NORTHWESTERN UNIVERSITY

Store-Operated Calcium Channels in the Brain:
Functions in Astrocytes and a Role in Learning and Memory

A DISSERTATION

SUBMITTED TO THE GRADUATE SCHOOL

IN PARTIAL FULFILLMENT OF THE REQUIREMENTS

for the degree

DOCTOR OF PHILOSOPHY

Field of Neuroscience

(Northwestern University Interdepartmental Neuroscience Program)

By

Anna Bettina Tóth

EVANSTON, ILLINOIS

September 2019

ABSTRACT

Store-operated Ca^{2+} entry (SOCE) is a principal mechanism for generating cellular Ca^{2+} signals. Store-operated Ca^{2+} release-activated Ca^{2+} (CRAC) channels serve an essential role in generating Ca^{2+} elevations needed for transcriptional, enzymatic, and secretory effector cascades in many cell types. CRAC channels, comprised of the ER Ca^{2+} sensor STIM and the plasma membrane Ca^{2+} channel Orai, were discovered in the immune system but have been increasingly recognized for widespread roles throughout the organism. Here, we investigated the functional roles of CRAC channels in the nervous system, with a specific focus on their role in the hippocampus for astrocyte physiology and animal behavior.

Astrocytes are the major glial subtype in the brain and mediate numerous functions ranging from metabolic support to gliotransmitter release through signaling mechanisms controlled by Ca^{2+}. Despite intense interest, the Ca^{2+} influx pathways in astrocytes remain obscure, hindering mechanistic insights into how Ca^{2+} signaling is coupled to downstream astrocyte-mediated effector functions. In the first part of this dissertation, we identified store-operated CRAC channels encoded by Orai1 and STIM1 as a major route of Ca^{2+} entry for driving sustained and oscillatory Ca^{2+} signals in astrocytes after stimulation of metabotropic purinergic and protease-activated receptors. Using synaptopHluorin as an optical reporter, we showed that the opening of astrocyte CRAC channels stimulated vesicular exocytosis to mediate the release of gliotransmitters, including ATP. Furthermore, slice electrophysiological recordings showed that activation of astrocytes by protease-activated receptors stimulated interneurons in the CA1 hippocampus to increase inhibitory postsynaptic currents on CA1 pyramidal cells. These results reveal a central

role for CRAC channels as regulators of astrocyte Ca^{2+} signaling, gliotransmitter release, and astrocyte-mediated tonic inhibition of CA1 neurons.

Ca^{2+} elevations are essential for many neuronal processes that form the neurochemical basis of learning and information storage in the brain. CRAC channels are highly expressed in brain regions critical for learning, memory, and cognition, including the hippocampus. However, their role in mediating the Ca^{2+} signals driving learning and memory are not well understood. In the second part of this dissertation, we investigated the role of CRAC channels in regulating cognitive and behavioral functions using conditional Orai1 knockout mice. We showed that these mice are impaired in working, spatial, and associative memory tasks, suggesting that Orai1 channels play a role in processes essential for learning and memory.

Together, these studies add new insight into the physiological functions of store-operated CRAC channels in the nervous system and the consequences of dysfunction in this Ca^{2+} signaling pathway.

ACKNOWLEDGMENTS

This work would not have been possible without the help and support of many people who have contributed time, energy, ideas, encouragement, and motivation during the course of my graduate studies. First, I would like to express my gratitude to my advisor, Dr. Murali Prakriya, for the opportunity to work with him. He has been a fantastic mentor and I greatly appreciate the time and effort he has put into helping me grow as a scientist and person. Thank you, Murali, for all the lessons, conversations, and support over these past years.

I am fortunate to have had the opportunity to learn from other experienced and accomplished scientists who have contributed their time and energy to helping me succeed during this phase of my life. I would like to thank my thesis committee: Drs. Richard Miller, Marco Martina, and Savio Chan. I greatly appreciate the feedback and constructive criticism that they provided during my committee meetings, which helped move my project forward. I would like to thank other Northwestern faculty who have collaborated on projects or taught me during my training: Drs. Jelena Radulovic, Geoffrey Swanson, and Anis Contractor. I would also like to thank the directors and administrators of the Medical Scientist Training Program (MSTP), the Northwestern University Interdepartmental Neuroscience (NUIN) program, and the Northwestern Department of Pharmacology. And thank you to my undergraduate research advisor at the University of Michigan, Dr. Hisashi Umemori, for introducing me to neurobiology research and inspiring me to pursue a PhD.

To the members of the Prakriya lab: thank you all for your help and for making it fun to come to work every day. Specifically, thank you to former lab members Amit, Agila, Leida, Lauren, and Ann. Thank you to Andrew, who helped me with immunostaining and other

techniques and once saved my laptop from a nearly deadly coffee spill; and Chelsea and Natalie, who were always fun to talk to and invaluable for all their help with the mice. Thank you to my collaborators in lab: Kotaro Hori, who worked hard on setting up slice electrophysiology in our lab and contributed greatly to this project; Mikki Novakovic, whose coding and tireless troubleshooting in MatLab helped immensely with data analysis in this project; and Mehdi Maneshi, who is putting tremendous effort into continuing the learning and memory project. Thank you to my wonderful office-mates, Megumi and Priscilla, for all their advice, fun conversations, and for setting up a flower garden in our office. Thank you to lab members Nisha, Tim, Shogo, and Toneisha for their scientific enthusiasm and Martinna for her quick learning and help with the mice. I thank everyone for all the helpful discussions and delicious contributions to the lab potlucks.

I extend many thanks to others who have assisted with this work: my collaborators Natalie Bernstein and Laurie Lambot for their help with viral injections, Drs. Dina Arvanitis and Joshua Rappoport in the Center for Advanced Microscopy for their assistance with imaging, Dr. Craig Weiss and Mary in the Behavioral Phenotyping Core for their assistance and advice on behavioral techniques, and Anita and Mariah in the Radulovic lab for their help with fear conditioning experiments.

I would like to thank all of my graduate school friends and classmates, who have gone through this long journey with me, especially my friends Anu and Sherry. I would also like to express my heartfelt gratitude to other very important people in my life: to Shivani, for being my longest and closest friend, and for regularly helping me escape the stress of graduate school with adventurous trips abroad. To Colin, for his support every day, for providing balance in my life,

and importantly, for home-cooked meals after long days in lab. And to my little brother Bence, for his lifelong friendship and for always believing in me.

Finally, I would like to express my deepest appreciation to my amazing parents. They have been my strongest cheerleaders through good days and bad, and without their support, I certainly wouldn't be here. I thank them from the bottom of my heart for always encouraging me to follow my dreams.

TABLE OF CONTENTS

LIST OF FIGURES

CHAPTER 1

CHAPTER 2

CHAPTER 3

CHAPTER 4

CHAPTER 5

CHAPTER 6

CHAPTER 1

INTRODUCTION

Store-Operated Ca^{2+} Entry

Calcium (Ca^{2+}) is a versatile intracellular second messenger that regulates a remarkable diversity of cellular functions spanning from early development to cell death (1). Underlying the effectiveness of Ca^{2+} as a signaling molecule is the 20,000-fold gradient that cells maintain between their intracellular (~50-100 nM resting) and extracellular (~1-2 mM) concentrations and the careful control cells exert over the concentration and spatiotemporal nature of the intracellular Ca^{2+} signal using a collection of Ca^{2+} channels, pumps, buffers, and binding proteins (2). Cells keep the resting cytosolic Ca^{2+} levels low using sarcoendoplasmic reticular Ca^{2+} ATPases (SERCA) to pump Ca^{2+} into the endoplasmic reticulum (ER), the major intracellular store (~400-600 μM resting [Ca^{2+}]), and plasma membrane Ca^{2+} ATPases (PMCA) to pump Ca^{2+} out of the cell. Two primary mechanisms of mobilizing cytosolic [Ca^{2+}] elevations are the release of Ca^{2+} from stores in the ER, and the influx of Ca^{2+} from outside the cell through Ca^{2+}-permeable ion channels in the plasma membrane (PM). In many cells, these two processes are coupled by a unique Ca^{2+} influx pathway called store-operated Ca^{2+} entry (SOCE) (3).

SOCE is typically activated by the engagement of cell surface receptors that activate phospholipase C (PLC) through G-proteins or tyrosine kinase cascades to cleave phosphatidylinositol 4,5-bisphosphate (PIP_2) and produce inositol 1,4,5-trisphosphate (IP_3). IP_3 then binds to IP_3 receptors on the ER membrane to release Ca^{2+} from ER stores (4). The ensuing depletion of intracellular Ca^{2+} stores activates a family of store-operated channels (SOCs) on the PM, resulting in Ca^{2+} influx down its chemical gradient from the extracellular space into the

cytoplasm (**Fig. 1.1**). SOCE is named for its mode of activation – reduction of the ER Ca^{2+} store – and SOCs play a homeostatic role by providing Ca^{2+} to refill the ER stores and also serve to directly elevate cytosolic [Ca^{2+}] to trigger a variety of effector functions. Whereas the Ca^{2+} capacity of the ER is finite and release can only generate transient Ca^{2+} signals, the influx of Ca^{2+} through SOCs can be sustained for much longer timescales of minutes to hours to drive biological processes such as gene expression, proliferation, exocytosis, and secretion.

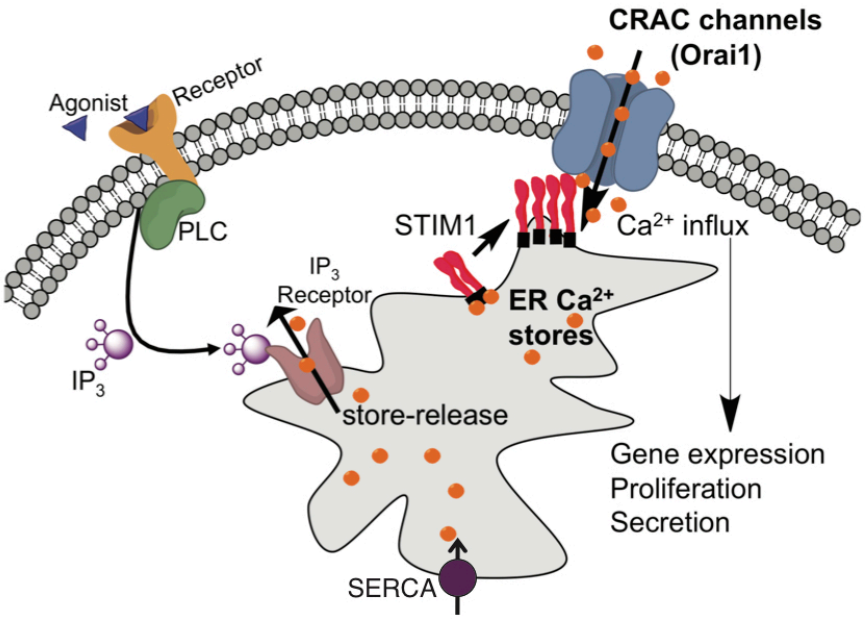

Figure 1.1. Signaling mechanism of store-operated Ca^{2+} entry. Stimulation of cell surface receptors that activate PLC results in the production of IP_3 and the depletion of ER stores through IP_3 receptors. ER store depletion triggers the plasma membrane store-operated channels (CRAC channels), resulting in Ca^{2+} influx into the cytosol. The molecular components of SOCE – STIM1 and Orai1 – are described in detail below. Figure adapted from Leidamarie Tirado-Lee.

The idea of SOCE was first described in 1986 by James Putney, who proposed that Ca^{2+} store depletion was responsible for a sustained Ca^{2+} influx from the extracellular space, following an initial release of ER Ca^{2+} triggered by IP_3 (5, 6). The first direct measurement of the SOCE pathway came from recordings of small, voltage-independent Ca^{2+} currents activated by

physiological agonists in T cells and mast cells (7, 8). The introduction of SERCA inhibitors as experimental tools helped establish the link between these Ca^{2+} currents and SOCE. The most widely used of these is thapsigargin (TG), a plant-derived lactone and selective inhibitor of SERCA that depletes ER stores by unmasking a continuous passive Ca^{2+} leak from the ER. TG permitted the experimental depletion of ER Ca^{2+} stores while bypassing receptor stimulation and the generation of IP_3 (9, 10). The observation that TG triggered PM Ca^{2+} influx that was the same as influx triggered by IP_3, and that IP_3 and TG had non-additive effects on Ca^{2+} influx, suggested that they were activating the same Ca^{2+} entry pathway (9). Subsequent studies in T cells and mast cells recognized the similarities in the Ca^{2+} current induced by physiological agonists and by direct Ca^{2+} store depletion, establishing falling store content as the stimulus for channel activation (11-14). The current was named the Ca^{2+} release-activated Ca^{2+} (CRAC) current, I_{CRAC}, and the channel, the CRAC channel (13). CRAC channels are characterized by their voltage-independence, exquisite Ca^{2+} selectivity, inwardly-rectifying current-voltage relationship, and low unitary conductance (15, 16).

For two decades after the SOCE pathway was first proposed, the pharmacological and electrophysiological properties of the CRAC channel were described in detail (3), but the molecular identities of the CRAC channel components eluded scientists. Numerous CRAC channel candidates were proposed, most prominently various members of the transient receptor potential (TRP) channel family (17-19), although none had all the biophysical properties of CRAC channels. In 2005, stromal interaction molecule 1 (STIM1) was identified as the ER Ca^{2+} sensor that links store-depletion to channel activation (20-22) and in 2006, Orai1 was identified as the pore-forming subunit of the CRAC channel (23-25). The molecular mechanism of CRAC channel activation begins with Ca^{2+} release from the ER. Upon store depletion, STIM1 oligomerizes and

translocates from the bulk ER to ER-PM junctions, where it physically activates the Orai1 channel (**Fig. 1.1**) (26).

STIM: the ER Ca^{2+} Sensor

STIM1 was identified in 2005 as the ER Ca^{2+} sensor for SOCE using RNAi screens for SOCE suppressors in *Drosophila* S2 cells (22) and HeLa cells (21). STIM1 is a 77kDa single-pass transmembrane (TM) protein located predominantly in the ER membrane, and knockdown of STIM1 significantly reduces SOCE and I_{CRAC} in mammalian cells. The ER luminal N-terminal portion of STIM1 contains an EF-hand motif, which allows the protein to sense Ca^{2+} content (20), and a sterile alpha motif (SAM), which regulates oligomerization (27). The cytosolic C-terminal portion binds to Orai channels, and contains a critical ~100 amino acid region, most commonly called the CRAC activation domain, which is the minimal region of STIM1 that is necessary and sufficient to activate CRAC channels (28-30).

Mammals express two homologs of STIM, STIM1 and STIM2, which have about 75% sequence similarity (4). STIM2 can also induce SOCE upon ER store depletion, but its activation kinetics, affinity for Ca^{2+}, and tissue expression differ from STIM1 (31). The EF-hand domain of STIM1 binds Ca^{2+} with a dissociation constant (K_D) of ~200 μM, and STIM2 binds with a K_D of ~500 μM (32). Therefore, STIM2 is partially active at resting ER Ca^{2+} levels and more sensitive to small changes in ER luminal [Ca^{2+}]. It has therefore been suggested to play a homeostatic role in maintaining basal cytosolic and ER Ca^{2+} levels (33). STIM2 is also characterized by slower oligomerization kinetics and less effective in Orai1 binding and activation than STIM1 (34).

Orai: the pore-forming subunit of the CRAC channel

Orai1 was identified through linkage mapping in a family with severe combined immunodeficiency (SCID) lacking SOCE and CRAC channel function (35), combined with genome-wide RNAi screens in *Drosophila* for genes regulating SOCE (35, 36). Orai1 is a four-transmembrane domain PM protein that forms the ion-conducting pore of the CRAC channel (23). Orai1's identity as the pore-forming subunit of the CRAC channel was established based on findings that the mutation of an acidic residue (E106) in TM1 diminished Ca^{2+} influx and changed ion selectivity of the pore (23-25). The crystal structure of *Drosophila* Orai in the closed state revealed that the channel is assembled as a hexamer of Orai subunits arranged around a central ion pore (37). A ring of six glutamate residues (E178, corresponding to E106 in the mammalian Orai1) on the extracellular side constitutes the selectivity filter.

There are three Orai homologs: Orai1, Orai2, and Orai3. The transmembrane domains are highly conserved among the 3 Orai isoforms. When coexpressed with STIM1, all three Orai isoforms function as Ca^{2+}-selective store-operated channels, but differ in some of their biophysical properties including inactivation and permeation, and in their sensitivity to pharmacological inhibitors (38-41). Orai2 expression is particularly high in the brain, lung, spleen, and small intestine, and Orai3 is abundant in many solid organs, but neither are well-defined functionally and their physiological roles are largely unclear.

Recently, in T cells, Orai2 has been shown to modulate the magnitude of SOCE and T cell-mediated immune responses (42). Whereas deletion of Orai1 reduced SOCE and CRAC currents, deletion of Orai2 enhanced SOCE and CRAC currents in naïve T cells and macrophages. These effects are explained by the ability of Orai2 to form heteromeric channels with Orai1 to attenuate CRAC channel currents, likely due to its enhanced Ca^{2+}-dependent inactivation properties (42).

Molecular choreography of CRAC channel activation

The complex choreography of CRAC channel activation has been extensively studied and it involves a unique coupling process between the loss of Ca^{2+} from the ER lumen to the opening of Ca^{2+} permeable channels in the plasma membrane (26). When ER stores are full, the luminal EF-hand domain of STIM1 is bound to Ca^{2+}, and STIM1 is uniformly distributed throughout the ER membrane. Upon store depletion, Ca^{2+} unbinds from the EF-hand of STIM1, triggering a conformational change involving STIM1 oligomerization and translocation to PM-ER junctions where it forms distinct puncta (20, 27, 43-46). Orai1 also redistributes within the PM to accumulate at sites opposite to STIM1 (47). This juxtaposition allows for several protein-protein interactions to occur, leading to channel activation and Ca^{2+} entry into the cytosol (29, 46). Ca^{2+} is transferred into the ER by the SERCA pump and once the store is refilled, Ca^{2+} rebinds the luminal EF-hand, and the STIM1 activation process is reversed. STIM1 dissociates from Orai1 and SOCE is shut off (48). Each time an agonist stimulates ER Ca^{2+} release, a fraction of the released Ca^{2+} is transported out of the cell by PM Ca^{2+} ATPase pumps and the Na^{+}/Ca^{2+} exchanger. Therefore, SOCE plays a homeostatic role in ensuring adequate repletion of the stores. CRAC channels also play an active role in producing Ca^{2+} oscillations and waves that drive both short-term (i.e. secretion) as well as long-term (i.e. gene expression) signaling pathways.

Physiological Functions of SOCs

CRAC channels are highly evolutionarily conserved from *Drosophila melanogaster* to humans, and have a widespread expression in almost all mammalian tissues, underlying their role as a fundamental Ca^{2+} entry pathway. The pathophysiological relevance of CRAC channels was first revealed in studies that showed that CRAC channel activation and the ensuing Ca^{2+} signals

were vital to immune cell function (49-53). Over the years since, the contribution of store-operated CRAC channels to function has been described in the literature for numerous cell types and systems, including smooth muscle and skeletal muscle (54, 55), endothelial cells (56), platelets (57, 58), microglia (59), astrocytes (60), and neurons (61-63).

Studies in Human Patients

Early studies on CRAC channels established them as a primary pathway for Ca^{2+} influx in human T cells (51, 64). The link between aberrant CRAC channel activity and human disease was recognized in the first reports of a defective I_{CRAC} in the lymphocytes of young patients with primary immunodeficiencies (49, 50). Other studies showed that the T cells of two infant brothers with a form of severe combined immunodeficiency (SCID) characterized by an increased propensity for fungal and viral infections had a primary defect in SOCE and CRAC channel function (52, 53). Later the genetic defect of the two SCID patients was identified as a homozygous missense mutation in exon 1 of the ORAI1 gene, identifying Orai1 as an essential component of the CRAC channel (35). These and other patients with loss-of-functions mutations in Orai1 or STIM1 exhibit a severe form of immunodeficiency due to impairment of T cell activation and cytokine production resulting in predisposition to life-threatening infections. In addition, these patients are afflicted by congenital myopathy, characterized by muscular hypotonia, and ectodermal dysplasia, characterized by abnormalities in sweat glands and/or teeth, and in the case of STIM1 deficiency, autoimmunity (65-67). The findings that mutations in either Orai1 or STIM1 are associated with a similar phenotype further reveal that a faulty CRAC channel pathway is the basis for these pathological features.

The fact that patients with loss-of-function mutations in Orai1 and STIM1 primarily show severe immune dysfunction despite CRAC channels having a widespread and possibly ubiquitous expression, does not exclude a functional role for Orai1, STIM1, and SOCE in other cell types and systems. In other cell types, Orai1 and STIM1 may have partially redundant roles, with the possibility that Orai2, Orai3, STIM2, or other non-store-operated Ca^{2+} influx pathways functionally compensate, at least in part, for their loss in the individual (65, 68).

SOCs in Brain and Behavior

Although CRAC channels were originally described and characterized in immune cells, they have been demonstrated to be highly expressed throughout the body, including the brain (69). In the brain, Ca^{2+} regulates a myriad of critical processes including neuronal excitability, transmitter exocytosis, synaptic transmission, and neuronal development. Whereas the literature on voltage- and ligand- gated Ca^{2+} channels in the brain is extensive, the role of CRAC channels in neurobiological processes remains poorly understood.

All three Orai isoforms are expressed in the cortex, hippocampus, cerebellum, and spinal cord (63, 69, 70). STIM1 and STIM2 are both expressed throughout the brain and spinal cord in neurons and glia, with reports that STIM2 is the predominant isoform in neurons of the hippocampus and cortex, while STIM1 has strong expression in the cerebellum (63, 71-75). Numerous studies have implicated CRAC channels and SOCE in various neuronal functions including neurotransmitter release (76), synaptic plasticity (62, 77, 78), neural progenitor and neuronal gene expression (79, 80), nociception (61, 70, 81), and motor function (82, 83). Consequently, dysregulation of SOCE in neurons and glia can disrupt intracellular Ca^{2+} homeostasis and may contribute to the pathogenesis of numerous neurological diseases. Indeed,

dysfunctional SOCE has been implicated in hypoxic neuronal cell death (75), epilepsy (73), amyotrophic lateral sclerosis (84), and Alzheimer's disease (85, 86). Given the central importance of Ca^{2+} for regulating essential neurobiological processes, it is of considerable consequence to elucidate the Ca^{2+} signaling pathways in the nervous system. Yet despite increasing interest in the field, many questions remain to be resolved.

SOCE in the Nervous System

Neuronal Store-Operated Ca^{2+} Signaling

Ca^{2+} signaling mediates many essential roles in neurons including gene expression, neurotransmitter release, and synaptic plasticity. Therefore, identifying the Ca^{2+} influx pathways mediating these vital processes has been of great interest in neurobiology. Even before the identification of STIM and Orai, Ca^{2+} imaging experiments showed that TG evoked SOCE in cultured hippocampal neurons and freshly dissociated cortical neurons (87, 88). Now, Orai and STIM have been shown to be expressed in many brain regions including the hippocampus and the cortex, although their cellular roles are still unclear.

One area in which SOCE may make important contributions is synaptic plasticity. Plasticity is commonly manifested in dendritic spines, where Ca^{2+} elevations are essential for driving processes such as long-term potentiation (LTP) and spine maturation (89). At the CA3 Schaffer collateral- CA1 synapse in the hippocampus, strong synaptic activity evokes Ca^{2+} signaling in dendritic spines, which activates downstream signaling programs such as Ca^{2+}/calmodulin protein kinase II (CaMKII) activation that result in strengthening of the synapse through the insertion of new AMPA receptors and changes in spine morphology. Ca^{2+} entry through NMDA receptors is known to be essential for evoking spine Ca^{2+} elevations to induce

plasticity, but NMDA receptors may not be the only Ca^{2+} influx pathway, and growing evidence indicates that Ca^{2+} stores and store-operated CRAC channels may also contribute (62, 76, 77, 90).

Stim and Orai proteins have been shown to be expressed throughout the brain and reported to play roles in synaptic transmission and higher cognitive functions (91). Moreover, SOCE dysregulation has been suggested as a factor in the pathogenesis of neurodegenerative diseases like Alzheimer's disease (92-95). In particular, STIM2 has been implicated as a predominant player in SOCE and the proper functioning of hippocampal neurons. In knockout mouse studies, STIM2-deficient mice showed an impairment in hippocampus-dependent spatial learning (75). A potential mechanism for this defect comes from a study by Sun et al., which showed that STIM2 regulates steady-state activity of the enzyme CaMKII to stabilize mushroom spines in hippocampal neurons (86). They further showed that familial Alzheimer's disease mutations and aging compromise SOC activation, resulting in impaired spine maturation. STIM2 activation or overexpression in hippocampal neurons could rescue mushroom spine loss, protect spines from amyloid synaptotoxicity, and rescue impaired LTP in an Alzheimer's disease mouse model (85, 86, 96). On the other hand, familial Alzheimer's disease mutations have also been shown to promote cleavage of STIM1, impairing SOCE and destabilizing dendritic spines, a defect which could be rescued by overexpression of STIM1 (97).

Thus, evidence exists for the involvement of CRAC channels in neuronal physiology and pathophysiology. Yet, the available literature shows striking gaps in our understanding of the molecular mechanisms and functional roles of CRAC channels proteins including Orai1 in neurons, underscoring the need for future studies.

Astrocyte Store-Operated Ca^{2+} Signaling

Astrocytes are the primary glial cell type in the brain and regulate many aspects of brain function including neurogenesis and synaptogenesis, regulation of blood flow and metabolic support, ion homeostasis, clearance of neurotransmitters, neural repair following injury, and modulation of synaptic transmission (98-103). As electrically nonexcitable cells, astrocytes exhibit a form of excitability based on intracellular Ca^{2+} elevations.

Evidence from studies *in vitro*, *in situ*, and *in vivo* have demonstrated that astrocytes express a large repertoire of G protein-coupled receptors (GPCRs) which can be activated by neurotransmitters released from presynaptic terminals during neural activity (104-106). This includes purinergic, glutamatergic, GABAergic, adrenergic, muscarinic, and peptidergic receptors (107). Many of these are G_q-coupled GPCRs that act through the PLC-IP_3 signal transduction pathway to stimulate the release of Ca^{2+} from ER stores via IP_3R Ca^{2+} release channels (108) (**Fig. 1.2**). These characteristic rises in cytosolic Ca^{2+} levels, typically manifested as Ca^{2+} waves and oscillations, define the "Ca^{2+} excitability" of astrocytes (109, 110). The Ca^{2+} excitability of astrocytes is increasingly recognized as having a complex and dynamic spatiotemporal profile (111), underscoring the need to understand how Ca^{2+} homeostasis and signaling is regulated in astrocytes. Because Ca^{2+} mediates numerous effector functions including ion homeostasis, metabolism, gene expression, cell growth, and secretion (2), identification of the mechanisms by which Ca^{2+} enters the cell to evoke astrocyte Ca^{2+} signals is of great interest.

Yet, the available literature shows striking gaps in our understanding of the "Ca^{2+} excitability" of astrocytes. What pathways are involved in generating astrocyte Ca^{2+} elevations? What are the dynamic properties of these Ca^{2+} signals? How are they coupled to downstream effector functions? Progress in resolving these questions has been slow, largely because the

sources of Ca^{2+} mobilization and Ca^{2+} entry in astrocytes remain poorly understood (109, 110, 112-114). There is strong evidence for the involvement of Ca^{2+} release from intracellular stores (101, 110, 112, 115, 116). However, because release of Ca^{2+} from intracellular stores is typically coupled to activation of SOCE and previous studies were not designed to discriminate between SOCE and store release, the possibility that SOCE could contribute to astrocyte Ca^{2+} signaling has not been seriously considered in past work.

Orai1 and STIM1 are expressed in glioblastoma cell lines (117), cortical astrocytes (118, 119), spinal astrocytes (60), and white matter glia of the optic nerve (120), where they mediate SOCE in response to TG-mediated depletion of ER Ca^{2+} stores. Some studies have also argued for a key role of TRPC channels, especially TRPC1 and TRPC3, in mediating SOCE in primary astrocytes (109, 114, 121, 122). Therefore, the contribution of CRAC channels for regulating the Ca^{2+} excitability of astrocytes, particularly in response to physiological agonists, and their role in downstream effector functions remains unresolved.

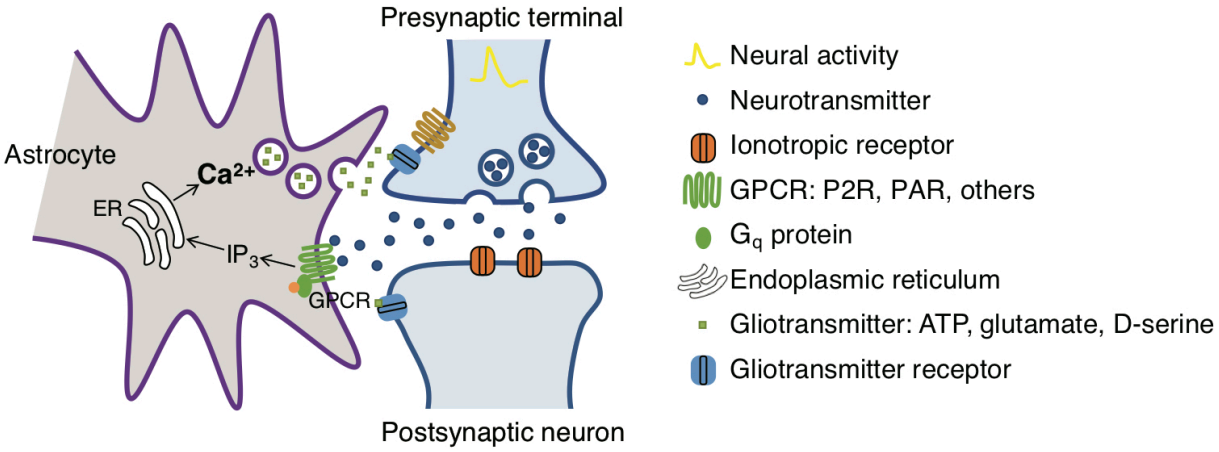

Figure 1.2. Ca^{2+} signaling in astrocytes. At many synapses, astrocyte processes interact with pre- and post-synaptic neurons in a functional structure called the "tripartite synapse." Depolarization of presynaptic terminals triggers release of neurotransmitters, which act on astrocyte G-protein coupled receptors. The ensuing increase in astrocytic $[Ca^{2+}]_i$ can stimulate release of gliotransmitters from the astrocyte to reciprocally modulate neuronal activity. The mechanisms underlying gliotransmitter exocytosis are unresolved.

Ca^{2+} Signaling and Gliotransmitter Release

Historically thought to serve solely as structural and trophic support cells for neurons, the modern viewpoint of astrocytes has undergone significant revision. It has been almost 30 years since the first evidence challenging the role of astrocytes as passive bystanders to neuronal activity was published. In 1990, Cornell-Bell et al. first observed that activation of glutamate receptors on astrocytes elevated their intracellular Ca^{2+} levels (123). This finding that astrocytes can sense glutamatergic synaptic transmission with their Ca^{2+} responsiveness eventually expanded with the discovery that astrocyte Ca^{2+} dynamics can mediate not just neuron to astrocyte signaling, but also astrocyte to neuron; in other words, bi-directional communication between neurons and astrocytes (124, 125).

There is now abundant evidence that astrocytes play a direct role in modulating neuronal activity and synaptic functions through the release of neuroactive molecules called gliotransmitters (111, 126). To support their role in synaptic physiology, the end feet of astrocyte processes are physically and functionally associated with many presynaptic and postsynaptic neurons, in a specialized anatomical structure known as the tripartite synapse (127-129). The close morphological apposition of astrocytes and synaptic structures allows astrocytes to not only sense neurotransmitters released from synaptic terminals, but also to modulate the function of synapses by releasing gliotransmitters (**Fig. 1.2**). Dysregulation of the reciprocal communication between astrocytes and neurons is thought to be involved in a number of brain pathologies including epilepsy, stroke, and ALS (84, 130, 131).

While the molecular mechanisms involved in the release of gliotransmitters such as glutamate, ATP, and D-serine are not completely understood, there is compelling evidence that it involves Ca^{2+}-dependent exocytosis analogous to the vesicle release mechanism in neurons and

endocrine cells (132). In support of this mechanism, astrocytes have been shown to synthesize and store chemical transmitters in secretory compartments, express the core machinery that is critical for exocytosis including SNARE complex proteins and a Ca^{2+} sensor, and release transmitters upon stimulation (133-141). Furthermore, the release of gliotransmitters is inhibited by Ca^{2+} buffering and by toxins targeting the SNARE proteins (142), as expected for a Ca^{2+}-dependent exocytotic process.

When released from astrocytes, gliotransmitters activate neuronal receptors and modulate neural activity. Because astrocytes can release multiple gliotransmitters which can act on multiple targets even in the same circuit, there is a high degree of complexity in the physiological effects of astrocyte gliotransmission. The hippocampus is often the focus of studies on gliotransmission, as many hippocampal synapses have astrocyte coverage and the circuits have been well-defined. ATP is known to be a major neuronal-glial signaling molecule and Ca^{2+} elevations in astrocytes have been shown to trigger release of ATP, which regulates synaptic activity and plasticity in the hippocampus (143-145). In addition to direct actions mediated by P2 purinoceptors, ATP released from astrocytes can have secondary neuromodulatory effects mediated by P1 receptors after rapid degradation to adenosine (146). In the same circuit, astrocytic Ca^{2+} elevations trigger glutamate release, which can modulate synaptic transmission by acting on both presynaptic mGluRs as well as postsynaptic NMDARs (147-149). Thus, through their Ca^{2+}-dependent secretion of gliotransmitters, astrocytes can exert diverse modulatory actions on neuronal activity. However, the specific mechanisms and sources of Ca^{2+} signaling that govern regulated secretion remain poorly understood.

There remain many questions and controversies about gliotransmission in the field (110, 150-152). Several studies have questioned the existence of Ca^{2+}-mediated gliotransmission based

largely on two negative findings: A) Stimulation of an exogenously-expressed orphan GPCR (MrgA1) in astrocytes failed to modulate synaptic activity or plasticity despite provoking bulk rises in astrocyte $[Ca^{2+}]_i$ (153); and B) Deleting the Ca^{2+} release pathway, IP_3R2, which is enriched in astrocytes, had no effect on synaptic transmission or synaptic plasticity in the CA1 despite reducing astrocyte $[Ca^{2+}]_i$ (154). The precise reasons are unclear for the discrepancy between these studies and many others that found that manipulating Ca^{2+} signals in astrocytes does affect synaptic transmission. However, it is possible that bulk Ca^{2+} elevations evoked by the activation of MrgA1 are not functionally coupled to gliotransmitter release pathways, and that IP_3R2 is not the only trigger of gliotransmitter release. Indeed, others have reported recently that IP_3R2 KO mice still show abundant Ca^{2+} signals, predominantly in processes (115, 116, 155), and IP_3R2-independent ER Ca^{2+} release pathways exist in astrocytes including the other IP_3Rs, IP_3R1 and IP_3R3 (156, 157). These complexities highlight the importance of defining the pathways that regulate astrocyte Ca^{2+} signaling and how they are connected to gliotransmission.

Summary

Ca^{2+} is a ubiquitous signaling messenger essential to the proper functioning of cells. Among the many Ca^{2+} signaling mechanisms that contribute to driving biological processes, SOCE through CRAC channels is a widespread and clinically important pathway. Originally described in the immune system, CRAC channels are now known to be highly expressed in the brain, including in astrocytes and neurons. Yet the properties and physiological roles of these channels in the nervous system are not well-defined. In my thesis dissertation, I investigate the role of CRAC channels for astrocyte Ca^{2+} excitability and gliotransmitter release using genetic knockouts of Orai1 and STIM1, and wide-field, two-photon, and total internal reflection (TIRF) microscopy.

Additionally, I explore the behavioral effects of deleting Orai1 in the brain and the role of Orai1 in learning and memory.

Chapter 2 focuses on the pharmacological and molecular properties of store-operated Ca^{2+} entry in astrocytes, showing that CRAC channels formed by Orai1 and STIM1 are a major route of Ca^{2+} entry in hippocampal astrocytes. Chapter 3 explores the physiological activators of this signaling pathway in astrocytes, demonstrating that CRAC channels are essential for generating Ca^{2+} signals in astrocytes following metabotropic receptor stimulation. Chapter 4 explores the functional consequences of CRAC channel activation in cultured astrocytes, showing that stimulation of CRAC channels by store depletion and metabotropic agonists directly triggers slow vesicular release of gliotransmitters including ATP. Chapter 5 focuses on our studies in hippocampal slices, demonstrating that Orai1 is essential for generating Ca^{2+} signals in astrocyte processes, and that activation of Orai1 in astrocytes can modulate neuronal circuits by increasing the activity of GABAergic interneurons in the CA1 hippocampus. Finally, Chapter 6 explores the functional consequences of conditional deletion of Orai1 in the brain to understand how CRAC channels contribute to cognition and behavior.

CHAPTER 2

HIPPOCAMPAL ASTROCYTES EXHIBIT STORE-OPERATED CALCIUM ENTRY MEDIATED BY ORAI1 AND STIM1

Adapted from: Toth et al., Sci Signal, 2019 (158)

Introduction

Astrocytes display intracellular Ca^{2+} fluctuations implicated in many downstream effector functions including release of gliotransmitters (134, 159, 160). However, the contributions of specific plasma membrane Ca^{2+} entry pathways that shape the nature of these intracellular Ca^{2+} signals and mediate astrocyte functions are poorly understood. In many non-excitable cells, store-operated Ca^{2+} entry (SOCE) is a primary mechanism of mobilizing $[Ca^{2+}]_i$ elevations. SOCE occurs through the opening of CRAC channels, encoded by the Orai genes (Orai1-3) and activated by the ER Ca^{2+} sensors, STIM1 and STIM2. Recent studies indicate that astrocytes exhibit SOCE, however the molecular identity and functional downstream role of SOCE in hippocampal astrocytes is unknown.

In this chapter, we explore a potential role for CRAC channels in generating cytosolic Ca^{2+} elevations in cultured hippocampal astrocytes. We identify store-operated Ca^{2+} entry as a major mechanism of generating Ca^{2+} signals in hippocampal astrocytes, with pharmacological properties characteristic of CRAC channels. We further identify Orai1 and STIM1 as the molecular players mediating SOCE in hippocampal astrocytes, with Orai2 playing a modulatory role.

Results

Pharmacological properties of SOCE in hippocampal astrocytes

To begin to explore the mechanisms and functions of SOCs in astrocytes, we measured cytosolic Ca^{2+} transients following depletion of ER Ca^{2+} stores with the SERCA inhibitor TG in cultured hippocampal astrocytes. TG was administered in a Ca^{2+}-free Ringer's solution and SOCE was quantified using the classical method of measuring the rate and extent of Ca^{2+} influx after readdition of extracellular Ca^{2+}. These experiments revealed that mouse hippocampal astrocytes exhibited robust SOCE with the typical pharmacological hallmarks of CRAC channels (161), including blockade by low concentrations of the trivalent ion La^{3+} (**Fig. 2.1A**), inhibition by the channel inhibitor BTP2 (**Fig. 2.1A**), and potentiation at low doses and inhibition at high doses by the compound 2-aminoethyldiphenyl borate (2-APB) (**Fig. 2.1, B and C**). These results indicate that store-operated CRAC channels are functionally expressed in mouse brain astrocytes and mediate robust SOCE.

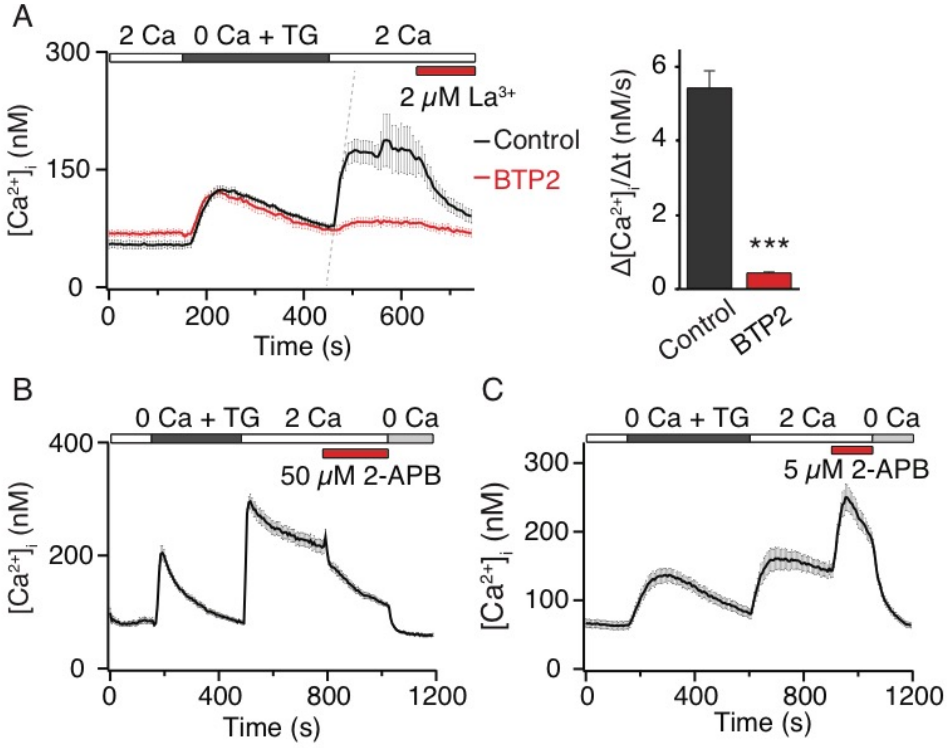

Figure 2.1. Pharmacological properties of SOCE in hippocampal astrocytes. (A) Depletion of ER Ca^{2+} stores with TG (1 μM) in a Ca^{2+}-free Ringer's solution evoked store release and subsequent SOCE

when extracellular Ca^{2+} (2 mM) was added back. SOCE was blocked by 2 μM $LaCl_3$ and after preincubation with BTP2 (1 μM for 2 hrs). The right graph shows the summary of the Ca^{2+} influx rate in control and BTP2-treated cells. Summary data are means ± SEM of n=35-36 cells for each group from 3 independent experiments. Ca^{2+} influx rates were calculated by measuring the initial slope of Ca^{2+} entry over 18 s after readdition of 2 mM Ca^{2+} solution (as shown by the dotted line for the control condition). ***P < 0.001 by unpaired t-test. **(B)** Administration of high dose 2-APB (50 μM) inhibited SOCE in cultured hippocampal astrocytes. n=11 cells, representative of 3 experiments. **(C)** Administration of low dose 2-APB (5 μM) potentiated SOCE, as previously described for CRAC channels (46, 162). n=6 cells, representative of 3 experiments.

Molecular determinants of SOCE in astrocytes

The best-described CRAC channels are formed by Orai1 and activated by the ER Ca^{2+} sensor, STIM1. Immunostaining revealed that Orai1 is expressed in the glial fibrillary acidic protein (GFAP)-positive hippocampal astrocytes from wild-type (WT) but not from Orai1 knockout (KO) cultures (**Fig. 2.2A**). Moreover, expression of a dominant negative pore-mutant of Orai1, E106A, suppressed SOCE, suggesting the involvement of Orai proteins in this pathway (**Fig. 2.2B**). To directly determine the contribution of Orai1 and STIM1 for mediating SOCE in astrocytes, we examined Ca^{2+} signals in brain-specific KO mice of these proteins, which were generated by crossing $Orai1^{fl/fl}$ (or $STIM1^{fl/fl}$) mice with mice expressing Cre-recombinase driven by the *nestin* promoter (80). Because nestin is expressed in neural stem/progenitor cells early in brain development, the progeny of this cross ($Orai1^{fl/fl\ nestin\text{-}Cre}$ or $STIM1^{fl/fl\ nestin\text{-}Cre}$) should lack Orai1 or STIM1 in both neurons and glia in the brain (163, 164). Consistent with this expectation, examination of TG-mediated Ca^{2+} entry in primary astrocytes obtained from Orai1 or STIM1 KO mice indicated that SOCE was abrogated upon loss of Orai1 or STIM1 (**Fig. 2.2, C and D**) with no change in the resting baseline $[Ca^{2+}]_i$ levels or the amount of Ca^{2+} released from ER stores (**Fig. 2.2, E and F**). The decrease in SOCE showed a gene dosage effect with the homozygous Orai1 KO cells showing significantly greater impairment in Ca^{2+} influx compared to Orai1 heterozygous

(HET) cells **(Fig. 2.2C)**. SOCE was observed in astrocytes derived from the hippocampus or the cortex, and La^{3+} sensitivity and dependence on Orai1 did not differ between astrocytes from these two regions (**Fig. 2.2, G and H**).

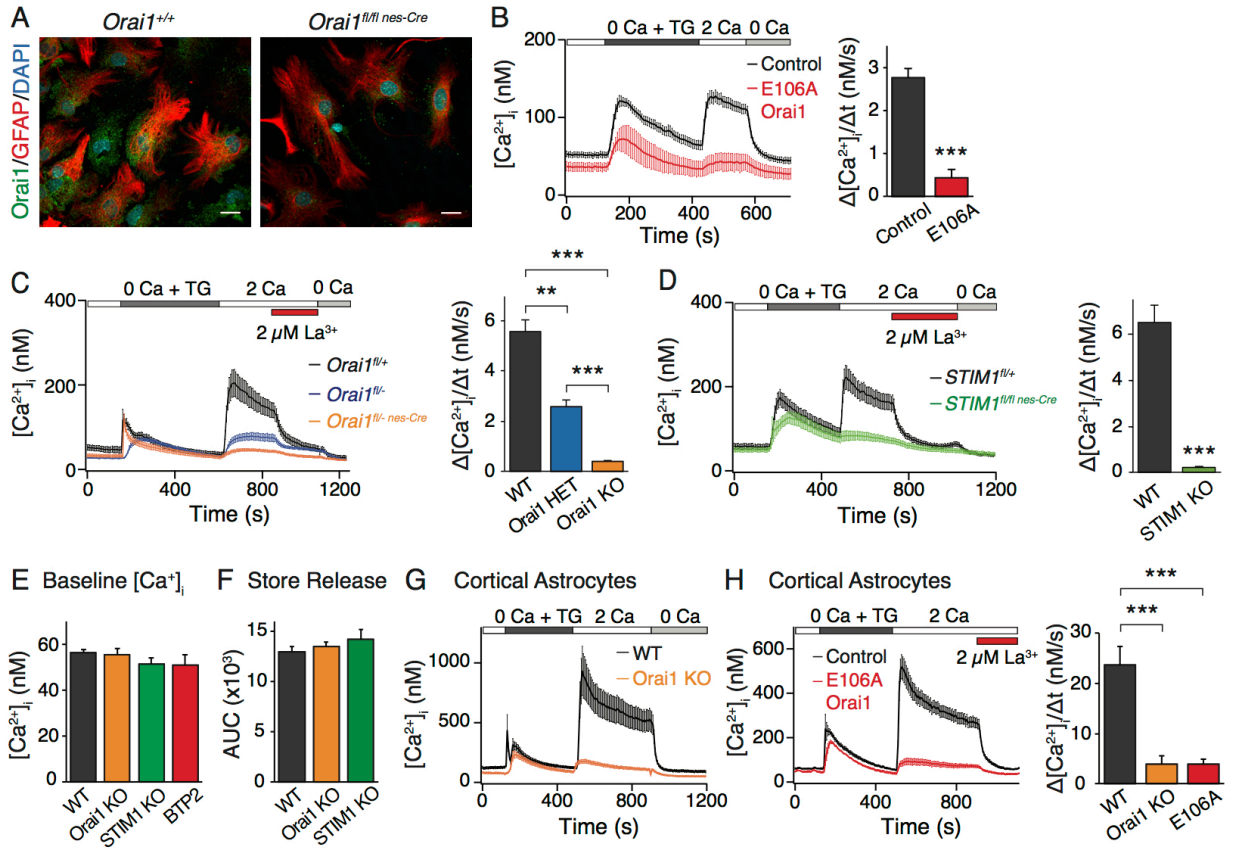

Figure 2.2. Astrocyte SOCE is mediated by Orai1 and STIM1. (A) Orai1 was expressed in cultured astrocytes. Hippocampal astrocyte cultures were immunolabeled for Orai1 and glial fibrillary acidic protein (GFAP). Orai1 labeling (green) was absent in cultured astrocytes from Orai1 KO (*Orai1*$^{fl/fl\ nestin\text{-}Cre}$) mice. Scale bar, 20 µm. **(B)** Overexpression of a dominant negative mutant of Orai1 (E106AOrai1-YFP) (23) significantly suppressed SOCE in cultured hippocampal astrocytes. Summary data are means ± SEM, n=10-20 cells for each group from 3 independent experiments. **(C)** SOCE is abolished in cultured hippocampal astrocytes from brain-specific Orai1 KO mice. Ca^{2+} influx rates were attenuated after readdition of external Ca^{2+}. The right graph shows the summary of the rate of Ca^{2+} influx in WT (*Orai1*$^{fl/+}$ and *Orai1*$^{fl/fl}$), Orai1 HET (*Orai1*$^{fl/+\ nestin\text{-}Cre}$ and *Orai1*$^{fl/-}$), and Orai1 KO (*Orai1*$^{fl/fl\ nestin\text{-}Cre}$ and *Orai1*$^{fl/-\ nestin\text{-}Cre}$) cells. Summary data are means ± SEM, n=39-56 cells for each group from 4-6 independent experiments. **(D)** SOCE was abolished in cultured astrocytes from STIM1 KO mice (*STIM1*$^{fl/fl\ nestin\text{-}Cre}$). Summary data (right graph) are means ± SEM, n=25-30 cells for each group from 3-4 independent experiments. (**E**) Summary of the baseline $[Ca^{2+}]_i$ for WT (n=72 experiments), Orai1 KO (n=50 experiments), STIM1 KO (n=16 experiments), and BTP2-treated (n=8 experiments) astrocytes. Data are means ± SEM. (**F**) Quantification

of store Ca^{2+} release (area under the curve, AUC) during application of TG in Ca^{2+}-free solution for 300 s. Data are means ± SEM for n=33-152 cells for each group from 4-11 independent experiments. (**G**) Cultured cortical astrocytes showed SOCE. SOCE is abolished in cortical astrocytes from Orai1 KO mice (*Orai1*$^{fl/fl\ nestin\text{-}Cre}$ and *Orai1*$^{fl/-\ nestin\text{-}Cre}$). Summary data are means±SEM, n=20-30 cells for each group from 3 independent experiments. (**H**) Overexpression of a dominant negative mutant of Orai1 (E106AOrai1-YFP) in cortical astrocytes significantly suppressed SOCE. Summary data are means ± SEM, n=8-36 cells for each group from 3 independent experiments. **P < 0.01; ***P < 0.001 by analysis of variance (ANOVA) followed by Tukey test for comparison of multiple groups (C, H) or by unpaired t-test for comparison of two groups (B, D).

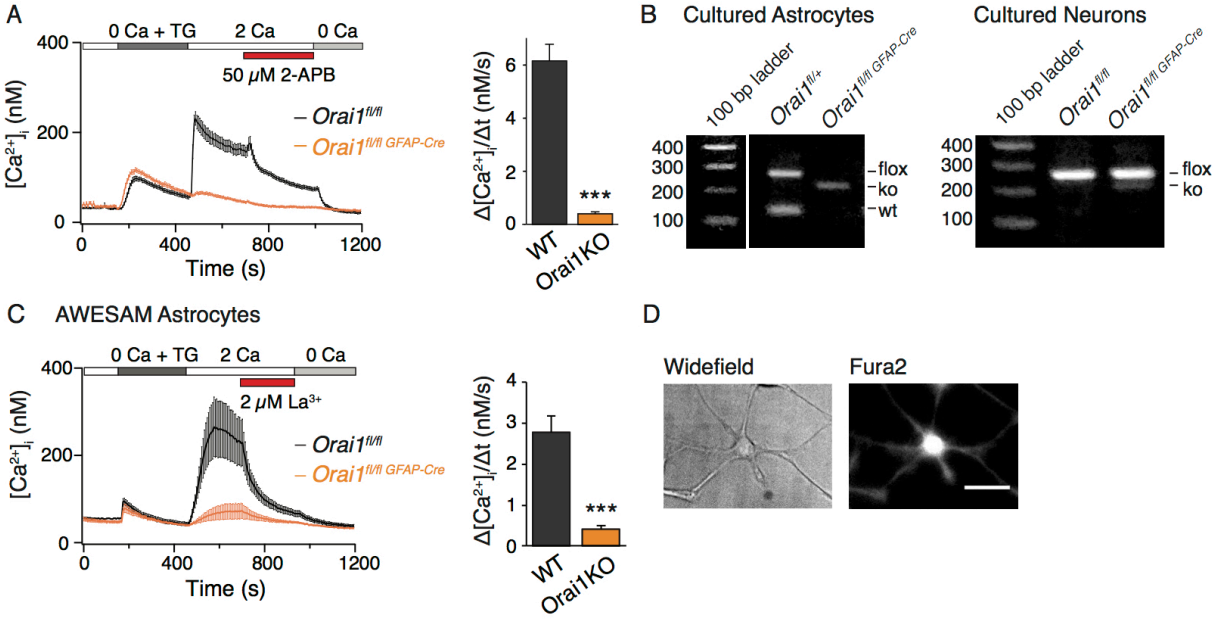

Figure 2.3. SOCE is abolished in cultured astrocytes from astrocyte-specific Orai1 KO mice. (A) Depletion of ER Ca^{2+} stores with TG (1 μM) in a Ca^{2+}-free Ringer's solution evoked store release and subsequent SOCE when extracellular Ca^{2+} (2 mM) was added back. Ca^{2+} influx rates were attenuated in *Orai1*$^{fl/fl\ GFAP\text{-}Cre}$ astrocytes. Summary data are means ± SEM, n=34-40 cells for each group from 3 independent experiments. **(B)** PCR of genomic DNA isolated from cultured astrocytes demonstrated complete deletion of the Orai1 gene in astrocytes from *Orai1*$^{fl/fl\ GFAP\text{-}Cre}$ mouse hippocampi. By contrast, the floxed band was largely preserved in neuronal cultures from *Orai1*$^{fl/fl\ GFAP\text{-}Cre}$ hippocampi. **(C)** Loss of Orai1 abrogated SOCE in astrocytes grown in cultures using the AWESAM culture protocol. Summary data are means ± SEM, n=31-43 cells for each group from 3 independent experiments. **(D)** Example images of the morphology of astrocytes grown using the AWESAM culture protocol in wide-field (left) and loaded with Fura2-AM (right). Scale bar, 10 μm. ***P < 0.001 by unpaired t-test.

SOCE was also lost in cultured astrocytes derived from astrocyte-selective *Orai1*$^{fl/fl\ GFAP\text{-}Cre}$ mice **(Fig. 2.3A)**, in which Orai1 was deleted by crossing *Orai1*$^{fl/fl}$ mice with *mGFAP-Cre* transgenic mice. Polymerase chain reaction (PCR) measurements in these mice indicated that

Orai1 was deleted in astrocytes from *Orai1*$^{fl/fl\ GFAP\text{-}Cre}$ mice but largely preserved in neurons (**Fig. 2.3B)** providing a second, more astrocyte-selective genetic line for probing the role of Orai1 in astrocytes. In addition, astrocytes grown using the "AWESAM" protocol that yields stellate astrocytes with complex morphology, long processes, and a more in vivo-like transcriptome than traditional astrocyte cultures (165, 166) exhibited robust SOCE which was lost in Orai1 KO astrocytes *(***Fig. 2.3, C and D***)*. Collectively, these results indicate that Orai1 and STIM1 are essential for mediating SOCE in mouse astrocytes.

Role of Orai2 in astrocyte SOCE

Another one of the three Orai isoforms - Orai2 - is highly expressed in the brain, particularly the hippocampus (http://mouse.brain-map.org/gene/show/92825). Yet, very little is known about its role in regulating Ca^{2+} signaling in the brain. To explore this question, we cultured hippocampal astrocytes from whole-animal Orai2 KO mice (*Orai2*$^{-/-}$) and examined TG-mediated SOCE. In stark contrast to Orai1, deletion of Orai2 strongly *enhanced* SOCE in hippocampal astrocytes. The rate of Ca^{2+} influx upon readdition of extracellular Ca^{2+} increased nearly threefold.

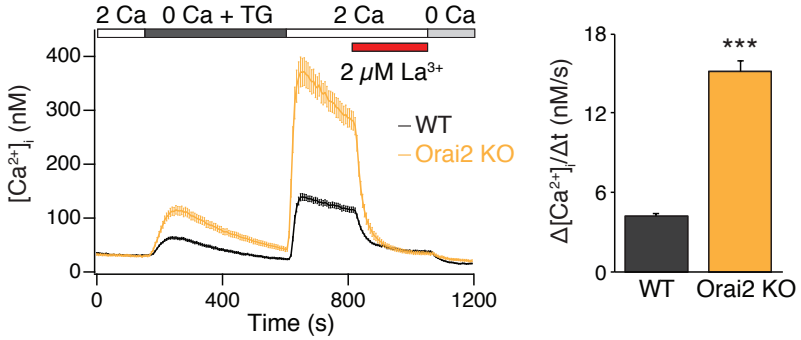

Figure 2.4. SOCE is enhanced in astrocytes from Orai2 KO mice. SOCE evoked by store depletion with 1 μM TG is increased in Orai2 KO (*Orai2*$^{-/-}$) vs WT hippocampal astrocytes. SOCE was blocked by 2 μM La^{3+} in both WT and Orai2 KO cells. Summary data are means ± SEM, n=52-66 cells for each group from 4 experiments. ***P<0.001 by unpaired t-test.

Discussion

In this chapter, we demonstrate that cortical and hippocampal astrocytes exhibit SOCE with the pharmacological and biophysical hallmarks of CRAC channels, including blockade by low concentrations of La^{3+}, modulation by 2-APB, and inhibition by the CRAC channel inhibitor BTP2. SOCE in astrocytes was abrogated by conditional KO of Orai1 and STIM1, consistent with previous observations (60, 118-120). Our data do not directly rule out a role for the CRAC channel molecules Orai3 and STIM2, or a contribution from other potential Ca^{2+} channels in astrocytes like TRP channels. However, TG-mediated SOCE was >95% abolished by deletion of Orai1 and STIM1, indicating that Orai1 and STIM1 are necessary for the bulk of SOCE in hippocampal astrocytes.

In striking contrast to the loss of SOCE seen in Orai1 KO astrocytes, Orai2 KO astrocytes show a significant gain of SOCE. This finding is consistent with recent studies showing that deletion of Orai2 results in increased SOCE and CRAC currents in lymphocytes, macrophages, mast cells, chondrocytes, and enamel cells (42, 167-169). This result suggests that in astrocytes, Orai1 and Orai2 could form heteromeric channels, with Orai2 acting as negative regulator of Orai1 (42). Therefore, in the Orai2 KO cells, Orai1 may be forming homomeric channels in which the modulation by Orai2 is removed, resulting in increased SOCE.

Our results are qualitatively and quantitatively similar in hippocampal astrocytes cultured from either brain-specific Orai1 KO mice ($Orai1^{fl/fl\ nestin\text{-}Cre}$) or astrocyte-selective Orai1 KO mice ($Orai1^{fl/fl\ GFAP\text{-}Cre}$). While the distinction between these two mouse lines does not matter much in the simplified system of purified astrocyte cultures, it has great significance in an intact system with both astrocytes and neurons. In our hippocampal slice experiments presented below, we probe

the role of Orai1 in astrocytes by using *Orai1*$^{fl/fl\ GFAP\text{-}Cre}$ conditional KO mice to preferentially target the deletion of Orai1 to astrocytes, while leaving neurons relatively intact.

It is also worth noting that astrocytes cultured using the AWESAM protocol also exhibit SOCE mediated by Orai1. In the astrocyte literature, there is often criticism of data obtained in the standard culture preparation, due to the property of astrocytes to change their gene expression profiles depending on the specific culture conditions (170). The recently developed AWESAM protocol is reported to more closely resemble *in vivo* astrocytes in terms of morphology, mRNA expression profile, and Ca^{2+} fluctuations than other astrocyte monocultures (165). The fact that we see similar SOCE properties in astrocytes cultured using either the AWESAM protocol or the standard protocol suggests that SOCE is not merely a culture artifact in standard preparations. In experiments presented below, we further explore the role of Orai1 in the astrocytes of hippocampal slices, which even more closely capture the complex environment and properties of astrocytes *in vivo*.

CHAPTER 3

SOCE IN ASTROCYTES IS ACTIVATED BY GPCR SIGNALING PATHWAYS

Adapted from: Toth et al., Sci Signal, 2019 (158)

Introduction

Neurotransmitters including glutamate and ATP bind to high affinity G-protein coupled receptors (GPCRs) on astrocytes to evoke IP_3-mediated release of Ca^{2+} from ER Ca^{2+} stores (104, 105) and induce astrocyte Ca^{2+} signaling behaviors ranging from sustained signals to oscillations (109, 110). In astrocytes, GPCRs constitute a major class of receptors which include purinergic, glutamatergic, GABAergic, adrenergic, muscarinic, and protease-activated receptors (PARs) (107). Purinergic receptors, including metabotropic P2Y GPCRs, are implicated in the Ca^{2+} excitability of astrocytes and the reciprocal communication between neurons and glia (136, 143, 171, 172). Likewise, PARs, which are abundantly expressed in astrocytes (173-175), are linked to many astrocyte functions including gliotransmitter release (176), production of proinflammatory mediators (177), and astrogliosis (178). In this chapter, we asked whether physiological activators of GPCRs on astrocytes activate Ca^{2+} signaling through store-operated CRAC channels.

Results

To investigate the physiological activators of SOCE in astrocytes, we surveyed several agonists of G protein-coupled purinergic, glutamatergic, cholinergic, and protease-activated receptors that can evoke depletion of ER Ca^{2+} stores. We administered these agonists in Ca^{2+}-free solution to release intracellular Ca^{2+} stores and examined SOCE after readdition of extracellular

Ca^{2+}. The purinergic agonist ATP, the P2Y-specific ($P2Y_2$ and $P2Y_4$) receptor agonist uridine triphosphate (UTP), and the PAR agonist thrombin robustly activated SOCE in astrocytes **(Figs. 3.1 and 3.2)**.

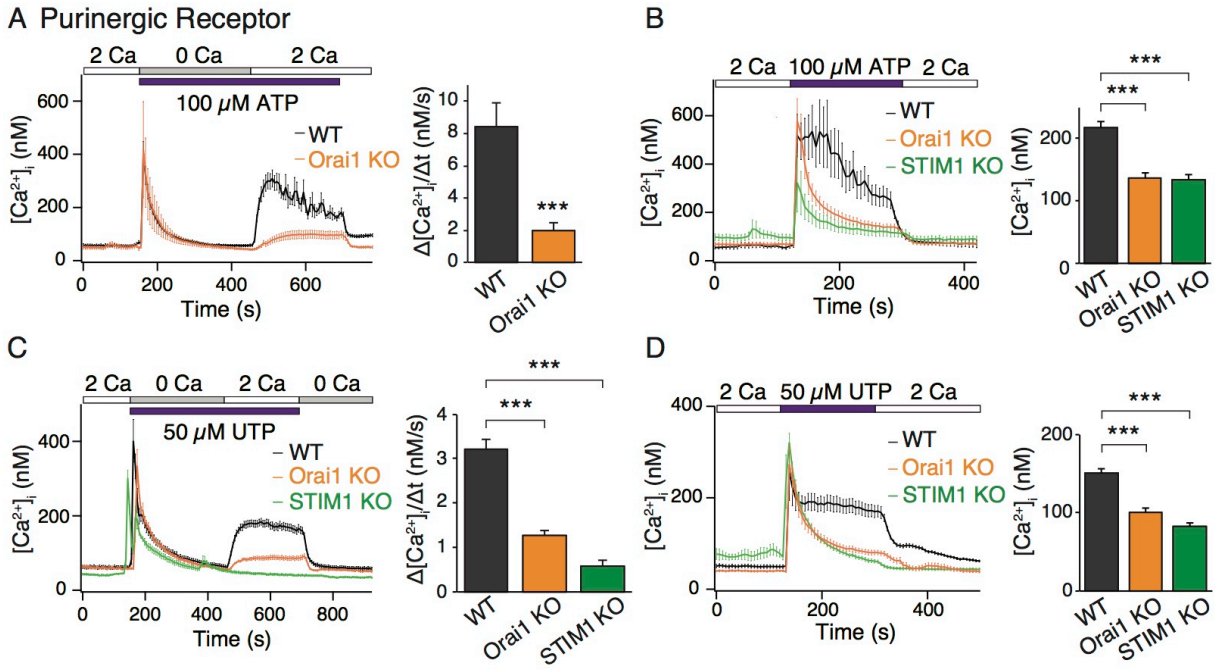

Figure 3.1. Stimulation of purinergic GPCRs activates SOCE in hippocampal astrocytes. (A) Cultured hippocampal astrocytes were treated with ATP (100 μM) in a Ca^{2+}-free Ringer's solution to deplete internal Ca^{2+} stores. Readdition of 2 mM extracellular Ca^{2+} elicited SOCE that was significantly decreased in Orai1 KO (*Orai1*$^{fl/fl\ nestin\text{-}Cre}$ and *Orai1*$^{fl/fl\ GFAP\text{-}Cre}$) cells, as measured by the rate of Ca^{2+} influx. Summary data are means ± SEM of n=22-26 cells for each group from 3-4 independent experiments. **(B)** In the standard extracellular 2 mM Ca^{2+} Ringer's solution, ATP (100 μM) evoked a biphasic $[Ca^{2+}]_i$ elevation, with the sustained phase abolished in Orai1 KO (*Orai1*$^{fl/fl\ GFAP\text{-}Cre}$) and STIM1 KO (*STIM1*$^{fl/fl\ nestin\text{-}Cre}$) astrocytes. Right graph shows the summary of the average $[Ca^{2+}]_i$ measured 120 s after ATP application. Data are means ± SEM, n=26-76 cells for each group from 3-10 experiments. **(C)** Stimulation of P2Y receptors with UTP (50 μM) activated store release in Ca^{2+}-free solution and subsequent sustained SOCE in 2 mM Ca^{2+} solution. SOCE was significantly attenuated in Orai1 KO (*Orai1*$^{fl/fl\ GFAP\text{-}Cre}$) and STIM1 KO (*STIM1*$^{fl/fl\ nestin\text{-}Cre}$) astrocytes. Summary data are means ± SEM of n=25-57 cells for each group from 3-6 independent experiments. **(D)** In 2 mM Ca^{2+} Ringer's solution, UTP (50 μM) evoked a biphasic $[Ca^{2+}]_i$ elevation, with the sustained phase abolished in Orai1 KO (*Orai1*$^{fl/fl\ GFAP\text{-}Cre}$) and STIM1 KO (*STIM1*$^{fl/fl\ nestin\text{-}Cre}$) astrocytes. Right graph shows the summary of the average $[Ca^{2+}]_i$ measured 120 s after UTP application. Data are means ± SEM, n=27-109 cells for each group from 3-12 experiments. ***P < 0.001 by ANOVA followed by Tukey test for comparison of multiple groups (B, C, D) or by unpaired t-test for comparison of two groups (A).

These experiments indicated that application of ATP or UTP in a Ca^{2+}-free solution produced a transient Ca^{2+} rise followed by a sustained Ca^{2+} elevation when extracellular Ca^{2+} was reapplied. The rate and extent of Ca^{2+} influx after readdition of extracellular Ca^{2+} was attenuated in astrocytes from Orai1 KO and STIM1 KO mice (**Fig. 3.1, A and C**). In a complementary test, application of ATP or UTP in the presence of extracellular Ca^{2+} resulted in a biphasic Ca^{2+} signal, the sustained phase of which was lost in Orai1 KO and STIM1 KO astrocytes (**Fig. 3.1, B and D**). Similarly, application of thrombin elicited Ca^{2+} signals consistent with SOCE, which were diminished in Orai1 KO and STIM1 KO astrocytes (**Fig. 3.2, A to C**). These results indicate that CRAC channels contribute to the Ca^{2+} signals mediated by purinergic receptors and PARs. In contrast to astrocytes, neurons failed to show elevations in $[Ca^{2+}]_i$ after administration of thrombin (**Fig. 3.2D**), consistent with previous studies showing that PAR-linked Ca^{2+} signaling is active primarily in hippocampal CA1 astrocytes but not neurons (174, 175). Together, these findings suggest that Orai1 channels are essential for mediating the intracellular Ca^{2+} rises downstream of metabotropic stimuli in astrocytes.

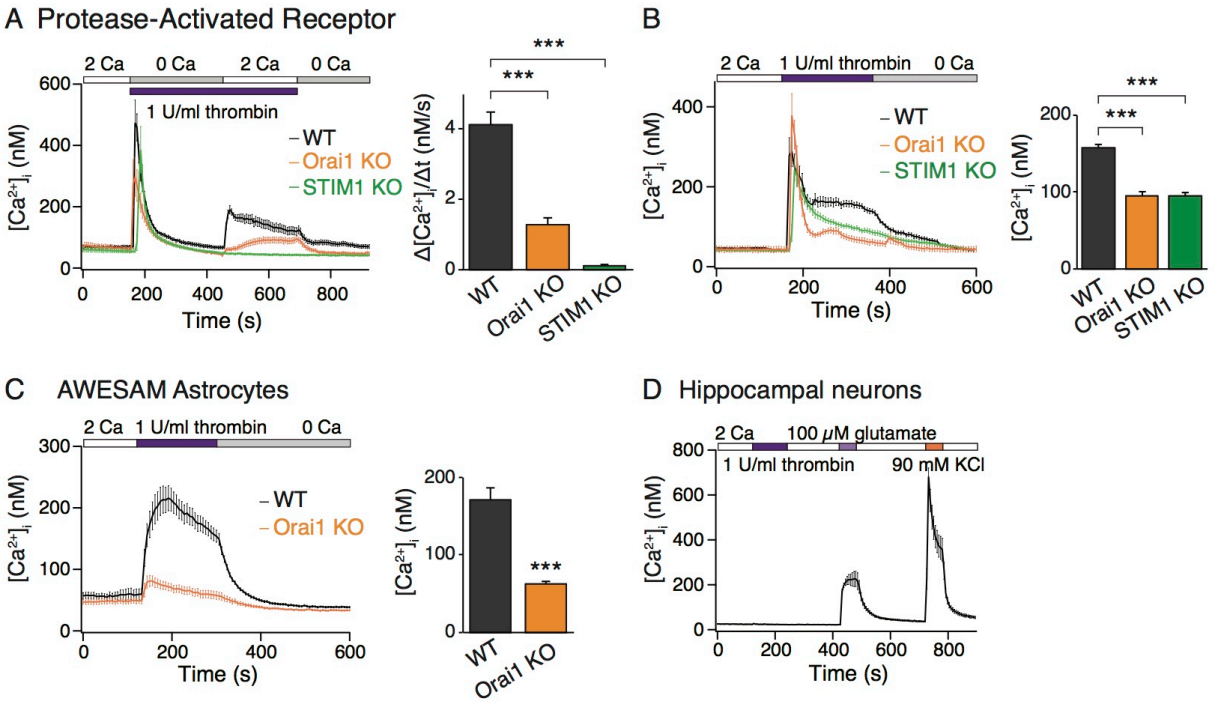

Figure 3.2. Stimulation of PAR GPCRs activates SOCE in hippocampal astrocytes. (A) Stimulation of PARs with thrombin (1 U/ml) activated store release in Ca^{2+}-free solution followed by SOCE in 2 mM Ca^{2+} solution. SOCE was significantly attenuated in Orai1 KO (*Orai1*$^{fl/fl\ GFAP\text{-}Cre}$) and STIM1 KO (*STIM1*$^{fl/fl\ nestin\text{-}Cre}$) astrocytes. Summary data are means ± SEM of n=24-53 cells for each group from 3-6 independent experiments. **(B)** In 2 mM Ca^{2+} Ringer's solution, thrombin (1 U/ml) evoked a biphasic $[Ca^{2+}]_i$ elevation, with the sustained phase abolished in Orai1 KO (*Orai1*$^{fl/fl\ GFAP\text{-}Cre}$) and STIM1 KO (*STIM1*$^{fl/fl\ nestin\text{-}Cre}$) astrocytes. Right graph shows the summary of the average $[Ca^{2+}]_i$ measured 120 s after thrombin application. Data are means ± SEM, n=25-141 cells for each group from 3-16 experiments. **(C)** In WT astrocytes from AWESAM cultures, thrombin (1 U/ml) evoked a $[Ca^{2+}]_i$ elevation which was abrogated in Orai1 KO (*Orai1*$^{fl/fl\ GFAP\text{-}Cre}$) astrocytes. Right graph shows the summary of the average $[Ca^{2+}]_i$ measured 120 s after thrombin application. Data are means ± SEM, n=38-43 cells for each group from 4-5 experiments. **(D)** Administration of thrombin (1 U/ml) failed to evoke $[Ca^{2+}]_i$ elevations in cultured hippocampal neurons. By contrast, neurons showed a robust increase in $[Ca^{2+}]_i$ following application of glutamate (100 μM) and 90 mM K^+ solution. n=7 cells, representative of 3 experiments. ***P<0.001 by ANOVA followed by Tukey test for comparison of multiple groups (A, B) or by unpaired t-test for comparison of two groups (C).

Discussion

Loss of Orai1 abrogated sustained and oscillatory Ca^{2+} signals evoked by the GPCR agonists ATP, UTP, and thrombin without detectably affecting Ca^{2+} release from intracellular stores. These results indicate that CRAC channels function as a major route of Ca^{2+} entry in hippocampal astrocytes after stimulation of various GPCRs. Because astrocytes express a large

repertoire of GPCRs for neurotransmitters and hormones (107) whose activation is linked to many downstream effects including gliotransmitter release, cytokine production, and proliferation (60, 101, 145, 176), the finding that Orai1 channels play an essential role in triggering astrocytic Ca^{2+} elevations in response to GPCR activation suggests that CRAC channels could serve as a key Ca^{2+} entry pathway for driving these and other downstream effector functions.

CHAPTER 4

THE ROLE OF ORAI1 CHANNELS IN GLIOTRANSMITTER RELEASE

Adapted from: Toth et al., Sci Signal, 2019 (158)

Introduction

Growing evidence indicates that astrocytes play a direct role in modulating neuronal activity and synaptic functions through the Ca^{2+}-dependent release of neuroactive gliotransmitters (104, 105, 179). These small molecules such as glutamate, ATP, adenosine, and D-serine (111, 132, 180) can directly modulate brain functions such as plasticity (143, 181), synchronization of neuronal spiking (182), and even modulation of behavior (183). The finding that Orai1 channels are critical for receptor-mediated mobilization of Ca^{2+} influx into astrocytes led us to next ask whether Orai1-mediated Ca^{2+} entry can evoke Ca^{2+}-dependent release of gliotransmitters. We addressed this question using several different methods: monitoring vesicular exocytosis with the genetically encoded fluorescent reporter, synaptopHluorin (spH), and the styryl dye FM1-43, and directly measuring specific gliotransmitters released into the external media.

Results

Activation of Orai1 channels stimulates vesicular exocytosis measured by spH

spH is a fusion protein made up of the transmembrane synaptic vesicle protein VAMP2 (synaptobrevin 2) and a pH-sensitive green fluorescent protein called pHluorin fused to its C-terminus inside the vesicle lumen (184). The highly acidic intraluminal environment of vesicles (pH ~ 5.5) causes pHluorin fluorescence [pKa ~ 7.1 (where K_a is the acid dissociation constant)] to be quenched. However, upon vesicular fusion, the intraluminal pH equilibrates with the neutral

pH of the extracellular medium (pH ~ 7.4) resulting in rapid dequenching and ~20-fold increase in spH fluorescence. Fluorescence is quenched once again following endocytosis and reacidification. We transiently transfected spH into hippocampal astrocytes and monitored spH fluorescence 24 to 48 hours later using TIRF microscopy, which enabled us to detect distinct exocytotic events on the footprint of spH-expressing astrocytes (**Fig. 4.1A**). At rest, the exocytotic

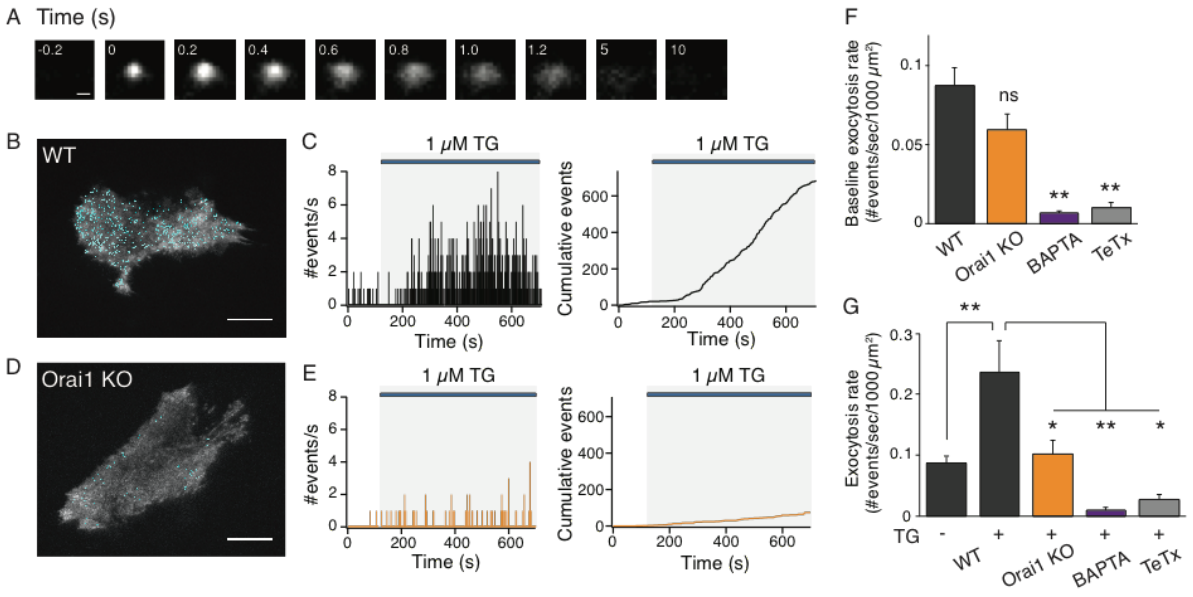

Figure 4.1. Orai1 channels stimulate vesicular exocytosis following store depletion. (A) Fluorescence changes during a single vesicle fusion event monitored with spH. Images were captured every 200 ms and the time of appearance of the fusion event was set to 0. Scale bar, 1 µm. (**B**) Location of spH events (shown in blue dots) are mapped onto the footprint of a TG-stimulated WT (*Orai1*$^{fl/+}$) astrocyte. Scale bar, 20 µm. **(C)** Histogram of the number of spH fusion events measured each second. The right plot shows the integral of these events over the time course of the experiment. Stimulation with TG evoked an increase in the rate of exocytosis. (**D**) Location of the spH events (blue dots) mapped onto the footprint of a TG-stimulated Orai1 KO (*Orai1*$^{fl/fl\ GFAP\text{-}Cre}$) astrocyte. Scale bar, 20 µm. **(E)** Histogram of the number of spH fusion events measured each second. The right plot shows the integral of these events over the time course of the experiment. (**F**) Summary of the average exocytosis rate during a 2-min unstimulated baseline for each of the indicated conditions. (**G**) Summary of the average exocytosis rate for each of the indicated conditions. The average exocytosis rate during TG (1 µM) treatment was calculated from the maximum slope of the cumulative events plot over a 200-sec window. TG-evoked spH exocytosis was significantly suppressed in Orai1 KO cells, by preincubation with BAPTA-AM (5 µM), or by co-expressing the light chain of tetanus toxin (TeTx) in astrocytes. WT, n=21 cells; Orai1 KO, n=17 cells; BAPTA, n=7 cells; TeTx, n=5 cells. Bar graphs show means ± SEM. *P<0.05, **P<0.01 by ANOVA followed by Tukey test. ns, not significant.

events occurred with an average frequency of 0.09 ± 0.01/s or 5 ± 1 fusions/min per 1000 μm^2 of astrocyte footprint. The fluorescence of the events decayed with heterogeneous kinetics with an average decay half-width of ~1.7 s in resting cells (**Fig. 4.2, A to C**). These kinetic features are comparable to the properties of spontaneous spH fusion events previously described, and could, as previously suggested, reflect a mix of both kiss-and-run and full fusions (159, 160).

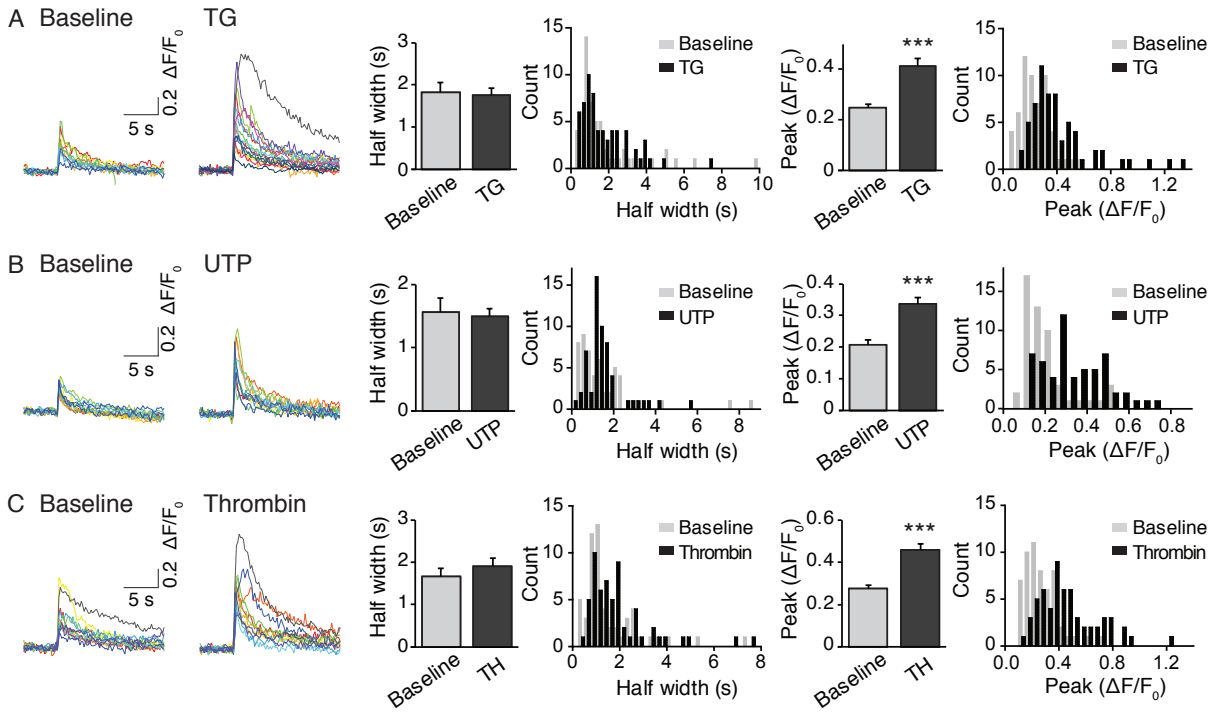

Figure 4.2. Kinetics of individual spH fusion events in WT astrocytes. (**A**) Traces of fluorescence changes for individual spH events during baseline and after stimulation with 1 μM TG. The half widths (s) and peaks ($\Delta F/F_0$) of each event were measured and plotted as averages and histograms. Data show means ± SEM, n=57-63 events for each group from 5 independent experiments. (**B**) Traces of fluorescence changes for individual spH events during baseline and after stimulation with 50 μM UTP. Summary data show means ± SEM, n=52-57 events for each group from 5 independent experiments. (**C**) Traces of fluorescence changes for individual spH events during baseline and after stimulation with 1 U/ml thrombin. Summary data show means ± SEM, n=56-59 events for each group from 5 independent experiments. ***P < 0.001 by paired t-test.

Stimulating WT cells with TG to activate CRAC channels enhanced the rate and extent of exocytosis (**Fig. 4.1, B and C**). TG also caused the appearance of large amplitude exocytotic

events with similar half-widths as seen at baseline (**Fig. 4.2A**). The average rate of exocytosis increased about threefold to 14 ± 3 fusions/min per 1000 μm^2 of astrocyte footprint, reaching its peak value 267 ± 30 s after TG administration. In contrast to astrocytes from WT mice, exocytosis evoked by TG was significantly impaired in astrocytes from Orai1 KO mice (**Fig. 4.1, D and E**). Basal exocytosis was not significantly altered in the Orai1 KO mice (**Fig. 4.1F**). Rather the primary defect appeared to be in the extent of the increase in secretion rate after cell stimulation, which was significantly smaller in Orai1 KO astrocytes in response to TG stimulation (**Fig. 4.1G**).

To verify that the spH events we observed were truly vesicle fusions, we examined the effects of co-expressing the light chain of tetanus toxin (TeTx), a protease toxin that cleaves VAMP2 and prevents SNARE (soluble *N*-ethylmaleimide-sensitive factor attachment protein receptor)-mediated exocytosis (185). spH exocytosis was abrogated with TeTx both at baseline (**Fig. 4.1F**) and in response to TG (**Fig. 4.1G)**, indicating that spH-monitored vesicular fusion events in astrocytes are driven by SNARE-mediated exocytosis. Furthermore, chelating intracellular Ca^{2+} with BAPTA-AM nearly completely abolished spH fusion events at baseline (**Fig. 4.1F**) and after TG stimulation (**Fig. 4.1G**), consistent with the role of $[Ca^{2+}]_i$ elevations in inducing vesicular exocytosis.

Next, we stimulated astrocytes with the GPCR agonists UTP and thrombin (**Fig. 4.3, A and B**). UTP and thrombin increased the rate of exocytosis to 14 ± 2 and 19 ± 3 fusions/min per 1000 μm^2 of astrocyte footprint, respectively. UTP and thrombin evoked exocytosis considerably faster than TG, with the maximal rates peaking at 161 ± 29 s and 133 ± 30 s after agonist application, respectively, suggesting that receptor-mediated Ca^{2+} entry was more effective at triggering exocytosis than Ca^{2+} entry triggered by passive depletion of ER stores. In addition to evoking an increase in the rate of exocytosis, UTP and thrombin caused an increase in the

amplitude of exocytotic events (**Fig. 4.2, B and C**). As seen for TG, deletion of Orai1 resulted in a significant decrease in the rate of exocytosis in response to cell stimulation by UTP and thrombin (**Fig. 4.3, C and D**). In astrocytes with stellate morphology grown using the AWESAM protocol, thrombin stimulation also evoked increased spH exocytotic events in WT astrocytes, but not in similarly grown Orai1 KO astrocytes (**Fig. 4.4, A to D**). Together, these results indicate that Orai1 channels are essential for store depletion-evoked and receptor-stimulated vesicular exocytosis in hippocampal astrocytes.

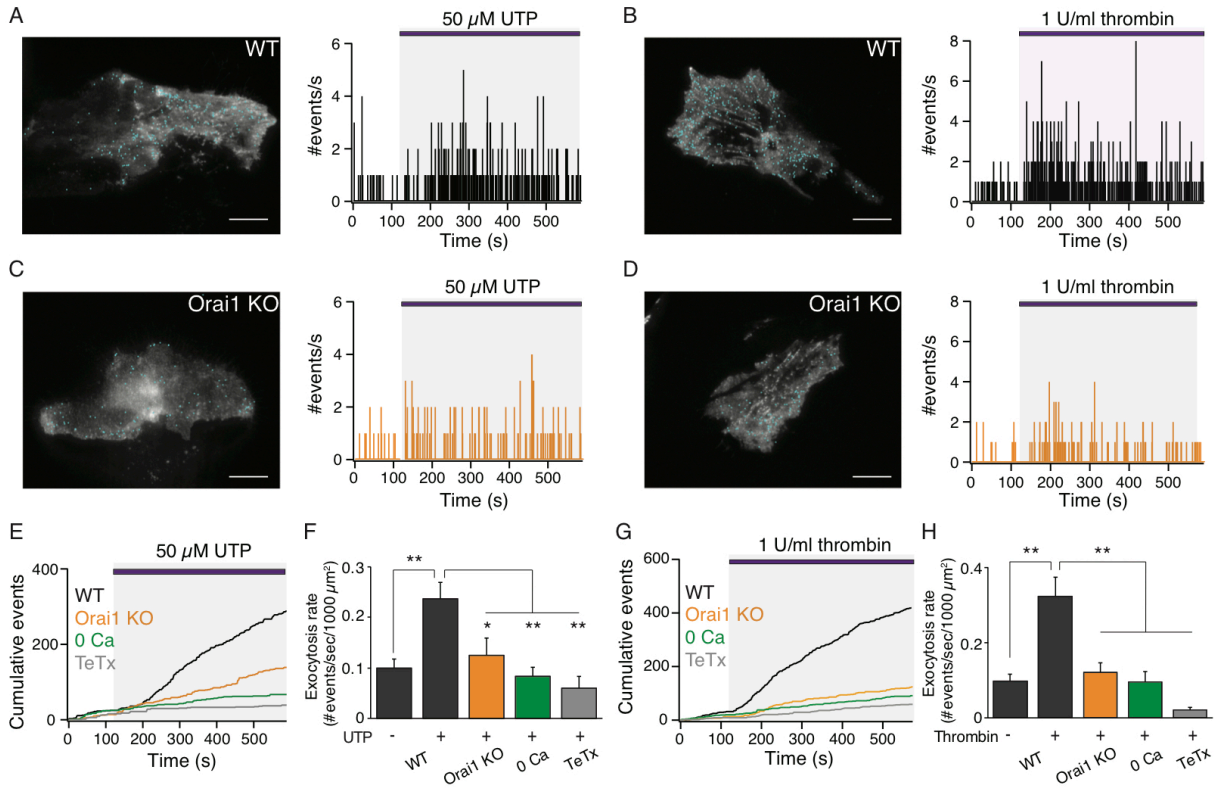

Figure 4.3. Exocytosis evoked by UTP and thrombin is abrogated in Orai1 KO astrocytes. (**A**) Location of spH events (blue dots) mapped onto the footprint of a WT (*Orai1*$^{fl/+}$) astrocyte stimulated with 50 μM UTP (left image). Histogram of the number of spH fusion events measured each sec (right plot). UTP was administered after a 2-min baseline. (**B**) Location of spH events (blue dots) mapped onto the footprint of a WT (*Orai1*$^{fl/+}$) astrocyte stimulated with 1 U/ml thrombin (left). Histogram of the number of spH fusion events measured each sec (right). Thrombin was administered after a 2-min baseline. (**C-D**) Location of spH events mapped onto the footprint of an Orai1 KO (*Orai1*$^{fl/fl\ GFAP\text{-}Cre}$) astrocyte stimulated with 50 μM UTP (C) or 1 U/ml thrombin (D). Histogram of the number of spH fusion events measured each sec (right). (**E**) Cumulative event plots for WT, Orai1 KO, Ca^{2+}-free, and TeTx-expressing astrocytes

stimulated with UTP. (**F**) The average rate of UTP-evoked exocytosis per 1000 µm^2 was significantly suppressed in Orai1 KO cells, in Ca^{2+}-free solution, or by TeTx. WT, n=19 cells; KO, n=12 cells; Ca^{2+}-free, n=10 cells; TeTx, n=7 cells. (**G**) Cumulative event plots for WT, Orai1 KO, Ca^{2+}-free, and TeTx-expressing astrocytes stimulated with thrombin. (**H**) The average rate of thrombin-evoked exocytosis per 1000 µm^2 in the indicated conditions. WT, n=18 cells; KO, n=17 cells; Ca^{2+}-free, n=7 cells; TeTx, n=9 cells. Scale bars, 20 µm. Bar graphs show means ± SEM. *P<0.05, **P<0.01 by ANOVA followed by Tukey test.

Administration of UTP or thrombin in a Ca^{2+}-free Ringer's solution did not substantively induce exocytosis (**Fig. 4.3, E to H**), despite mobilization of $[Ca^{2+}]_i$ (**Fig. 3.1C and 3.2A**), indicating that store release by itself does not drive vesicular exocytosis. Together, these data show that Ca^{2+}-dependent vesicular exocytosis evoked by GPCR stimulation requires Ca^{2+} entry through Orai1 channels across the plasma membrane.

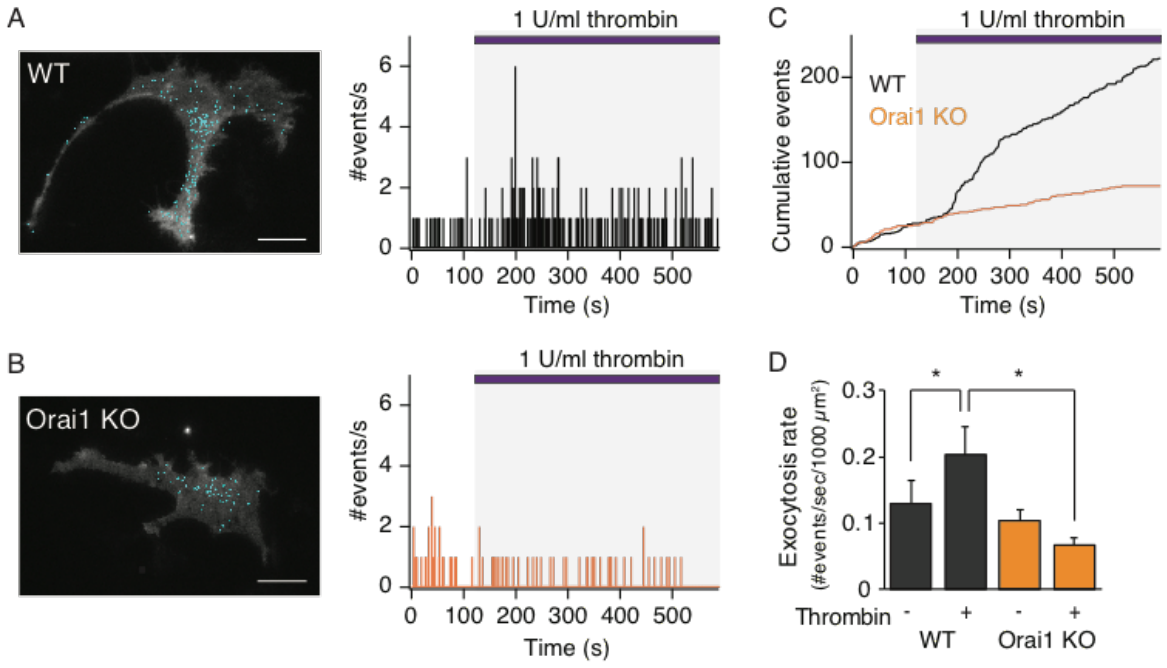

Figure 4.4. spH-monitored vesicular exocytosis in AWESAM stellate astrocyte cultures. (A) In WT astrocytes, stimulation with thrombin evoked a significant increase in the rate of spH exocytosis. **(B)** Thrombin-evoked spH-labeled vesicular exocytosis was abolished in Orai1 KO (*Orai1*$^{fl/fl\ GFAP\text{-}Cre}$) astrocytes. **(C)** Cumulative event plots for WT and Orai1 KO astrocytes. (**D**) Summary of the average rate of exocytosis per 1000 µm^2 in the indicated conditions. WT, n=14 cells; Orai1 KO, n=8 cells. Bar graph shows means ± SEM. *P<0.05 by paired t-test (comparison between baseline and thrombin) or unpaired t-test (comparison between WT and Orai1 KO). Scale bars, 20 µm.

Vesicular exocytosis is mediated by local Ca^{2+} signals around CRAC channels

The finding that store release alone in the absence of SOCE was less efficient at evoking gliotransmitter release led us to next consider whether vesicle fusion events were coupled to local spatial microdomains around CRAC channels rather than global Ca^{2+} rises. To explore this idea, we studied the differential effects of fast and slow Ca^{2+} chelators, BAPTA and EGTA, on vesicle fusion. Chelators reduce the lateral spread of the Ca^{2+} microdomain to an extent determined by the chelator's on-rate. EGTA and BAPTA have similar affinities for Ca^{2+}, but the Ca^{2+} binding on-rate of EGTA is 150-fold slower. Therefore, EGTA suppresses global [Ca^{2+}] elevations but produces a local region of relatively unbuffered [Ca^{2+}] around the pore. In contrast, BAPTA has a faster Ca^{2+} binding on-rate, causing Ca^{2+} to rapidly drop to resting levels within tens of nanometers of the Ca^{2+} channel, suppressing both local and global Ca^{2+} elevations. The differential effects of EGTA and BAPTA on Ca^{2+} buffering have been used to map the local coupling of Ca^{2+} channels to BK channels (186), the neurotransmitter release machinery (187, 188), and gene transcription (80, 189, 190). We found that both EGTA and BAPTA strongly suppressed the TG- and thrombin-mediated global rises in $[Ca^{2+}]_i$ resulting from activation of CRAC channels as measured by Fura-2 (**Fig. 4.5A**). However, whereas BAPTA nearly completely suppressed both spontaneous and UTP-evoked vesicle fusion events, EGTA was less effective (**Fig. 4.5, B and C**). Similar results were seen in thrombin-stimulated cells (**Fig. 4.5, D and E**). These results suggest that vesicular fusion events in response to CRAC channel activation are stimulated primarily by local sub-membrane Ca^{2+} elevations rather than global Ca^{2+} rises.

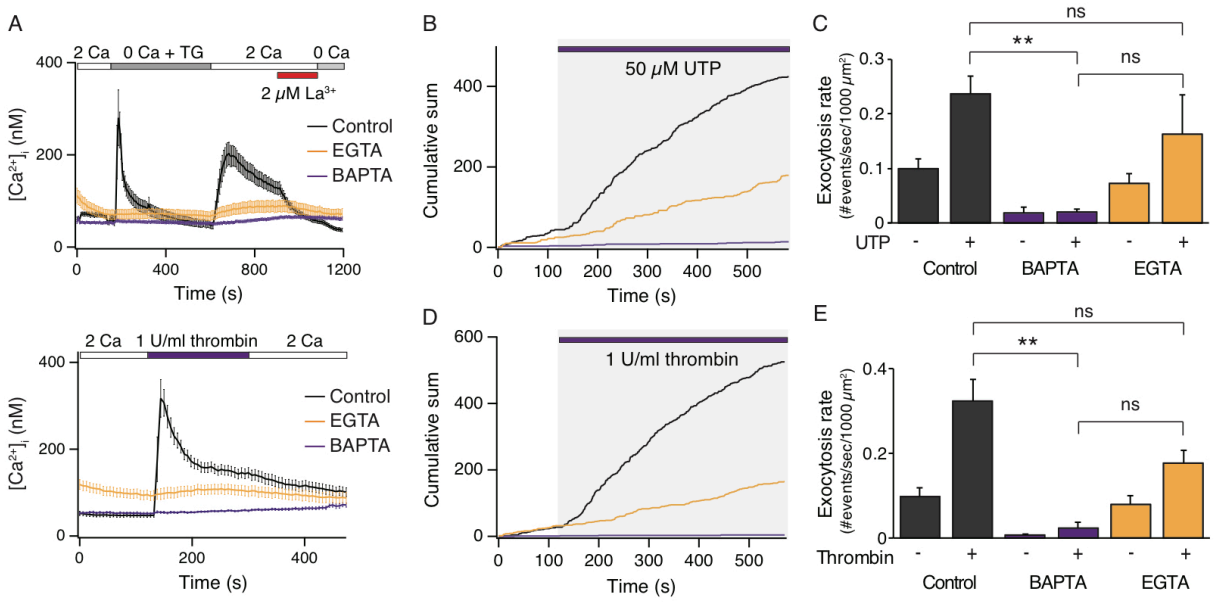

Figure 4.5. Local Ca^{2+} signals contribute to CRAC channel-mediated vesicular exocytosis. (**A**) $[Ca^{2+}]_i$ elevations produced by SOCE in EGTA- or BAPTA-treated cells in response to TG (top) and thrombin (bottom). (**B**) UTP-evoked spH fusion events were strongly suppressed by BAPTA but not EGTA. (**C**) Average rates of the baseline and UTP-evoked spH fusion events in the presence of BAPTA or EGTA. WT, n=19 cells; BAPTA, n=6 cells; EGTA, n=7 cells. (**D**) Thrombin-evoked spH fusion events were strongly suppressed by BAPTA but not EGTA. (**E**) Average rates of the baseline and thrombin-evoked spH fusion events in the presence of BAPTA or EGTA. WT, n=18 cells; BAPTA, n=6 cells; EGTA, n=8 cells. Bar graphs show means ± SEM. **P<0.01 by ANOVA followed by Tukey test.

Loss of Orai1 impairs exocytosis as monitored by FM1-43

In a second method to monitor exocytosis, we used the dye FM1-43, which reversibly binds to synaptic membranes and can be incorporated into synaptic vesicles and has been used to monitor vesicular exocytosis in many cell types, particularly neurons (191, 192). FM1-43 is reported to preferentially label lysosomal-like vesicles (134), raising the possibility that this method may provide a readout of lysosomal secretion. We found that activation of SOCE by store-depletion stimulated exocytosis of FM1-43-labeled vesicles in cultured hippocampal astrocytes (**Fig. 4.6A**). FM1-43 destaining was markedly attenuated by deleting Orai1 and suppressed after preincubation with the CRAC channel inhibitor BTP2 (**Fig. 4.6, B-D**). These results are consistent with the

previous findings using spH and further support a crucial role for Orai1 in mediating gliotransmitter exocytosis from astrocytes.

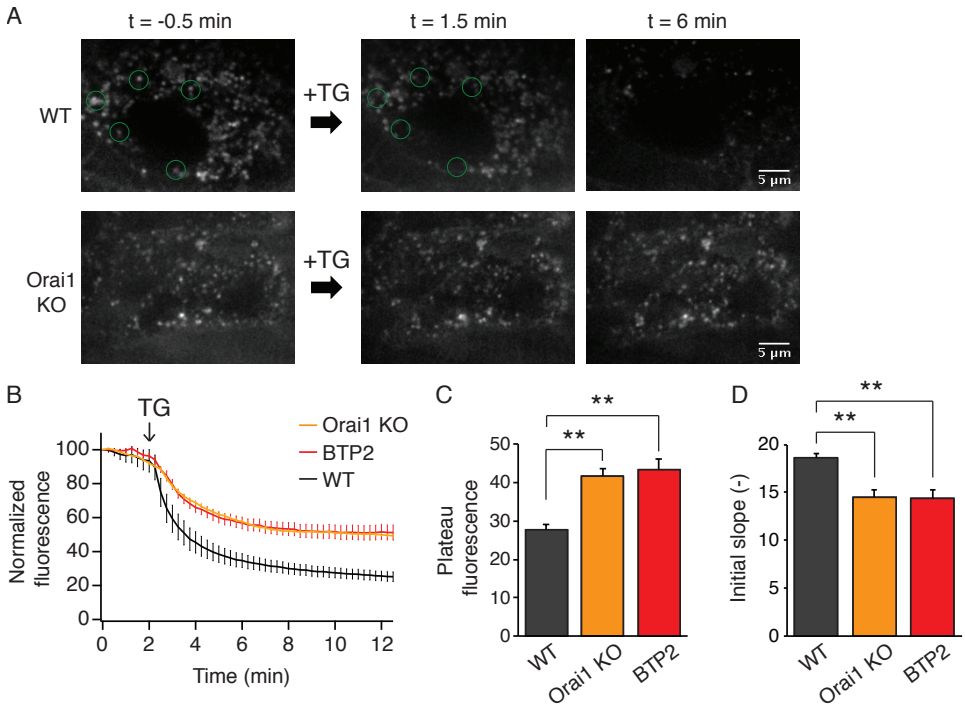

Figure 4.6. Exocytosis as monitored by FM1-43 is impaired in Orai1 KO astrocytes. (A) Fluorescence changes in FM1-43 track exocytosis in cultured astrocytes. Confocal images showing that application of TG (1 µM) at t=0 caused a loss of FM1-43-loaded vesicles (circles) and overall decrease in FM1-43 fluorescence of WT astrocytes. (**B**) After a 2-min baseline, FM1-43 destaining was evoked by TG (1 µM). Destaining was suppressed after preincubation with the CRAC channel inhibitor BTP-2 (1 µM for 2 hr) and in Orai1 KO astrocytes. Destaining for each cell was quantified as the change in fluorescence normalized to the initial fluorescence at the start of the experiment. (**C**) Summary data of the FM1-43 experiments showing the extent of de-staining as measured by the average normalized fluorescence over the last minute each of experiment. Data are means ± SEM, n=20-63 cells for each group from 3-9 independent experiments. (**D**) Summary data showing the initial rate of destaining as measured by the average slope of the fluorescence decrease over 2 minutes following TG application. Data are means ± SEM, n=20-63 cells for each group from 3-9 independent experiments. **P<0.01 by ANOVA followed by Tukey test.

Activation of CRAC channels evokes ATP release from hippocampal astrocytes

Although pHluorins and FM1-43 provide a convenient way to monitor regulated exocytosis, these tools do not reveal the identity of the gliotransmitters being released. ATP is a prominent gliotransmitter released from astrocytes that regulates the physiology of neurons and

astrocytes (193-196). To determine whether CRAC channels are involved in the release of this key gliotransmitter, we measured ATP in the supernatant of cultured astrocytes. These measurements revealed that CRAC channel activation in response to depletion of ER Ca^{2+} stores by TG (**Fig. 4.7A**) or thrombin (**Fig. 4.7B**) significantly enhanced ATP secretion. ATP secretion was impaired in Ca^{2+}-free solution (**Fig. 4.7A**), suggesting that store release by itself was insufficient to stimulate secretion. Deletion of Orai1 attenuated both TG- and thrombin-evoked ATP secretion (**Fig. 4.7, A and B**). Likewise, blockade of CRAC channel-mediated Ca^{2+} influx with BTP2 also abrogated TG-induced ATP release from astrocytes (**Fig. 4.7A**). Together, these results provide evidence that Orai1-mediated CRAC channels are essential for the secretion of ATP from astrocytes.

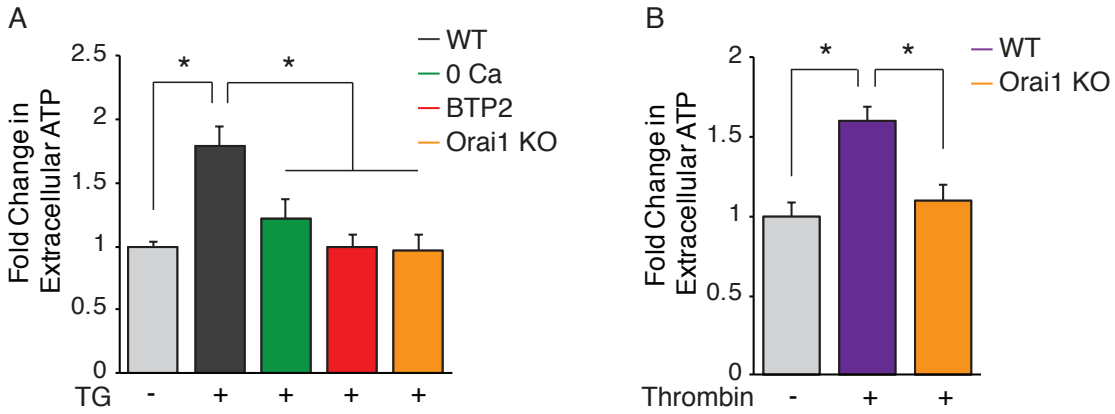

Figure 4.7. Agonist-evoked ATP secretion is abrogated in Orai1 KO astrocytes. (A) SOCE stimulates ATP secretion from cultured astrocytes. ATP levels were measured using a luciferin-luciferase luminescence assay from the supernatant of multiwell plates after 10 min stimulation. TG-mediated ATP secretion depended on external Ca^{2+} and was suppressed in Orai1 KO astrocytes and WT astrocytes after preincubation with CRAC channel inhibitor BTP2 (1 μM for 2 hrs). n=14-28 wells for each group from 3-5 independent cultures. (**B**) Thrombin stimulated ATP secretion from cultured WT astrocytes, but not Orai1 KO astrocytes. n=18-24 wells for each group from 3-4 independent cultures. Bar graphs show means ± SEM. *P<0.05 by ANOVA followed by Tukey test.

Discussion

The experiments in chapter 3 showed that Orai1 channels play an essential role in triggering astrocytic Ca^{2+} elevations in response to GPCR activation. Because the activation of GPCRs on astrocytes has been linked to gliotransmitter release, these findings suggested that Orai1 could serve as a key Ca^{2+} entry pathway for driving this effector function. Consistent with this possibility, measurements of vesicular exocytosis using spH and FM1-43 showed that loss of Orai1 impaired TG- and GPCR-evoked gliotransmitter release. Specifically, spH measurements showed that the increase in vesicular exocytosis triggered by TG, UTP, or thrombin was essentially eliminated in Orai1 KO astrocytes. Likewise, FM1-43 measurements similarly showed that loss of Orai1 markedly attenuated the extent of FM1-43 destaining. Last, direct measurements of ATP showed that the release of this key gliotransmitter was impaired in Orai1 KO astrocytes. These results indicate that CRAC channels are essential for evoked vesicular exocytosis after stimulation of purinergic receptors and PARs in astrocytes.

It is worth noting that the loss of Orai1 did not impair Ca^{2+} store release in response to stimulation of P2Y receptors and PARs (**Figs. 3.1 and 3.2**), yet evoked vesicular exocytosis and ATP secretion were markedly impaired (**Figs. 4.3 and 4.7**). The inability of IP_3R-mediated store release to evoke substantive vesicular exocytosis in the absence of Ca^{2+} influx points to an essential requirement for Ca^{2+} entry across the plasma membrane to evoke exocytosis from astrocytes. This conclusion challenges prevailing viewpoints that have attributed GPCR-mediated Ca^{2+} elevations and gliotransmitter release primarily to Ca^{2+} release from stores (110, 114, 152, 153). However, these previous studies of IP3R-mediated Ca^{2+} transients did not directly probe whether GPCR-evoked Ca^{2+} signals in fact are the exclusive result of Ca^{2+}-release from stores or also include Ca^{2+} entry across the plasma membrane through store-operated channels. On the basis of results

presented here, we favor the interpretation that store release alone is insufficient and that Ca^{2+} entry through SOCE is essential for vesicular exocytosis. The ability of the slow Ca^{2+} chelator EGTA to block global Ca^{2+} signals but not vesicular exocytosis as effectively as the fast Ca^{2+} chelator BAPTA is also consistent with this notion, reaffirming the importance of local Ca^{2+} signals close to sites of Orai1 channels for initiating exocytosis.

A notable feature of astrocytic vesicular release is its slow and sustained nature, which differs from the considerably faster and precisely-timed nature of exocytosis in neurons (197). In response to cell stimulation by TG, UTP, or thrombin, we observed that the increase in the rate of exocytosis developed slowly, especially after TG stimulation, and was typically maintained for minutes after agonist administration. These observations are consistent with previous findings showing significant delays in exocytosis of spH- or Syb2-mOrange2-labeled vesicles after cell stimulation with ATP (160) or ionomycin (134). Similar observations have been made for astrocyte secretory lysosomes labeled with EGFP-LAMP1, or FITC-dextran, or quinacrine (196, 198). We believe that the slow kinetics of astrocytic exocytosis likely reflects the slow kinetics of CRAC channel activation which requires accumulation of STIM1 and trapping of Orai1 at the ER-plasma membrane junctions (4).

An additional feature of vesicular release in astrocytes is that unlike neurons, astrocytes do not exhibit defined anatomical structures akin to synapses specialized for vesicular fusion. In particular, electron microscopy studies have demonstrated that astrocytes lack structurally organized vesicle clusters typical of the active zone present in presynaptic terminals of neurons (133, 199). Consistent with these observations, we observed spH fusion events at locations throughout the entire cell, including in the processes. The slow and distributed nature of astrocyte gliotransmitter release suggests that rather than affecting individual fast synaptic events, astrocytes

play a role in modulating the homeostatic state or global activity of neuronal circuits by targeting extrasynaptic low-affinity receptors (101, 112).

CHAPTER 5

ASTROCYTE ORAI1 CHANNEL STUDIES IN SITU

Adapted from: Toth et al., Sci Signal, 2019 (158)

5.1 Orai1 channels generate GPCR-mediated Ca^{2+} fluctuations in astrocytes processes in slice

Introduction

The results presented above indicated that CRAC channels function as a major route of receptor-mediated Ca^{2+} entry in primary cultured hippocampal astrocytes. Does this phenomenon also occur in astrocytes in their normal environment in situ? Astrocytes in vivo display complex morphology, with numerous intricate branches and fine tertiary processes that propagate intracellular Ca^{2+} fluctuations and waves (116, 155). In culture, this extensive three-dimensional morphology, particularly in the fine distal processes, is lost. Given that the majority of Ca^{2+} activity in hippocampal and cortical astrocytes occurs in the processes (200-202), and not the soma, it is important to examine these signals in a more intact system. As in primary cultured astrocytes, Ca^{2+} fluctuations in astrocytes in brain slices are also mediated largely through Ca^{2+} influx across the plasma membrane (116, 155), but the identity of the channels responsible for Ca^{2+} entry remains unclear.

Results

To visualize Ca^{2+} signals in astrocyte fine processes in their native environment and examine the role of Orai1 channels for these Ca^{2+} signals, we used the genetically encoded fast Ca^{2+} indicator GCaMP6f to image Ca^{2+} fluctuations using two-photon laser scanning microscopy

(2PLSM) in acutely prepared slices from WT and conditional Orai1 KO mice. GCaMP6f was selectively expressed in hippocampal CA1 astrocytes by injecting the dorsolateral hippocampus in adult mice (P35-P57) with an AAV5 viral expression vector carrying the GfaABC$_1$D astrocyte-specific promoter (116). We imaged Ca^{2+} activity using 2PLSM in single GCaMP6f-expressing astrocytes in transverse hippocampal slices from WT and *Orai1*$^{fl/fl\ GFAP\text{-}Cre}$ (Orai1 KO) mice (**Fig. 5.1A**). We focused our studies on astrocytes in the CA1 stratum radiatum layer because these astrocytes have been implicated in many functions including uptake and release of transmitters and modulation of hippocampal neural circuits by ATP-mediated stimulation of interneuron activity (145, 203, 204).

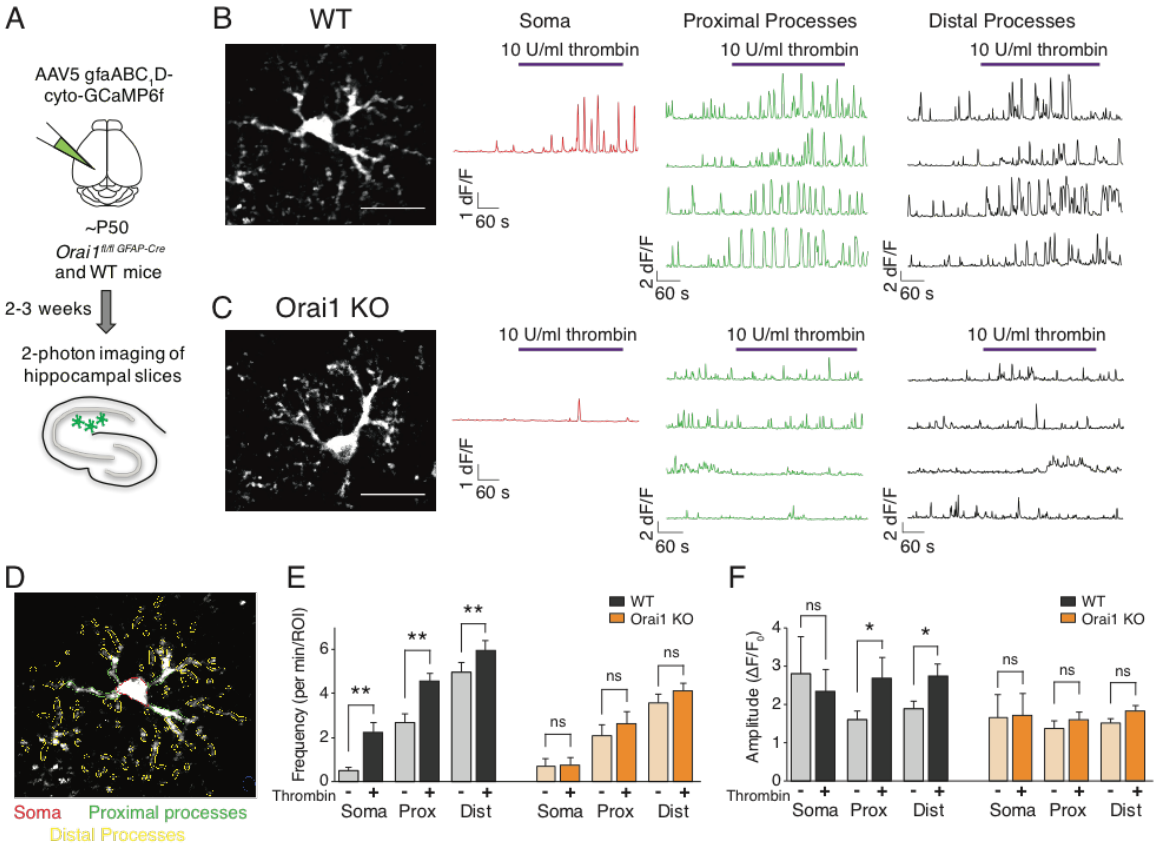

Figure 5.1. Orai1 channels generate GPCR-mediated Ca^{2+} fluctuations in astrocytes in situ. (A) Illustration of the experimental approach. GCaMP6f was expressed in astrocytes of the hippocampal CA1

using stereotaxic injections of AAV5 virus with an astrocyte-specific gfaABC$_1$D promoter. After 2-3 weeks to allow for expression, Ca^{2+} fluctuations in astrocytes expressing GCaMP6 were imaged using 2PLSM. (**B, C**) Images of GCaMP6f-expressing WT (*Orai1*$^{fl/fl}$) (B) or Orai1 KO (*Orai1*$^{fl/fl\ GFAP\text{-}Cre}$) (C) astrocytes. Each image is the maximum intensity projection of the time series (540s). Scale bar, 20 μm. Traces on the right show representative Ca^{2+} fluctuations measured in the soma, proximal processes, and distal processes. Thrombin (10 U/ml) was used to activate G_q protein-coupled PARs on astrocytes and evoke Ca^{2+} signaling. (**D**) Method for demarcating regions of interest (ROIs) for analysis of GCamP6f signals. ROIs were drawn on the maximum intensity projection of the time series (~540s) in each experiment around the soma, the primary proximal processes coming off the cell body, and the distal tertiary processes. The areas and numbers of ROIs drawn on the proximal and distal processes were similar between WT and Orai1 KO cells. (**E-F**) Summary of the Ca^{2+} oscillation frequency (**E**) and amplitude (**F**) at baseline and after administration of thrombin in WT (*Orai1*$^{fl/fl}$, black bars) and Orai1 KO (*Orai1*$^{fl/fl\ GFAP\text{-}Cre}$, orange bars) astrocytes. (WT, n=11 cells from 5 mice; Orai1 KO, n=8 cells from 4 mice). Statistical analysis was done using paired t-test. Bar graphs show means ± SEM, *P<0.05, **P<0.01. ns, not significant. Prox, proximal processes. Dist, distal processes.

Examination of GCaMP6f-expressing astrocytes using 2PLSM revealed an intricate pattern of astrocyte arborization expected of astrocytes in situ. In contrast to cultured astrocytes, astrocytes in situ showed robust on-going spontaneous activity seen as transient rises in Ca^{2+} in the soma as well as in the processes. To compare the behavior of WT and Orai1 KO astrocytes, we mapped Ca^{2+} fluctuations in three anatomically-defined compartments: the soma, the primary proximal processes coming off the cell body, and the distal tertiary processes **(Fig. 5.1, B-D**). These measurements revealed that WT astrocytes have spontaneous Ca^{2+} oscillations, which occur at a relatively low frequency of 0.5 ± 0.14/min in the soma, but at considerably higher frequencies in the proximal and distal processes (2.7 ± 0.4/min per ROI and 5.0 ± 0.4/min per ROI, respectively) (**Fig. 5.1E**). We observed Ca^{2+} signals with a traveling wave-like quality as well as more compartmentalized, local Ca^{2+} signals in the processes, similar to the observations by Srinivasan *et al.* (116). Consistent with previous observations (116, 155), spontaneous Ca^{2+} activity declined in the absence of extracellular Ca^{2+}, indicating that it critically depends on Ca^{2+} entry across the plasma membrane (**Fig. 5.2**).

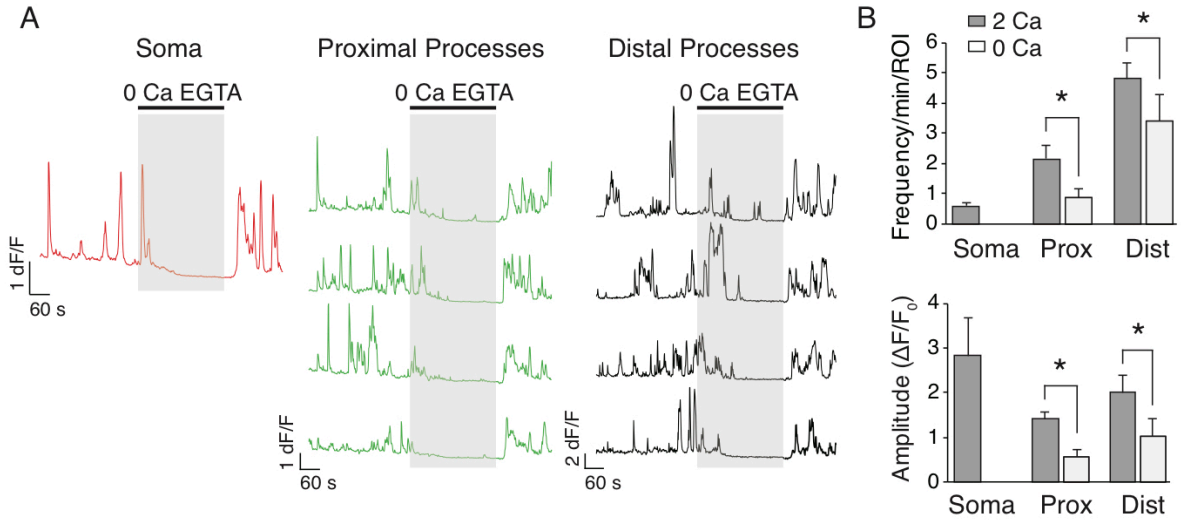

Figure 5.2. Ca^{2+} fluctuations in astrocytes in situ decline in the absence of extracellular Ca^{2+}. (A) Removal of extracellular Ca^{2+} through administration of a Ca^{2+}-free aCSF (with 1 mM EGTA) diminished spontaneous Ca^{2+} fluctuations in astrocytes in all compartments (soma, proximal processes, and distal processes). (**B**) Summary data of frequency and amplitude of Ca^{2+} fluctuations are means ± SEM, n=6 cells. *P<0.05 by paired t-test.

To examine how these Ca^{2+} signals are altered by GPCR stimulation, we used the PAR agonist thrombin, which evokes robust Orai1-dependent Ca^{2+} signals in astrocytes as described above (**Fig. 3.2)**. Application of thrombin increased Ca^{2+} activity in all three astrocyte compartments – soma, proximal processes, and distal processes, with the frequency of somatic Ca^{2+} oscillations in WT astrocytes increasing nearly fivefold (from 0.5 ± 0.14 to 2.3 ± 0.5/min per ROI) (**Fig. 5.1E**). Thrombin also significantly increased both the amplitude and frequency of Ca^{2+} fluctuations in the proximal and distal processes (**Fig. 5.1, E and F**), with the amplitude of Ca^{2+} fluctuations in the proximal processes increasing by 65% and those in the distal processes increasing by 45%. Analysis of the amplitude distributions revealed that the increase in the overall amplitude of the thrombin-evoked Ca^{2+} fluctuations occurred primarily because of emergence of large amplitude oscillations in the proximal and distal processes **(Fig. 5.3**).

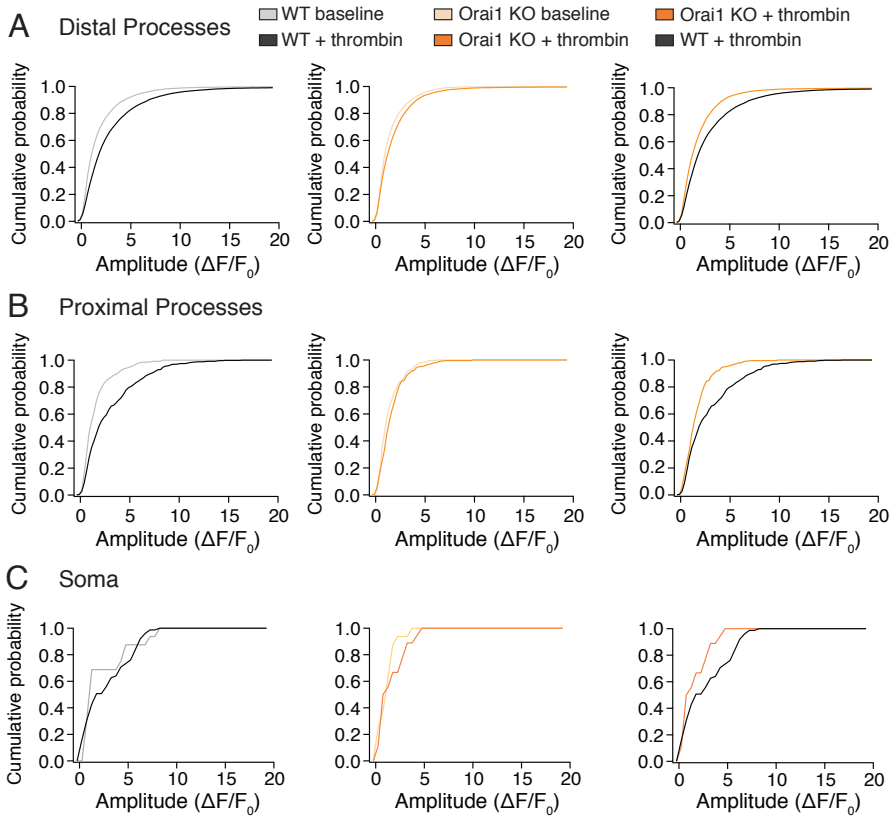

Figure 5.3. Cumulative probability plots of baseline and thrombin-evoked astrocyte Ca^{2+} fluctuations. Cumulative probability plots of the amplitudes of each Ca^{2+} oscillation in each ROI measured in the distal (**A**) and proximal (**B**) processes and the somata (**C**) of astrocytes from WT (*Orai1*$^{fl/fl}$) and Orai1 KO (*Orai1*$^{fl/fl\ GFAP\text{-}Cre}$) mice. Proximal processes: WT, n=333 events (baseline), n=564 events (thrombin); Orai1 KO, n=193 events (baseline), n=243 events (thrombin). Distal processes: WT, n=8211 events (baseline), n=10040 events (thrombin); Orai1 KO, n=6319 events (baseline), n=7464 events (thrombin). Somata: WT, n=16 events (baseline), n=75 events (thrombin); Orai1 KO, n=16 events (baseline), n=18 events (thrombin).

Examination of the behavior of Orai1 KO astrocytes revealed that, at baseline, the frequency and amplitude of Ca^{2+} oscillations in the cell body and proximal processes were similar to those seen in WT astrocytes **(Fig. 5.4A)**. The only notable difference from WT astrocytes was a modest decline (~30%) in the frequency of baseline Ca^{2+} oscillations in the distal processes (**Fig. 5.4A)**. However, the amplitude of these signals was comparable to those seen in WT astrocytes

(Fig. 5.4B). Thus, these results suggest that in unstimulated astrocytes, CRAC channels make only minor contributions to spontaneous baseline Ca^{2+} signals.

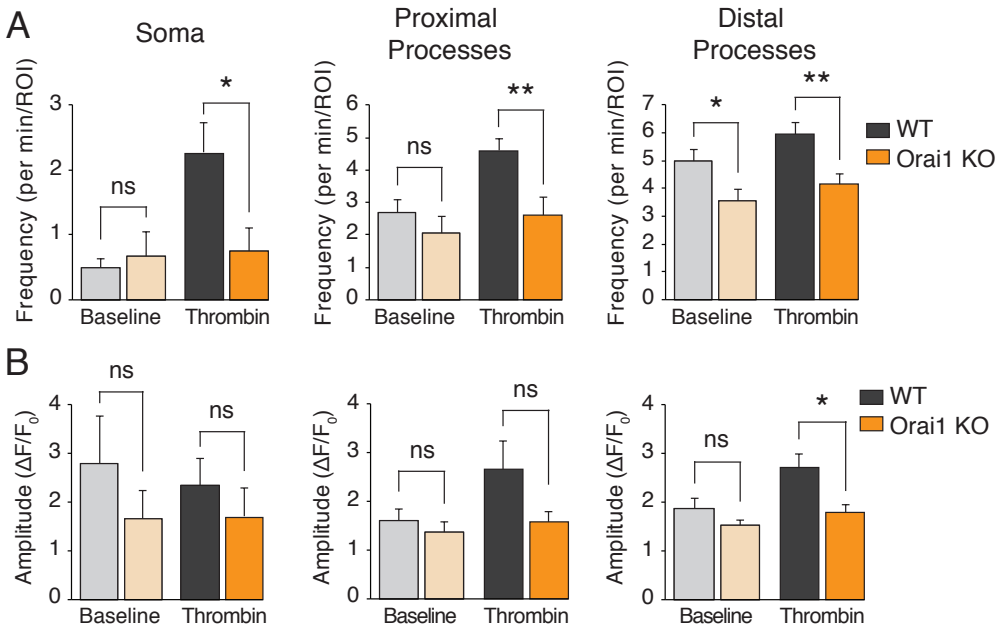

Figure 5.4. Baseline and thrombin-evoked Ca^{2+} fluctuations in WT versus Orai1 KO cells. Comparison of WT (*Orai1*$^{fl/fl}$) and Orai1 KO (*Orai1*$^{fl/fl\ GFAP\text{-}Cre}$) Ca^{2+} oscillations, at baseline and after thrombin application. Loss of Orai1 significantly reduced the frequency (**A**) and amplitude (**B**) of the Ca^{2+} fluctuations in the proximal and distal processes. Statistical analysis was done using unpaired t-test. Bar graphs show means ± SEM, *P < 0.05, **P < 0.01.

In response to thrombin, however, Orai1 KO astrocytes displayed several major differences from WT astrocytes. First, in contrast to the marked enhancement of Ca^{2+} fluctuations seen in WT astrocytes, thrombin failed to boost the frequency of Ca^{2+} fluctuations in Orai1 KO astrocytes (**Fig. 5.1E**). In all three compartments (cell body, proximal, and distal processes), the frequency of Ca^{2+} fluctuations did not change after thrombin administration. As a result, the frequency of Ca^{2+} fluctuations after thrombin stimulation was markedly lower in Orai1 KO astrocytes compared to WT astrocytes (**Fig. 5.4A**). Second, unlike WT astrocytes, Orai1 KO astrocytes also did not show an increase in the amplitude of Ca^{2+} fluctuations in response to thrombin administration (**Fig.**

5.1F). The amplitude of Ca^{2+} fluctuations after thrombin stimulation was also lower in Orai1 KO astrocytes compared to stimulated WT astrocytes in the distal processes (**Fig. 5.4B**). A direct comparison of distribution of the amplitudes of Ca^{2+} spikes further revealed that the proximal and distal processes of Orai1 KO astrocytes exhibited a significant lack of larger amplitude events seen in WT astrocytes in response to thrombin stimulation (**Fig. 5.3**). Together, these results indicate that loss of Orai1 substantially attenuates the frequency and amplitude of Ca^{2+} fluctuations both in the cell body and processes of astrocytes in situ after GPCR stimulation.

Discussion

Astrocyte morphology in intact tissue is complex, with numerous fine networks of processes extending from the soma. Unlike astrocytes in culture, measurements of astrocyte Ca^{2+} signals in brain slices using GCaMP6f revealed substantial spontaneous activity especially in the proximal and distal processes. These Ca^{2+} fluctuations were reduced in Ca^{2+}-free extracellular solutions, indicating that they were mediated in large part by transmembrane Ca^{2+} fluxes, in agreement with conclusions from past reports (116, 155, 205). However, loss of Orai1 elicited only a modest decrease in Ca^{2+} signaling at rest, indicating that Orai1 does not substantially account for the fluctuations seen in unstimulated cells. By contrast, stimulation of astrocytes in tissue slices evoked an increase in Ca^{2+} fluctuations that were dependent on the presence of Orai1 channels. Specifically, the thrombin-mediated increase in the frequency of Ca^{2+} fluctuations in the cell body and processes was essentially eliminated in the absence of Orai1 channels (**Fig. 6, D and H**). Loss of Orai1 also attenuated the amplitude of the thrombin-mediated Ca^{2+} rises in the distal processes.

The finding that Orai1 channels play an essential role in triggering astrocyte Ca^{2+} elevations in response to GPCR activation raises the possibility that CRAC channels could serve as a key Ca^{2+} entry pathway for the effector functions downstream of GPCR signaling, including gliotransmitter release. We have tested this possibility in cultured astrocytes (Chapter 4), and next examine the implications of Orai1-mediated gliotransmitter release on neural circuits in slice.

5.2 Astrocyte Orai1 channels regulate GABAergic transmission to CA1 pyramidal neurons

Introduction

The above findings indicating that Orai1 channels function as a major route of Ca^{2+} entry in astrocytes and that they stimulate gliotransmitter release led us to next examine the role of this pathway for modulating the activity of neighboring hippocampal neurons. To investigate this question, we used hippocampal CA1 slice electrophysiology to monitor the effects of astrocyte-mediated release of gliotransmitters on hippocampal neurons. Previous studies have shown that thrombin-mediated stimulation of PARs expressed in astrocytes enhances the activity of GABAergic interneurons in the stratum radiatum region, likely through astrocytic release of ATP and stimulation of P2Y receptors on interneurons (145). The ensuing increase in electrical activity of interneurons is then detected as a slow burst of inhibitory postsynaptic currents (IPSCs) on CA1 pyramidal neurons (145, 204). We examined the role of astrocyte Orai1 channels for this effect by recording IPSCs in CA1 pyramidal neurons using patch-clamp electrophysiology in hippocampal slices.

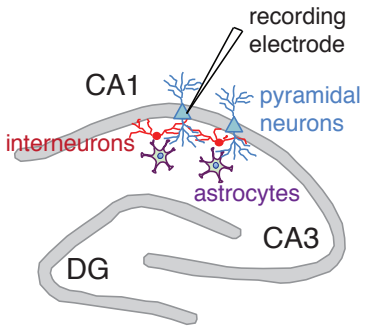

Figure 5.5. Schematic of the slice electrophysiology experiment. To monitor the effect of astrocyte stimulation on neuronal activity in the hippocampus, pyramidal neurons (blue) in the CA1 were patch-clamped. IPSCs were recorded, as a measure of the activity of interneurons (red) in the CA1. Astrocytes (purple) in the stratum radiatum region were stimulated by the application of thrombin.

Results

Consistent with previous reports (145, 204), we found that administration of thrombin to hippocampal slices evoked an increase in spontaneous IPSCs (sIPSCs) on CA1 pyramidal neurons that developed gradually over tens of seconds (**Fig. 5.6, A and B**). The frequency of sIPSCs increased twofold after thrombin administration, without an obvious change in the average amplitude of the events (**Fig. 5.6, C and D)**. This result indicates that stimulation of astrocyte Ca^{2+} signaling by thrombin increases the activity of GABAergic interneurons in the CA1 hippocampus. Moreover, the thrombin-mediated IPSC burst required action potential activity as measurements of the quantal miniature ISPC (mIPSC) responses in the presence of tetrodotoxin (TTX) showed no change in the mIPSC frequency or amplitude (**Fig. 5.6E**).

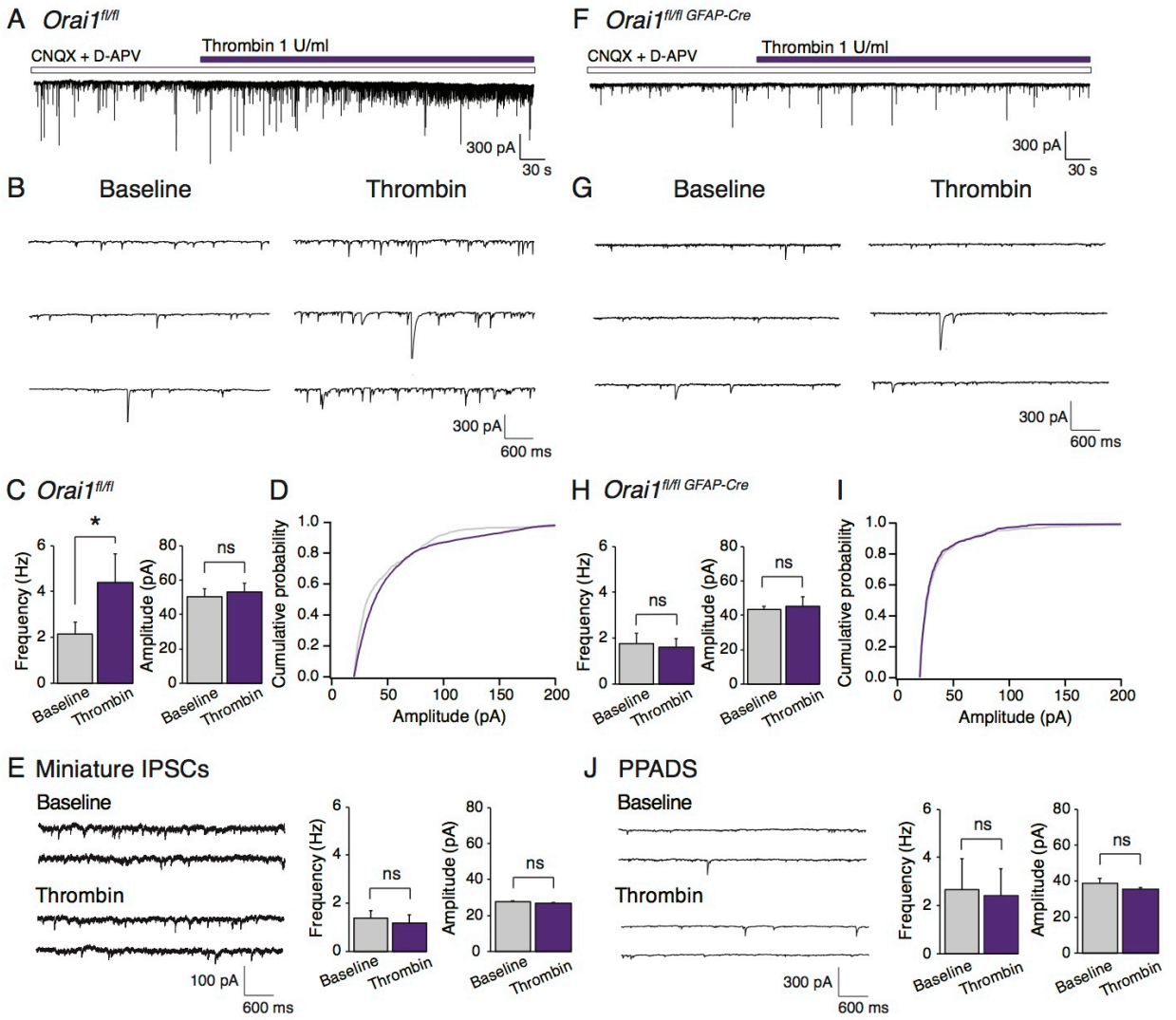

Figure 5.6. Astrocyte Orai1 channels regulate GABAergic input to CA1 pyramidal neurons. (**A**) Administration of thrombin evoked a burst of spontaneous IPSCs on *Orai1*$^{fl/fl}$ (WT) CA1 pyramidal neurons. Patch-clamp slice recordings were performed from CA1 pyramidal neurons held at -70 mV. (**B**) sIPSC traces from the experiment in (**A**) shown on an expanded timescale. (**C**) Summary of sIPSC frequency and amplitude in CA1 neurons from WT slices before and after application of thrombin. Thrombin evoked an increase in sIPSC frequency with no change in overall amplitude in WT slices (*P=0.02 by paired t-test, n=8 cells). (**D**) Amplitude distribution of the sIPSC events in the WT slice. (**E**) Thrombin did not alter the frequency or amplitude of mIPSCs in WT slices. mIPSCs were isolated in the presence of 1 µM TTX (n=8 cells). (**F**) The thrombin-induced sIPSC response in CA1 neurons was abolished in *Orai1*$^{fl/fl\ GFAP\text{-}Cre}$ (Orai1 KO) slices. (**G**) sIPSC traces from the experiment in (**F**) shown on an expanded timescale. (**H**) Summary of sIPSC frequency and amplitude in *Orai1*$^{fl/fl\ GFAP\text{-}Cre}$ slices before and after application of thrombin (n=6 cells). (**I**) Amplitude distribution of the sIPSC events in the Orai1 KO slice. (**J**) The broad-spectrum ATP inhibitor PPADS (30 µM) abolished the thrombin-mediated increase in frequency of sIPSCs in WT slices (n=4 cells). Bar graphs show means ± SEM, *P<0.05 by paired t-test. This experiment was performed by Kotaro Hori.

In conditional Orai1 KO (*Orai1*$^{fl/fl\ GFAP\text{-}Cre}$) mice, we observed that the frequency and amplitude of sIPSCs at baseline were unchanged compared to WT astrocytes (**Fig. 5.6, F to I**). This result suggests that in the absence of exogenous agonists, the inhibitory tone on CA1 pyramidal neurons was not altered by loss of astrocytic Orai1 channels. However, the thrombin-mediated enhancement of sIPSC response seen in WT mice was abolished in the *Orai1*$^{fl/fl\ GFAP\text{-}Cre}$ mice (**Fig. 5.6, F to H**). As a consequence, steady-state IPSC activity after thrombin administration was markedly lower in astrocytes from *Orai1*$^{fl/fl\ GFAP\text{-}Cre}$ mice compared to WT mice (**Fig. 5.6, C and H**). Further, administration of the broad-spectrum ATP receptor antagonist PPADS abolished the thrombin-mediated IPSC burst on CA1 pyramidal cells in WT slices (**Fig. 5.6J**), a finding consistent with previous reports indicating that astrocytic release of ATP modulates the activity of neighboring interneurons (145, 195, 204). Because PARs mediate Ca^{2+} signaling primarily in astrocytes but not in CA1 neurons (174, 175), these results suggest that thrombin-evoked activation of CA1 astrocytes results in the release of gliotransmitters to stimulate the excitability of nearby CA1 interneurons, which in turn increases GABAergic transmission to CA1 pyramidal neurons. Collectively, these results indicate that Orai1 channels in astrocytes are critical for astrocyte-mediated stimulation of stratum radiatum interneurons and astrocyte-mediated increase in tonic inhibition of CA1 pyramidal neurons.

Discussion

To examine the implications of Orai1-mediated gliotransmitter release on neural network activity, we used slice electrophysiology to monitor astrocyte-mediated modulation of interneuron activity. As shown in previous reports (145, 203), stimulation of astrocytes by the PAR agonist

thrombin increased IPSC activity on CA1 pyramidal neurons on slow timescales of tens of seconds lasting several minutes (**Fig. 7**). The thrombin-mediated increase in tonic inhibition on CA1 pyramidal neurons was lost in slices from *Orai1*$^{fl/fl\ GFAP\text{-}Cre}$ mice, indicating that astrocyte Orai1 channels have a vital role in driving the interneuron-mediated inhibition of CA1 neurons. Moreover, the ATP receptor antagonist PPADS abolished the thrombin-mediated IPSC burst in slices from WT mice, consistent with a model in which astrocyte stimulation enhances interneuron activity through Orai1-dependent release of ATP. These findings agree with previous findings showing that activation of astrocytes increases extracellular ATP levels, which can modulate neuronal (and astrocytic) function in myriad ways including increased inhibition in the neocortex (195, 203) and increased interneuron activity in the hippocampus CA1 (145, 203). Together, these results indicate that by driving astrocyte Ca^{2+} signaling and gliotransmitter release, astrocyte CRAC channels are likely to have a critical role in modulating hippocampal excitability under physiological conditions and may influence neuronal network activity in pathological conditions such as epilepsy and stroke.

A limitation to note of these experiments is the use of the *mGFAP-Cre* line to selectively delete Orai1 in astrocytes. Because neurons and astrocytes are derived from the same neural stem cells, the use of genetic methods to selectively target astrocytes is not straightforward. While the *mGFAP-Cre* is targeted primarily to postnatal astrocytes as shown previously by reporter gene expression (206), there is also some expression in postnatal GFAP-expressing neural stem cells and their progeny in the hippocampus, which could complicate the interpretation of results using this line (207). More recently, a transgenic line has been developed that specifically targets all adult brain astrocytes with no detectable neuronal contamination (207). These *Aldh1l1-Cre/ERT2* mice are also inducible, allowing for adult astrocytes to be specifically targeted, and circumventing

any issues of developmental or compensatory changes. Our hippocampal slice results could be strengthened by future experiments using this system to selectively abrogate Orai1 in adult astrocytes.

CHAPTER 6

THE ROLE OF ORAI1 IN LEARNING AND MEMORY

6.1 Hippocampal neurons exhibit store-operated calcium entry mediated by Orai1

Introduction

Our lab has previously shown that CRAC channels are a major route of Ca^{2+} entry in neural progenitor cells, where they regulate gene expression and proliferation (80). Neural progenitor cells are largely nonexcitable, in contrast to their mature neuron counterparts which upregulate expression of Ca^{2+} influx mechanisms such as voltage-gated Ca^{2+} channels. We wondered whether CRAC channels are also important for mobilizing Ca^{2+} signals in mature neurons. Several reports have shown SOCE in dorsal root ganglion neurons (81), dorsal horn neurons (61, 70), and cortical neurons (75, 208). We focused our studies on neurons in the hippocampus, where we have previously shown that Orai1 is highly expressed. In addition to expression in astrocytes, Orai1 expression is strong in the neurons of the CA1, CA3, and dentate gyrus (unpublished data). However, the specific functional roles of SOCE in hippocampal neurons remain unclear.

Results

To address a potential role for CRAC channels in generating cytosolic Ca^{2+} elevations in hippocampal neurons, we began our studies by measuring SOCE in cultured hippocampal neurons. Depleting ER Ca^{2+} stores in hippocampal neurons with TG revealed SOCE upon readdition of extracellular Ca^{2+} (**Fig. 6.1A**). SOCE in neurons exhibited the typical pharmacological hallmarks of Orai1 channels, including blockade by a low concentration of La^{3+} and inhibition by preincubation with BTP2 (**Fig. 6.1A**). SOCE was completely abrogated in hippocampal neurons

derived from brain-specific Orai1 KO mice (*Orai1*$^{fl/fl\ nestin\text{-}Cre}$) (**Fig. 6.1B**). In marked contrast to cells from Orai1 KO mice, hippocampal neurons from Orai2 KO mice showed increased SOCE, suggesting that Orai2 has a modulatory role in SOCE in neurons (**Fig. 6.1A**).

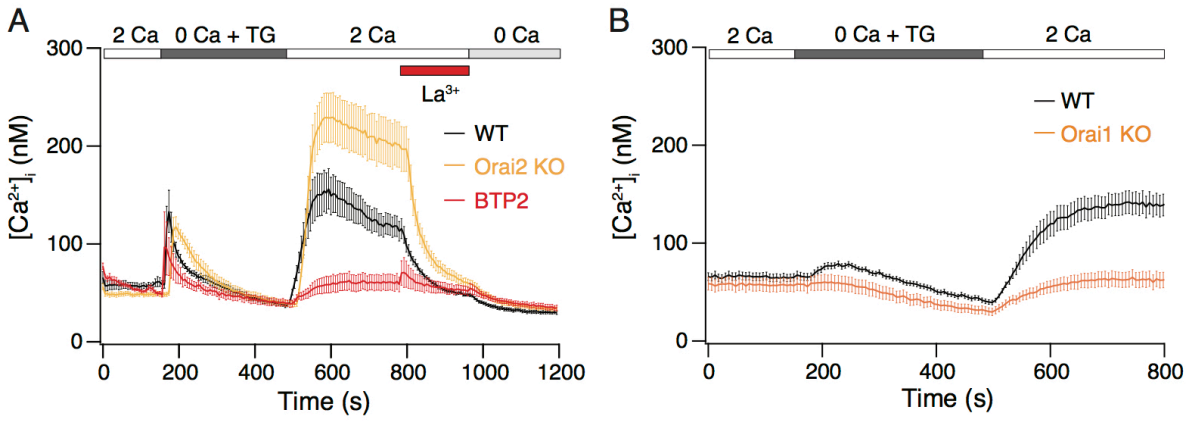

Figure 6.1. SOCE in hippocampal neurons. (**A**) Depletion of ER Ca^{2+} stores with TG evoked store release and subsequent SOCE after readdition of extracellular Ca^{2+}. SOCE was blocked by a low dose of La^{3+} (2 μM) and strongly attenuated by BTP2 (1 μM for 2 hrs). SOCE was markedly enhanced in hippocampal neurons from Orai2 KO (*Orai2*$^{-/-}$) mice. (**B**) SOCE was strongly attenuated in hippocampal neurons from Orai1 KO mice (*Orai1*$^{fl/-\ nestin\text{-}Cre}$).

Discussion

Our results show that Orai1 is essential for SOCE in hippocampal neurons. Like in astrocytes, our findings also demonstrate that loss of Orai2 increases SOCE in neurons. Orai2 is strongly expressed in the hippocampus, including in the dentate gyrus and pyramidal cell layer of the CA3 and CA1. Because of Orai2's powerful ability to modulate SOCE, it would be important to explore whether Orai2 is differentially expressed during development or in neurological disorders.

In our Ca^{2+} imaging experiments, we were able to measure cytosolic Ca^{2+} signals in the soma and some proximal processes of cultured hippocampal neurons. Considering that many

important Ca^{2+} signaling events that mediate synaptic transmission and plasticity take place in localized microdomains in small presynaptic and postsynaptic compartments at synapses (209), it will be important in future experiments to examine Ca^{2+} signals on these small scales. We are currently using GCaMP6f to monitor Ca^{2+} signals in dendrites and dendritic spines of WT and Orai1 KO mice to further investigate how Orai1 channels contribute to Ca^{2+} signaling in neurons. Future experiments in more intact preparations like hippocampal slices are also needed to determine if there are distinct features of SOCE in different cell populations of the hippocampus, such as excitatory pyramidal cells versus inhibitory interneurons.

6.2 Conditional deletion of Orai1 in the brain compromises learning and memory

Introduction

Ca^{2+} signaling regulates many essential roles in neurons including neuronal development and synaptic transmission. Ca^{2+} elevations in neurons also drive synaptic plasticity, including long-term potentiation (LTP), long-term depression (LTD), and spine morphogenesis (89). Because synaptic plasticity likely forms the neurochemical basis of learning and memory storage in the brain, the mechanisms driving plasticity and synaptic alterations are of considerable interest in neuroscience. A well-described form of synaptic plasticity occurs at the hippocampal CA3-CA1 synapse, where Ca^{2+} elevations in dendritic spines drive CaMKII activity to increase AMPA receptor activity and induce LTP (89). Ca^{2+} entry through NMDA receptors is essential for plasticity at this synapse, but alone may not be sufficient to induce LTP in all spines and conditions (210). Therefore, there are likely roles for additional Ca^{2+} pathways like SOCE in dendritic spines.

CRAC channels are expressed in several regions of the brain known to be critical for cognitive function, learning, and memory, including the hippocampus (69). This raises the

possibility that these channels play a role in cognition and behavior. Several studies have reported that STIM proteins can regulate behavior. Forebrain-specific STIM1 and STIM2 double KO mice have been shown to exhibit a pronounced impairment in spatial learning (211). Another study reported that STIM2 KO mice have a spatial learning defect (75). In contrast, overexpressing STIM1 in neurons or activating an optogenetic "OptoSTIM1" in the CA1 hippocampal region of mice can reinforce contextual memory formation (212, 213).

We showed above that loss of Orai1 strongly attenuates SOCE in hippocampal neurons. Considering the evidence in the field pointing to a role for CRAC channels in learning and memory, we next sought to explore the functional consequences of the loss of Orai1 in the brain using a battery of behavioral tests. Three well-described behavioral tests among those used to assess learning and memory in rodents are the Y-Maze, water maze, and fear conditioning. The Y-maze is a spatial working memory task which exploits the innate curiosity of rodents to explore novel environments (214, 215). Mice are placed on a Y-shaped maze and analyzed for spontaneous alternation, a hippocampal-dependent tendency to enter a less recently explored arm of the maze by using extra-maze visual cues. The task requires good working memory to maintain and update a mental log of recent arm entries, and young, healthy WT mice typically show a high percentage of alternations (75-80%).

The Morris Water Maze is a test for spatial memory, and it takes advantage of the natural swimming ability of rodents (216, 217). In a typical paradigm, mice learn to use distal spatial cues to locate a hidden escape platform in a pool of water over a period of 5 days. On the final day, the platform is removed and a probe trial is performed to assess memory. A mouse that has learned well will spend more time searching for the platform in the target quadrant of the pool.

Fear conditioning is an associative learning task in which mice learn to associate a neutral context (i.e. a box) or neutral stimulus (i.e. a tone) with an aversive stimulus (i.e. an electrical shock). This results in the expression of a fear response to the originally neutral context or stimulus (218). In a typical paradigm, mice in a conditioning chamber (context 1) are exposed to a tone (conditioned stimulus), followed by a brief pause (trace), and then an aversive foot shock (unconditioned stimulus). Twenty-four hours later (day 2), the mice are placed in a novel context (context 2) and tested for a fear response – freezing – in response to the conditioning tone and trace. Twenty-four more hours later (day 3), the mice are returned to the original chamber (context 1) and tested for their contextual freezing response. Fear conditioning is thought to involve both the amygdala and the hippocampus, with the hippocampus especially involved in contextual learning and trace fear conditioning when the conditioned stimulus and unconditioned stimulus are separated in time (219).

Results

Deletion of Orai1 in the brain compromises learning and memory

To begin to investigate the role for Orai1 in cognition, we performed learning and memory behavioral tests using WT and brain-specific Orai1 KO (*Orai1*$^{fl/fl\ nestin\text{-}Cre}$) mice. We noticed no gross abnormalities in life-span, weight, movement, feeding, or fertility in these mice, in contrast to whole-animal Orai1 null KOs which demonstrate perinatal lethality (220). However, the performance of Orai1 KO mice in learning tasks was significantly lower than the performance of their WT littermates (**Fig. 6.2 and 6.3**). In the Y-maze, Orai1 KO mice demonstrated fewer alternations than WT mice, suggesting a deficit in working memory. We observed similar results in both male and female mice (**Fig. 6.2, A and B**).

In the water maze, there were no differences between WT and Orai1 KO mice during a visible platform training phase, suggesting that there are no sensorimotor deficits preventing the mice from locating the maze visually and swimming to it (**Fig. 6.2, C and D**). In the hidden platform training phase, male mice were significantly impaired in their time to locate the platform in days 2 through 5 (**Fig. 6.2E**). In addition, male mice spent significantly less time in the target quadrant during the subsequent probe trial (**Fig. 6.2G**). In contrast, female Orai1 KO mice were not significantly impaired compared to WT mice in either the hidden platform or the probe trial, suggesting that there may be some sex differences in the impact of Orai1 loss on behavior (**Fig. 6.2, F and H**). Swimming speed was not different between WT and Orai1 KO in either male or female mice, again suggesting that there were no generalized motor deficits in the Orai1 KO mice (**Fig. 6.2, I and J**).

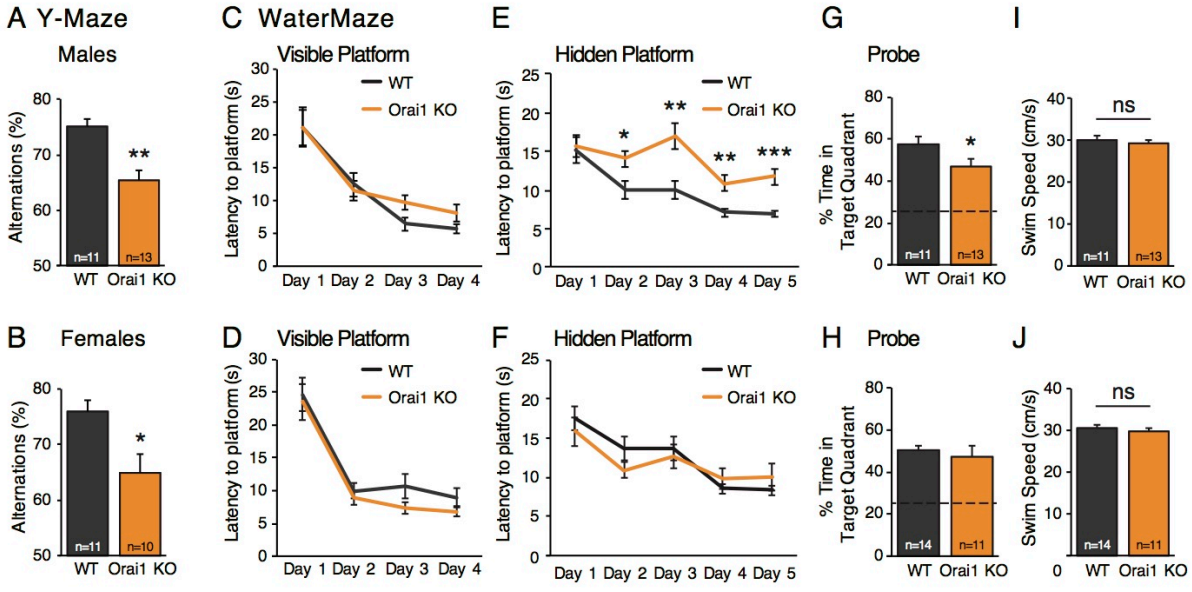

Figure 6.2. Orai1 KO mice show deficits in learning and memory. (**A-B**) Summary of alternations in Y-maze in WT and Orai1 KO (*Orai1*$^{fl/fl\ nestin\text{-}Cre}$) male (**A**) and female (**B**) mice. (**C-D**) Learning curves showing latency to a visible platform over 4 training days in the water maze for male (**C**) and female (**D**) mice. (**E-F**) Learning curves showing latency to a hidden platform over 5 days in the water maze for male (**E**) and female (**F**) mice. (**G-H**) Summary of the percent time spent in the target quadrant during the probe trial following the 5th day of the water maze hidden platform training for male (**G**) and female (**H**) mice. Dashed line indicates random chance (25%). (**I-J**) Average

swimming speed of the male (**I**) and female (**J**) mice during the probe trial. Data are means ± SEM, *P<0.05, **P<0.01, ***P<0.001 by unpaired t-test. n numbers of mice are indicated on the bars.

To test associative memory, we used the fear conditioning paradigm, as described in the introduction. Orai1 KO mice had a significant deficit in tone-dependent fear conditioning as well as contextual fear conditioning when compared to their WT littermates (**Fig. 6.3**). Lack of Orai1 did not affect locomotor activity in response to either the naïve context on day 1 or the electric shock (**Fig. 6.3, D and G**). Similar trends were seen in male and female mice.

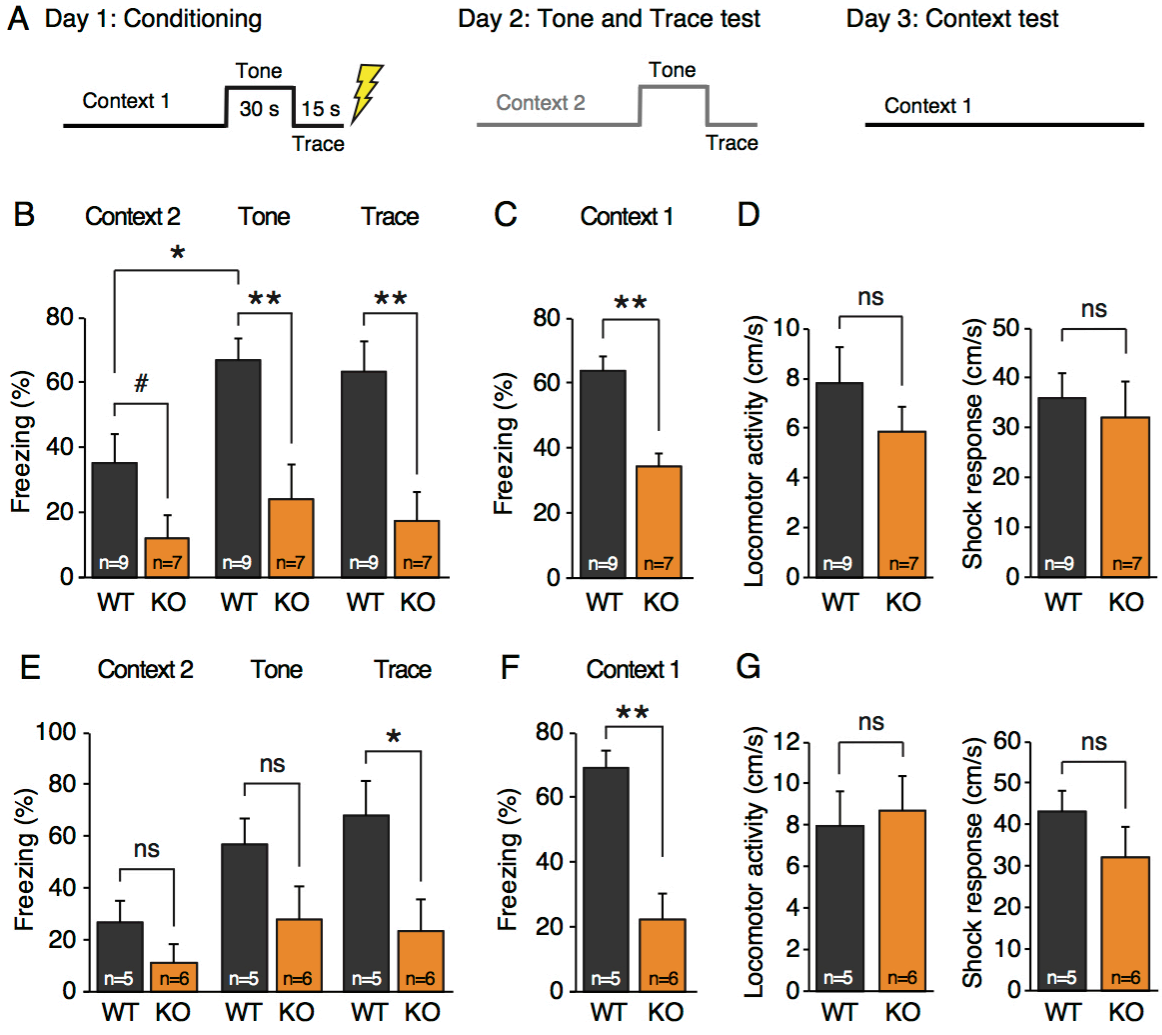

Figure 6.3. Orai1 KO mice show a defect in fear conditioning. (**A**) Schematic of the fear conditioning protocol. On day 1, mice were placed in context 1, where they received a conditioned stimulus (tone), followed by a 15 s interval

(trace), followed by the unconditioned stimulus (foot shock, depicted by the lightning bolt). On day 2, mice were placed in a novel context 2, where the percentage of freezing was measured in response to the conditioned tone and trace. On day 3, the percentage of freezing was measured in response to the original context 1. (**B**) Freezing responses to context 2, tone, and trace on day 2 in WT and Orai1 KO (*Orai1*$^{fl/fl\ nestin\text{-}Cre}$) male mice. #p=0.07, ns. (**C**) Freezing responses to context 1 on day 3 in male mice. (**D**) Similar locomotor activity (left) and shock response (right) of WT and Orai1 KO mice (on day 1). (**E**) Freezing responses to context 2, tone, and trace on day 2 in WT and Orai1 KO female mice. (**F**) Freezing responses to context 1 on day 3 in female mice. (**G**) Similar locomotor activity (left) and shock response (right) of WT and Orai1 KO mice (on day 1). Data are means ± SEM, *P<0.05,**P<0.01 by unpaired t-test. n numbers of mice are indicated on the bars.

Sensorimotor function is not grossly affected in brain-specific Orai1 KO mice

To assess general locomotive behavior and motor function, we used the open field test and the rotarod test. The open field test quantifies ambulation levels and exploratory behavior (221). It has also been used as a general test for anxiety, as more anxious mice will spend less time in the exposed center of the field. The rotarod test assesses cerebellar-dependent balance, coordination, and motor control by quantifying the amount of time a mouse can remain on a rotating rod before falling (222).

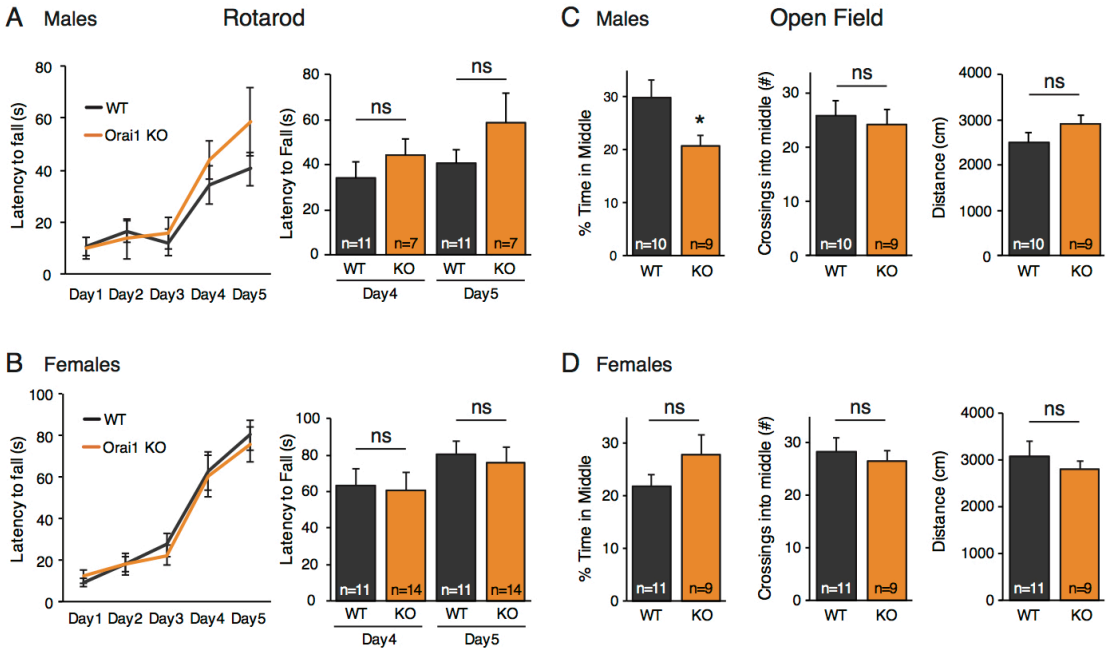

Figure 6.4. Orai1 KO mice are not impaired in motor tests. (**A-B**) The rotarod test reveals no differences in latency to fall or motor learning over a 5 day period between WT and Orai1 KO (*Orai1*$^{fl/fl\ nestin\text{-}Cre}$) mice. Results for male mice

are shown in (**A**) and female mice are shown in (**B**). (**C-D**) Summary of the open field test, showing percentage of time spent in the middle area of the field, the number of crossings into the middle, and the total distance traveled. Results for male mice are shown in (**C**) and female mice are shown are (**D**). Data are means ± SEM, *P<0.05 by unpaired t-test. n numbers of mice are indicated on the bars.

Orai1 KO mice performed similarly to WT in the rotarod and the open field tests, indicating that general locomotion and motor function are not compromised and these mice do not have generalized phenotypic abnormalities (**Fig. 6.4**). There was a moderate decrease in the percent time that male Orai1 KO mice spent in the middle of the open field test, suggesting increased anxiety in these animals, although the same phenotype was not seen in the female mice (**Fig. 6.4, C and D**).

Discussion

Using a battery of behavioral tests examining working, spatial, and associative memory in mice, we found that conditional deletion of Orai1 in the brain compromises learning and memory. Orai1 KO mice demonstrated deficits in the Y-maze, water maze, and fear conditioning. The decreased performance in these learning tests was likely not due to deficits in motor strength or coordination, as the Orai1 KO mice were not impaired in the rotarod and open-field tests. Because Y-maze, water maze, and fear conditioning all rely on proper hippocampal function, these results suggest that the loss of Orai1 weakens a fundamental aspect of plasticity in the hippocampus. We are currently following up these results by investigating the mechanistic basis of this phenotype. First, we are exploring the role of Orai1 in glutamate-evoked Ca^{2+} signals in dendritic spines, the locus for postsynaptic plasticity. We have found that glutamate uncaging-evoked Ca^{2+} signals in dendritic spines are impaired in Orai1 KO neurons, suggesting that Orai1 contributes to Ca^{2+} dynamics in dendritic spines.

Since LTP is believed to be a major contributor to the mechanistic basis of learning and memory, we are also investigating whether LTP at the Schaffer collateral-CA1 synapse is affected in Orai1 KO mice. And indeed, our preliminary results show that Orai1 KO mice have impaired LTP. Further, preincubation of hippocampal slices with the CRAC channel inhibitor BTP2 inhibits the induction of LTP, suggesting that the LTP deficit in Orai1 KO mice is not due to developmental alterations in hippocampal circuits. In addition, we are finding that CaMKII activation and AMPA receptor insertion are impaired in Orai1 KO neurons. These continuing studies in our lab establish a role for Orai1 in synaptic plasticity and suggest a cellular mechanism for the learning and memory deficits seen in Orai1 KO mice.

It is worth pointing out that in the learning and memory behavioral tests, there were some differences between male and female mice. In all three tests, the male mice were more significantly affected by the loss of Orai1, although in the Y-maze and fear conditioning, there were also learning deficits in the female mice. However, in the water maze, the male Orai1 KO mice showed reduced learning in the hidden platform and impaired performance during the probe trial, whereas the female Orai1 KO mice showed no difference from WT in either measure. Many studies have revealed sex differences in various learning behaviors (223, 224), although the results are often contradictory and reason is not well understood, making interpretation of these results difficult. Perhaps female Orai1 KO mice rely less on Orai1-mediated pathways for spatial learning, or have greater compensatory mechanisms for the loss of Orai1 than male mice. Interestingly, there has already been at least one report in the CRAC channel field of alterations in Orai1 expression affecting the sexes differently. A group found that context recognition behavior decreased only in female, and not male, mice overexpressing Orai1 in brain neurons (225). The intersection of sex

and behavior is complex, and underscores the importance for following up these studies in both male and female mice.

Our behavioral findings in mice may be relevant to 12q24.31 microdeletion syndrome in humans, in which there is a deletion of a small stretch of chromosome 12, that include the *Orai1* gene (226-229). This microdeletion syndrome is characterized by intellectual disability, autism, seizures, and craniofacial abnormalities. Although the mechanism for the cognitive defect in these patients is unknown, and there are several other genes deleted along with Orai1, it would be interesting to explore this potential link further.

Although whole-brain deletion of Orai1 provides important preliminary results related to the contribution of Orai1 channels for behavior, more studies will need to be done to determine the cell type mediating these altered behavioral phenotypes. Given the central role of the hippocampal excitatory neurons in producing synaptic plasticity, it is likely that the effects are mediated, as least in part, through excitatory neurons. We are currently testing this idea by crossing *Orai1*$^{fl/fl}$ mice with *CaMKII-Cre* mice to conditionally delete Orai1 expression in forebrain excitatory neurons (including the CA1 pyramidal cell layer) and investigating whether these mice phenocopy the whole-brain Orai1 KOs. However, the phenotype may be more complicated and involve dysregulation of Ca^{2+} signaling in other cell types also contributing to the abnormal behavior of Orai1 KO mice. We cannot rule out a contribution from astrocytes, which have also been implicated in plasticity and depressive behavior (143, 181, 183). Therefore, it would be interesting to explore whether astrocyte-specific Orai1 KO mice have these or other behavioral phenotypes.

The Orai isoform, Orai2, modulates store-operated Ca^{2+} signaling in neurons, as well as in astrocytes as described above. Although the expression of Orai2 is known to be particularly

prominent in the brain, especially in the hippocampus, virtually nothing is known about its role in regulating cell function in the brain. In contrast to Orai1 KO mice, which show decreased SOCE in neurons and astrocytes, Orai2 KO mice show increased SOCE in neurons and astrocytes, suggesting that Orai2 works as a negative modulator of Orai1. Therefore, it would be interesting to explore the performance of Orai2 KO mice in cognitive tasks including Y-maze, water maze, and fear conditioning. It remains to be determined from future studies whether an increase in store-operated Ca^{2+} signals disrupts Ca^{2+} homeostasis in a way that also impairs cognitive function, and whether the loss of Orai2 alters synaptic plasticity.

CHAPTER 7

CONCLUSIONS AND FUTURE DIRECTIONS

Despite evidence demonstrating that the "Ca^{2+} excitability" of astrocytes is important for many functions including the release of gliotransmitters (104, 121, 129, 193, 195, 230-232), the identity of the specific pathways that generate astrocyte Ca^{2+} signals, and how these are linked to effector functions is poorly understood. In this dissertation, we showed that CRAC channels formed by Orai1 and STIM1 are a major route of Ca^{2+} influx in hippocampal astrocytes and that their activation generates sustained Ca^{2+} signals and oscillations in response to stimulation of various GPCRs. Moreover, we showed that CRAC channel-mediated Ca^{2+} signals triggered gliotransmitter exocytosis and secretion of the gliotransmitter ATP. The release of ATP from astrocytes and the ensuing activation of purinergic receptors stimulated hippocampal interneurons to increase GABAergic transmission on CA1 pyramidal cells. These results reveal a function of CRAC channels as important regulators of astrocyte gliotransmission and identify astrocytic Orai1 channels as a new target for modulating neuronal activity.

To begin to understand the functional role of CRAC channels in the brain for cognition and behavior, we also conducted behavioral studies on mice with a conditional deletion of Orai1 in the brain. We found that these mice are cognitively impaired in tasks for working, spatial, and associative memory, with their motor behavior intact. Together, our results add valuable insight into the function of store-operated CRAC channels in the nervous system, but there are many additional interesting questions that remain.

While our studies in astrocytes have focused on gliotransmitter release, it is possible and indeed likely that CRAC channels could have other functional roles in astrocyte physiology.

Astrocytes have numerous functions and make essential contributions to many aspects of neural physiology including ion homeostasis, regulation of volume, neurotransmitter turnover, lactate production, synaptogenesis, synapse maturation and elimination, brain microcirculation, and response to injury, among many others. There is already evidence that Orai1 and STIMs regulate astrocyte cytokine production and may be involved in immune and pain responses (60). In addition, there are several reports that Ca^{2+} signaling through GPCRs regulates extracellular K^{+}, the mobilization of neuroprotective chemokines, and the release of vasoactive substances. However, it has not yet been explored whether store-operated CRAC channels specifically are involved in these vital processes.

Astrocytes are a very heterogeneous population in terms of morphology, physiology, and functionality (233). Just like neuronal populations, astrocyte populations are specialized to specific neural circuits, and they display diverse features and behaviors in different regions. There is already evidence to suggest that different groups of astrocytes display distinct features in spontaneous as well as agonist- and behavior-evoked Ca^{2+} signaling activity. We have limited our studies mainly to astrocytes of the CA1 hippocampus, but have evidence to show that CRAC channels also mediate store-operated Ca^{2+} influx in astrocytes of the cortex, and therefore may be involved in cortical astrocyte functions as well. It would be interesting to further explore how distinct groups of astrocytes in different areas of the brain utilize store-operated Ca^{2+} signaling.

What relevance do CRAC channels in astrocytes have to neurological pathologies? Studies have implicated dysfunctional astrocyte Ca^{2+} signaling in diseases such as Alzheimer's disease, Huntington's disease, stroke, and epilepsy. Several reports have already specifically demonstrated abnormal CRAC channel activity of astrocytes in diseases such as glioblastoma and amyotrophic lateral sclerosis. Our results suggest that Orai1 in astrocytes can increase the excitability of

hippocampal inhibitory interneurons by regulating the release of gliotransmitters. It would be interesting to examine whether the loss of astrocyte Orai1 can therefore contribute to disease states such as epilepsy which involve a downregulation or dysfunction of inhibitory circuits.

In summary, the findings presented here deepen our understanding of astrocyte physiology, yield new insight into the molecular players and signaling mechanisms controlling communication between glia and neurons, and provide evidence for a role for CRAC channels in cognition and behavior. Future studies that further clarify the functional roles of CRAC channels in the brain may illuminate neurological disorders involving dysregulated Ca^{2+} signaling in astrocytes and neurons and inform the search for therapeutic targets.

CHAPTER 8

MATERIALS AND METHODS

Transgenic mice

C57BL/6 mice were cared for in accordance with institutional guidelines and the Guide for the Care and Use of Laboratory Animals. Animals were group-housed in a sterile ventilated facility, under standard housing conditions (12:12-hour light/dark cycle with lights on at 7:00 am and temperatures of 20 to 22°C with *ad libitum* access to water and food), and maintained with in-house breeding colonies. Male and female mice were used in approximately equal numbers. All research protocols were approved by the Northwestern University Institutional Animal Care and Use Committee.

Tissue-specific deletion of Orai1 in the brain was accomplished as previously described (80). Briefly, $Orai1^{fl/fl}$ mice (provided by Amgen Inc.) and $Orai1^{fl/+}$ were crossed with *nestin-Cre* mice (003771 from the Jackson Laboratory) to generate $Orai1^{fl/fl\ nestin\text{-}Cre}$ (brain-specific KO) and $Orai1^{fl/+\ nestin\text{-}Cre}$ (brain-specific heterozygote). In addition to conditional deletion of Orai1 in the nervous system, the $Orai1^{fl/fl}$ x *nestin-Cre* cross also produced germline transmission in some instances, resulting in $Orai1^{fl/-}$ and $Orai1^{fl/-\ nestin\text{-}Cre}$ genotypes, which were used in some cases for Ca^{2+} imaging experiments from HET and Orai1 KO cultures, as indicated in the figure legends. To delete Orai1 selectively in astrocytes, $Orai1^{fl/fl}$ mice were crossed with *mGFAP-Cre* mice (012887 from the Jackson Laboratory) to yield $Orai1^{fl/fl\ GFAP\text{-}Cre}$ mice. In this line, Cre recombinase is controlled by a mouse GFAP regulatory sequence targeted to postnatal astrocytes. STIM1 KO mice were prepared by crossing $STIM1^{fl/fl}$ (courtesy of S. Feske, New York University) with *nestin-*

Cre mice to obtain *STIM1*$^{fl/fl\ nestin\text{-}Cre}$ mice. Orai2 KO mice (courtesy of Stefan Feske, NYU) were generated by replacing the protein-coding exons of *Orai2* with a LacZ reporter (42).

Primary cultures

Primary astrocytes were isolated from neonatal (P0-P3) mice by standard techniques for astrocyte cultures (165, 234) with minor modifications. Hippocampi or cortices were dissected and meninges removed under a dissection microscope in 4ºC dissection medium [10 mM HEPES in Hanks' balanced salt solution (HBSS)]. The tissue was minced and trypsinized (0.25% trypsin; Invitrogen) for 10 min in a 37°C water bath. Tissue was washed twice with HBSS and dissociated gently by trituration in culture media consisting of Dulbecco's modified Eagle's medium with 10% fetal bovine serum and 1% penicillin-streptomycin solution. Dissociated cells were filtered through a 70 μm strainer to collect cell suspension and cultured in 25 mm^2 tissue culture flasks with 10 ml of medium. Half of the medium was exchanged every 3 to 4 days and microglia were removed by forcefully shaking by hand for 10 to 15 s before each medium change. After cells reached near confluence (12 to 14 days in vitro), media was removed from the cells and exchanged with preheated trypsin-EDTA (0.05%). After 5 min in the incubator, culture medium was added to inactivate the trypsin, and cells were collected and centrifuged for 5 min. The supernatant was removed and the cell pellet was resuspended in culture medium. Cells were plated on poly-L-lysine-coated glass-bottom dishes (MatTek, 14 mm diameter, 10,000 to 15,000 cells per coverslip) or 24-well plates (15,000 to 20,000 cells per well), or six-well plates (~100,000 cells per well). Plated astrocytes were maintained in the incubator and used in experiments after 2 days and within 1 to 2 weeks of plating. Half of the media was exchanged with fresh medium every 4 days.

Stellate-like astrocytes were cultured using methods adapted from the recently developed AWESAM protocol (165, 166) with minor modifications. Astrocytes were cultured in flasks as described above. On day 7 to 10 in vitro, cells were trypsinized as described above and resuspended in NB+ medium containing Neurobasal (Invitrogen) with 5 ng/ml heparin-binding epidermal growth factor (HBEGF), 2% B-27 supplement (Invitrogen), 2 mM L-glutamine, and 1% penicillin-streptomycin solution. Cells were plated on poly-L-lysine-coated glass-bottom dishes (5,000 to 10,000 cells per coverslip) and maintained in the incubator for at least 1 week before use in experiments.

Primary neuronal hippocampal cultures were prepared from neonatal (P0 to P1) mice (235). Hippocampi were dissected as described above. Once the tissue was trypsinized and washed with HBSS, it was dissociated gently by trituration in neuronal media consisting of Neurobasal supplemented with 2% B-27, 2 mM L-glutamine, and 1% penicillin-streptomycin. Cells were plated on poly-D-lysine-coated glass-bottom dishes (~20,000 cells per coverslip) or 6-well plates (~200,000 cells per well) and maintained in the incubator for 2 to 3 weeks. Half of the neuronal medium was exchanged with fresh medium once a week.

DNA purification

Cultured hippocampal astrocytes or neurons were detached from six-well plates using a cell scraper. Detached cells and media were transferred to a 1.5 ml microcentrifuge tube and centrifuged for 5 min at 300xg. Supernatant was removed and the cell pellet was resuspended in phosphate-buffered saline (PBS). Total DNA was purified using the DNeasy kit (Qiagen), according to the manufacturer's instructions for cultured cells. Orai1 gene deletion was checked by PCR using the following primers: 5'-GGGACAAAACACTAACCTGTCAT-3', 5'-

GGAGTAGAATTCAGTGGGAGAGT-3', and 5'-TATGGTAAGGCTGGGAGACAC-3'. The expected sizes of the PCR products are: WT, ~131 base pairs (bp); floxed, ~257 bp; and KO, ~207 bp.

Viral microinjections

Postnatal day 35-57 *Orai1*$^{fl/fl\ GFAP\text{-}Cre}$ and WT littermate mice were deeply anesthetized with isoflurane and head-fixed on stereotaxic frame. Ophthalmic ointment was applied to protect the eyes during surgery. Thermal support was provided using a feedback-controlled heating pad (Warner). Mice were given preoperative analgesic coverage [buprenorphine 0.3 mg/kg, subcutaneously (sc)]. Small craniotomies were performed directly over hippocampus in the left hemisphere. The stereotaxic coordinates were as follows: 2.0 mm posterior to *bregma*; 1.5 mm lateral to midline; and 1.6 mm ventral to the pial surface. Injection pipettes were fabricated from glass capillary micropipettes (Wiretrol II, Drummond Scientific Company) by pulling (PP-830, Narishige) to a fine tip and beveling (Micro Grinder EG-400, Narishige) to a sharp edge. Pipettes were backfilled with mineral oil and then loaded with viral vector by tip filling. Pipettes were advanced slowly to their targets where the viral vector carrying a construct coding for the Cre-independent GCaMP6f (AAV5 gfapABC1D-cyto-GCaMP6f; Addgene plasmid no. 52925 at a titer of 1.4 x 10^{13} viral genomes/mL) was injected at a volume of 0.5 µl over 5 min. Syringes were left in place for 10 min before retraction to allow for virus diffusion. Animals received postoperative analgesic coverage (meloxicam 1.5 mg/kg, sc, once every 24 hours for 2 days).

Solutions and chemicals

The standard Ringer's solution used for wide-field Ca^{2+} imaging studies contained the following: 155 mM NaCl, 4.5 mM KCl, 10 mM D-glucose, 5 mM HEPES, 1 mM $MgCl_2$, 2 mM $CaCl_2$. The Ca^{2+}-free Ringer's solution contained 3 mM $MgCl_2$, 1 mM EGTA (Sigma-Aldrich), and no added $CaCl_2$. pH was adjusted to 7.4 with 1 N NaOH. Stock solution of TG, 2-APB, and YM-58483 (BTP2; Calbiochem) were dissolved in dimethyl sulfoxide and used at the indicated concentrations. ATP (Sigma-Aldrich), UTP (Sigma-Aldrich), and L-glutamic acid (Sigma-Aldrich) were all dissolved in water and used at the indicated concentrations. Thrombin was dissolved in 0.1% albumin and used at the indicated concentrations. EGTA-AM and BAPTA-AM (Invitrogen) were loaded into astrocytes by incubating the cells for 35 to 45 min with 5 μM AM buffer at 37ºC.

For GCaMP6 imaging and electrophysiological recordings of slices, the external artificial cerebrospinal fluid (aCSF) solution contained: 125 mM NaCl, 2.4 mM KCl, 1.2 mM Na_2PO_4, 25 mM $NaHCO_3$, 25 mM glucose, 2 mM $CaCl_2$ and 1 mM $MgCl_2$, equilibrated with 95% O2 and 5% CO_2. Ca^{2+} -free aCSF solution contained: 125 mM NaCl, 2.4 mM KCl, 1.2 mM Na_2PO_4, 25 mM $NaHCO_3$, 25 mM glucose, and 3 mM $MgCl_2$, with 1 mM EGTA, equilibrated with 95% O2 and 5% CO_2. The internal solution for electrophysiological recordings contained the following: 95 mM CsF, 25 mM CsCl, 10 mM HEPES, 10 mM EGTA, 2 mM Mg-ATP, 0.3 mM Na3-GTP, 10 mM QX-314, 5 mM tetraethylammonium chloride (TEA-Cl), 5 mM 4-aminopyridine (4-AP) (pH 7.3 with CsOH).

Wide-field Ca^{2+} imaging

Astrocytes grown on glass-bottom dishes were loaded with Fura-2 by incubating cells in 2 μM Fura-2-AM (Invitrogen) in growth medium for 35 min at 37°C. Fura-2-containing medium

was washed off and cells were incubated for an additional 5 to 10 min before imaging. All experiments were performed at room temperature. Single cell $[Ca^{2+}]_i$ measurements were performed as described previously (80). Image acquisition and analysis were performed using SlideBook (Denver, CO). Dishes were mounted on the stage of an Olympus IX71 inverted microscope and images were acquired every 6 s at excitation wavelengths of 340 and 380 nm, and an emission wavelength of 510 nm. For data analysis, ROIs were drawn around single cells, background was subtracted, and F_{340}/F_{380} ratios were calculated for each time point. A rise in the ratio of emission when excited at 340 nm over the ratio when excited at 380 nm indicated a rise in $[Ca^{2+}]_i$.

$[Ca^{2+}]_i$ was estimated from F_{340}/F_{380} ratio using the standard equation: $[Ca^{2+}]_i = ßK_d (R-R_{min})/(R_{max}-R)$, where R is the F_{340}/F_{380} fluorescence ratio and values of R_{min} and R_{max} were determined from an *in vitro* calibration of Fura-2 pentapotassium salt. ß was determined from the F_{min}/F_{max} ratio at 380 nm and K_d is the apparent dissociation constant of Fura-2 binding to Ca^{2+} (132 nM). The values of these parameters were as follows: $R_{min} = 0.36$, $R_{max} = 19.37$, ß = 12.18. For each cell, the rate of SOCE ($\Delta[Ca^{2+}]_i/\Delta t$) was calculated from the slope of a line fitted to three points (18 s) after the readdition of 2 mM Ca^{2+} Ringer's solution. Baseline $[Ca^{2+}]_i$ was calculated by averaging $[Ca^{2+}]_i$ values over a 2-min baseline for each experiment. Store release was calculated by measuring the area under the curve during TG application in Ca^{2+}-free solution.

Plasmids and transfection

Cultured astrocytes were transfected using Lipofectamine 2000 (Invitrogen) according to the manufacturer's instructions. The E106A Orai1-YFP (yellow fluorescent protein) plasmid has been described previously (46). spH was a gift from E. Kavalali (University of Texas

Southwestern). The TeTx light chain plasmid was purchased from addgene (pGEMTEZ-TeTxLC, plasmid no. 32640). Experiments were performed 24 to 48 hours after transfection.

SynaptopHluorin Imaging

Cultured astrocytes were transfected with 200 ng of spH plasmid per coverslip. After 24-48 hours, astrocyte growth medium was washed away and replaced with Ringer's solution. Dishes were mounted on the stage of Nikon X1 Spinning Disk Confocal equipped with TIRF illumination. spH fusion events were visualized on an Andor iXon3 EMCCD camera using a 60X objective and 488-nm laser filter set with the laser light brought to the angle for internal reflection. Images were acquired every 200 ms. Spontaneous events were imaged for a 2-min baseline before the solution was changed by pipette perfusion.

To determine the number, rate, and location of the vesicle fusion events, timelapse images were analyzed with a MATLAB program developed in-house by Michaela Novakovic. Time-lapse images (in the form of 16-bit .tiff files) were imported into MATLAB as three-dimensional matrices of one intensity value per pixel. The total cell area was calculated in the first frame by using the MATLAB edge detection function and multiplying the number of pixels within the edge of the cell by the area in a pixel. Background was removed by averaging the mean background intensity and subtracting it from all pixels in each frame. To reduce potential confounding factors of cell movement during solution exchange, the frames during and immediately after cell movement (generally a total ~15 s) were not analyzed. To detect events, each pixel was analyzed throughout the time-lapse imaging run to detect local intensity peaks. These local intensity peaks were then analyzed to see if they qualified as exocytotic events using criteria described by Schmoranzer *et al.* (236). Specifically, to count as an event, the intensity of the detected peak had

to exceed a threshold determined by the mean intensity plus three standard deviations of that pixel in frames 50 to 5 time points before the peak (the four time points immediately preceding the peak were excluded from this calculation to account for the rise-time of the signal). To account for the spatial spread of the fluorophore molecules, event spread was analyzed using two criteria: (i) The average of the four pixels immediately surrounding the peak had increased intensity compared with baseline in the following 0.6 s and (ii) the central pixel intensity decreased from its peak value after 0.6 s. If local intensity peaks were found to be exocytotic events according to these criteria, then their coordinates in the matrix and times were stored, so that their locations on the cell footprint and event times could be recovered.

FM1-43 imaging

Cultured astrocytes were incubated at room temperature in HBSS (with 1.2 mM Ca^{2+}) containing 8 μM FM1-43 lipophilic styryl dye (Invitrogen). After a 10-min loading period, the cells were washed three times with Ca^{2+}-free HBSS for 5 min before imaging. Fluorescence images were obtained at excitation wavelength 480 nm and emission wavelength 620 nm. Images were acquired every 15-sec for 10-15 min, background-subtracted, and normalized to the value at t=0.

ATP measurements

ATP released from astrocytes plated on 24-well plates was measured from the cell supernatant with the ENLITEN ATP luciferin-luciferase assay (Promega). Cells were washed twice with growth medium. After 30 min incubation at 37°C, medium was removed from cells and replaced with conditioned HBSS (with or without 1.2 mM Ca^{2+}). The ectonucleotidase inhibitor ARL67156 (200 μM) was applied to each well. The HBSS solution was collected after 10 min and

50 µl was mixed with 50 µl of luciferin/luciferase reagent. Bioluminescence was detected with a luminometer (Berthold Detection Systems). The intensity of the emitted light is proportional to ATP concentration. Data are expressed as a fold change in ATP concentration compared to unstimulated condition performed on the same day.

Immunostaining

Astrocytes plated on coverslips were fixed with 4% paraformaldehyde in PBS for 15 min at 4°C. Cells were washed with PBS, permeabilized by blocking in 4% bovine serum albumin/0.1% Triton X-100 in PBS for 1 hour. Cells were incubated with primary antibodies at 1:800 for GFAP (Sigma-Aldrich) and 1:200 for Orai1 (Alomone) overnight, followed by secondary antibody tagged to Alexa Fluor 488 or Alexa Fluor 594 at 1:500 for 1 hour. Nuclei were labeled with 4',6-diamidino-2-phenylindole.

Slice preparation

Hippocampal slices were cut from the brains of 3 to 5-week-old mice for electrophysiology and 14 to 22 days after viral injections for GCamP6f imaging. Animals were deeply anesthetized with isoflurane, and the brains were removed quickly. Horizontal slices either 250 µm (for GCamP6f imaging) or 300 µm (for slice electrophysiology), were cut using a tissue slicer (Compresstome model VF-200-0Z, Precisionary Instruments) in ice-cold sucrose aCSF. For the electrophysiological slice experiments, the composition of this solution was as follows: 85 mM NaCl, 2.5 mM KCl, 1.25 mM NaH_2PO_4, 25 mM $NaHCO_3$, 25 mM glucose, 75 mM sucrose, 0.5 mM $CaCl_2$ and 4 mM $MgCl_2$ saturated with saturated with 95% O_2 and 5% CO_2. For GCamP6f imaging, slices were cut in a solution containing the following: 110 mM Choline chloride, 2.5 mM

KCl, 25 mM $NaHCO_3$, 1.25 mM NaH_2PO_4, 25 mM D-glucose, 11.6 mM ascorbic acid, 3.1 mM pyruvic acid, 7 mM $MgCl_2$, and 0.5 mM $CaCl_2$, saturated with 95% O_2 and 5% CO_2. Slices were then quickly transferred into a recovery chamber with aCSF solution maintained at 30℃ and containing the following: 125 mM NaCl, 2.4 mM KCl, 1.2 mM Na_2PO_4, 25 mM $NaHCO_3$, 25 mM glucose, 1 mM $CaCl_2$ and 2 mM $MgCl_2$ saturated with 95% O_2 and 5% CO_2. After 30 min in the recovery chamber, slices were subsequently transferred into a storage chamber with aCSF containing 2 mM $CaCl_2$, where they were stored for 0.5 to 6 hours until they were used for calcium imaging using 2PLSM or electrophysiology.

GCamP6f imaging using 2-photon microscopy

GCamP6f signals were imaged in astrocytes expressing GCamP6f in brain slices using a Nikon A1R-MP+ multiphoton microscope with a Chameleon Vision titanium sapphire laser and 25X Nikon objective lens. The data were collected using Nikon Elements software. Astrocytes were selected from the CA1 stratum radiatum region and were typically located ~50 to 120 μm below the surface. The hippocampus (DG, CA1, and CA3) was identified using autofluorescence visible at 750 nm excitation at low magnification. Once the stratum radiatum region was identified, excitation was switched to 950 nm to visualize single GCaMp6f expressing cells at high magnification. Images were acquired at 1 frame/sec. Cells were excited at 950 nm at a laser power of 10%. Imaging was performed at room temperature. During the experiment, slices were continuously perfused with aCSF solution, which was switched for aCSF with thrombin (10 U/ml) or Ca^{2+}-free aCSF at the indicated times.

Slice electrophysiology

Patch-clamp recordings were performed using an Axopatch 200B amplifier interfaced to an ITC-18 input-output board and an iMac G5 computer. Currents were filtered at 2 kHz with a four-pole Bessel filter and sampled at 5 kHz. Stimulation, data acquisition, and analysis were performed using in-house routines developed on the Igor Pro platform. Recordings were performed from CA1 pyramidal neurons, and the holding potential was -70 mV. CA1 pyramidal cells were identified by their location in the pyramidal layer. IPSCs were isolated by the inclusion of 6-cyano-7-nitroquinoxaline-2,3-dione (CNQX) (10 μM) and D-(-)-2-amino-5-phosphonopentanoic acid (D-APV) (50 μM) in the extracellular solution to block glutamate receptors. mIPSCs were recorded in the presence of TTX (1 μM).

Behavioral tasks

Male and female mice were 9 to 14 weeks of age at the start of testing. The experimenter was blind to the genotype of each mouse during behavioral testing and analysis.

Y-maze. Mice were placed at the end of arm 3 in the Y-maze and allowed to enter any of the three arms for 8 min while activity was recorded by a video tracking system. The order of arm entries was analyzed manually for spontaneous alternation. A successful alternation was recorded for each set of three consecutive arm choices in which no repeated entries occurred. An unsuccessful alternation was recorded for each set of three consecutive arm choices in which a repeated entry occurred. An arm entry was counted if the entire body of the mouse (excluding tail) entered the arm. Each mouse was analyzed until it had completed 20 possible (successful and unsuccessful) alternations. The number of successful alternations was divided by the number of

possible alternations for the outcome measure, % alternation. Mice were excluded if they did not enter enough arms to complete 20 possible alternations. Chance level of alternation is 50%.

Morris water maze. The water maze apparatus consisted of a circular pool (1.2 m diameter), filled with water (21 to 22°C) made opaque with non-toxic white paint, with an overhead camera connected to a computer running WaterMaze video tracking software (Actimetrics). Before testing, all mice were trained with a visible platform for 4 days, with three starting locations (NE, SE, SW quadrants) corresponding to three platform locations (NW, SW, NE quadrants) repeated twice for a total of 6 trials per day. If the mouse failed to find the platform within 60 s, the experimenter guided the mouse to the platform location. To assess spatial reference memory, a hidden clear plastic platform was submerged 1 cm below the water's surface in a fixed location (NW quadrant). Large black visual navigation cues were hung from the walls surrounding the maze, corresponding to the four cardinal directions. Mice were tested with the hidden platform for 5 days, with three starting locations (NE, SW, SE quadrants) repeated twice for a total of 6 trials per day. The time to find the hidden platform and the path traveled were recorded for each trial. Two hours after the final trial on the last testing day, a probe trial was conducted with the hidden platform removed. Mice were started in the middle of the pool and the time spent searching in each quadrant of the pool was recorded over 60 s. Swimming speed of each mouse was also assessed during the probe trials.

Fear conditioning. Contextual and tone-dependent fear conditioning were tested using a computer-controlled activity monitor and tone/shock generator (TSE Systems). Mice were placed in Context 1 (Plexiglas chamber with a wire shock grid floor) for 173 s, followed by a 30 s tone (10 kHz; 75 dB), followed by a 15 s pause (trace), followed by a foot shock (2 s; 0.7 mA; constant current). After 24 hours, the mice were placed in a novel context (Context 2) for 60 s, followed by

exposure to the original tone for 30 s, followed by a 15 s trace. Freezing was measured every 10th second in the novel context, every 5th second during the tone, and every 3rd second during the trace. After 24 more hours, the mice were placed back in the original context 1 and contextual freezing was measured every 10th second during a 180 s exposure.

Open field. Mice were placed in the center of an open arena (56 x 56cm), and ambulation activity for 5 min was recorded by LimeLight software (Actimetrics). The open field was divided into a 5 x 5 grid of squares, with the outer 16 squares defining the 'outer' region and the inner 9 squares defining the 'inner' region. The software provided the total distance traveled, the percentage of time the mouse spent within each of the two regions, and the number of crossings from one region to the other.

Rotarod. Mice were tested on a RotaRod device (TSE Systems) over 5 days. For first three 'training' days, the mice were individually placed on the rod, which rotated at 12 rpm for 60 sec. The time at which the mouse fell off the rod was recorded. If the mouse remained on the rod without falling for the duration of the trial, 60 s was recorded as the time for that trial. For the last two 'test' days, the mice were individually placed on the rod, which rotated beginning at 4 rpm and accelerated to 40 rpm over 5 min. The time at which the mouse fell off the rod was recorded. Four trials per day were conducted for each mouse, spaced approximately 1 hour apart.

Data analysis

All data are expressed as means ± SEM. For datasets with two groups, statistical analysis was performed with two-tailed t-test to compare between control and test conditions. For datasets with greater than two groups, one-way ANOVA followed by Tukey post hoc test was used to

compare groups. Statistical analysis was performed with a confidence level of 95%, and results with $P < 0.05$ were considered significant.

The average rate of spH-labeled exocytosis was calculated by measuring the slope of a line fit to the cumulative events plot for each cell. The baseline rate was measured by fitting a line to the first 120 s of the experiment. For measurements of agonist-evoked exocytosis, the cursors were set at least 120 s after agonist application and spanned 200 s. For the Ca^{2+}-free exocytotic rate analysis, the cursors for the fit were set immediately after agonist application to obtain the store-release contribution to the release rate. No difference was seen in the exocytosis rates between *Orai1*$^{fl/fl\ nestin\text{-}Cre}$ and *Orai1*$^{fl/fl\ GFAP\text{-}Cre}$ astrocytes, and therefore the results from these cells were pooled into an "Orai1 KO" group.

spH event kinetics were measured with a line scan (12-pixel length (3.24 μm)) through the center of individual events. The fluorescence values were calculated as $\Delta F/F_0$, where F_0 was the average of the baseline fluorescence for 5 s (25 time points) before the event. The half width of each event was calculated using the Peak Analyzer function of OriginLab as the width of the curve at half of its maximum peak value.

The frequency and amplitude of Ca^{2+} fluctuations in GCaMP6f-expressing astrocytes in slices were analyzed using ImageJ and OriginLab. ROIs were drawn manually on the two-dimensional maximum intensity projection of the time series (~540s) in each experiment around the soma, the primary proximal processes coming off the cell body, and the distal tertiary processes (fig. S7A). The numbers and average sizes of the ROIs drawn around the soma, proximal processes, and distal processes were not significantly different between WT and *Orai1*$^{fl/fl\ GFAP\text{-}Cre}$ cells. Background was measured in a region of the imaging field not containing any GCamP6f expression. The background-subtracted mean intensity of each ROI was measured at each time

point using the ImageJ Multi Measure plugin and F_0 calculated by averaging the first 20 time points for each ROI. The intensity of the GCamP6f fluctuations at each time point was calculated as $\Delta F/F_0$ for each ROI, and frequency and amplitude of the fluctuations were measured using Peak Analyzer function of OriginLab. A moving baseline with asymmetric least squares smoothing was used and peaks were determined from the local maxima that exceeded a threshold of 10% over the local baseline. The frequency and amplitude for all the peaks in each ROI was averaged and calculated for each compartment (soma, proximal processes, distal processes) in each cell. Analysis was done over a 3-min duration immediately before and at least 90 s after the administration of thrombin. Cells were excluded from analysis if they had significant z-drift or x-y drift during the imaging.

IPSCs were analyzed using MiniAnalysis software (Synaptosoft Inc.). Events were analyzed over a 5-min duration immediately before and 3 min after the administration of thrombin. The threshold for detection of events was set at 20 pA.

REFERENCES

1. Berridge MJ, Lipp P, & Bootman MD (2000) The versatility and universality of calcium signalling. *Nat Rev Mol Cell Biol* 1(1):11-21.
2. Clapham DE (2007) Calcium signaling. *Cell* 131(6):1047-1058.
3. Parekh AB & Putney JW, Jr. (2005) Store-operated calcium channels. *Physiol Rev* 85(2):757-810.
4. Prakriya M & Lewis RS (2015) Store-Operated Calcium Channels. *Physiol Rev* 95(4):1383-1436.
5. Putney JW (1986) A model for receptor-regulated calcium entry. *Cell Calcium* 7:1-12.
6. Putney JW (1990) Capacitative calcium entry revisited. *Cell Calcium* 11(10):611-624.
7. Lewis RS & Cahalan MD (1989) Mitogen-induced oscillations of cytosolic Ca2+ and transmembrane Ca2+ current in human leukemic T cells. *Cell Regul* 1(1):99-112.
8. Matthews G, Neher E, & Penner R (1989) Second messenger-activated calcium influx in rat peritoneal mast cells. *J Physiol* 418:105-130.
9. Takemura H, Hughes AR, Thastrup O, & Putney JW (1989) Activation of calcium entry by the tumor promoter thapsigargin in parotid acinar cells. Evidence that an intracellular calcium pool and not an inositol phosphate regulates calcium fluxes at the plasma membrane. *J Biol Chem* 264(21):12266-12271.
10. Thastrup O, Cullen PJ, Drobak BK, Hanley MR, & Dawson AP (1990) Thapsigargin, a tumor promoter, discharges intracellular Ca2+ stores by specific inhibition of the endoplasmic reticulum Ca2+-ATPase. *Proc Natl Acad Sci U S A* 87(7):2466-2470.

11. Gouy H, Cefai D, Christensen SB, Debre P, & Bismuth G (1990) Ca2+ influx in human T lymphocytes is induced independently of ionositol phosphate production by mobilization of intracellular Ca2+ stores. A study with the Ca2+ endoplasmic reticulum-ATPase thapsigargin. *Eur J Immunol* 20(10):2269-2275.

12. Mason MJ, Mahaut-Smith MP, & Grinstein S (1991) The role of intracellular Ca2+ in the regulation of the plasma membrane Ca2+ permeability of unstimulated rat lymphocytes. *J Biol Chem* 266(17):10872-10879.

13. Hoth M & Penner R (1992) Depletion of intracellular calcium stores activates a calcium current in mast cells. *Nature* 355:353-356.

14. Zweifach A & Lewis RS (1993) Mitogen-regulated Ca2+ current of T lymphocytes is activated by depletion of intracellular Ca2+ stores. *Proc Natl Acad Sci U S A* 90(13):6295-6299.

15. Prakriya M & Lewis RS (2003) CRAC channels: activation, permeation, and the search for a molecular identity. *Cell Calcium* 33(5-6):311-321.

16. Prakriya M (2009) The molecular physiology of CRAC channels. *Immunol Rev* 231(1):88-98.

17. Yue L, Peng J-B, Hediger MA, & Clapham DE (2001) CaT1 manifests the pore properties of the calcium-release-activated calcium channel. *Nature* 410(6829):705-709.

18. Mori Y*, et al.* (2002) Transient Receptor Potential 1 Regulates Capacitative Ca2+Entry and Ca2+Release from Endoplasmic Reticulum in B Lymphocytes. *The Journal of Experimental Medicine* 195(6):673-681.

19. Philipp S*, et al.* (2003) TRPC3 mediates T-cell receptor-dependent calcium entry in human T-lymphocytes. *J Biol Chem* 278(29):26629-26638.

20. Zhang SL, *et al.* (2005) STIM1 is a Ca2+ sensor that activates CRAC channels and migrates from the Ca2+ store to the plasma membrane. *Nature* 437(7060):902-905.

21. Liou J, *et al.* (2005) STIM is a Ca2+ sensor essential for Ca2+-store-depletion-triggered Ca2+ influx. *Curr Biol* 15(13):1235-1241.

22. Roos J, *et al.* (2005) STIM1, an essential and conserved component of store-operated Ca2+ channel function. *J Cell Biol* 169(3):435-445.

23. Prakriya M, *et al.* (2006) Orai1 is an essential pore subunit of the CRAC channel. *Nature* 443(7108):230-233.

24. Vig M, *et al.* (2006) CRACM1 multimers form the ion-selective pore of the CRAC channel. *Curr Biol* 16(20):2073-2079.

25. Yeromin AV, *et al.* (2006) Molecular identification of the CRAC channel by altered ion selectivity in a mutant of Orai. *Nature* 443(7108):226-229.

26. Lewis RS (2007) The molecular choreography of a store-operated calcium channel. *Nature* 446(7133):284-287.

27. Luik RM, Wang B, Prakriya M, Wu MM, & Lewis RS (2008) Oligomerization of STIM1 couples ER calcium depletion to CRAC channel activation. *Nature* 454(7203):538-542.

28. Kawasaki T, Lange I, & Feske S (2009) A minimal regulatory domain in the C terminus of STIM1 binds to and activates ORAI1 CRAC channels. *Biochem Biophys Res Commun* 385(1):49-54.

29. Park CY, *et al.* (2009) STIM1 Clusters and Activates CRAC Channels via Direct Binding of a Cytosolic Domain to Orai1. *Cell* 136(5):876-890.

30. Yuan JP, *et al.* (2009) SOAR and the polybasic STIM1 domains gate and regulate Orai channels. *Nat Cell Biol* 11(3):337-343.

31. Hoth M & Niemeyer BA (2013) The neglected CRAC proteins: Orai2, Orai3, and STIM2. *Curr Top Membr* 71:237-271.

32. Zheng L, Stathopulos PB, Li GY, & Ikura M (2008) Biophysical characterization of the EF-hand and SAM domain containing Ca2+ sensory region of STIM1 and STIM2. *Biochem Biophys Res Commun* 369(1):240-246.

33. Brandman O, Liou J, Park WS, & Meyer T (2007) STIM2 is a feedback regulator that stabilizes basal cytosolic and endoplasmic reticulum Ca2+ levels. *Cell* 131(7):1327-1339.

34. Stathopulos PB, Zheng L, & Ikura M (2009) Stromal interaction molecule (STIM) 1 and STIM2 calcium sensing regions exhibit distinct unfolding and oligomerization kinetics. *J Biol Chem* 284(2):728-732.

35. Feske S*, et al.* (2006) A mutation in Orai1 causes immune deficiency by abrogating CRAC channel function. *Nature* 441(7090):179-185.

36. Zhang SL*, et al.* (2006) Genome-wide RNAi screen of Ca2+ influx identifies genes that regulate Ca2+ release-activated Ca2+ channel activity. *Proc Natl Acad Sci U S A* 103(24):9357-9362.

37. Hou X, Pedi L, Diver MM, & Long SB (2012) Crystal structure of the calcium release-activated calcium channel Orai. *Science* 338(6112):1308-1313.

38. Gross SA*, et al.* (2007) Murine ORAI2 splice variants form functional Ca2+ release-activated Ca2+ (CRAC) channels. *J Biol Chem* 282(27):19375-19384.

39. Lis A*, et al.* (2007) CRACM1, CRACM2, and CRACM3 are store-operated Ca2+ channels with distinct functional properties. *Curr Biol* 17(9):794-800.

40. Mercer JC*, et al.* (2006) Large store-operated calcium selective currents due to co-expression of Orai1 or Orai2 with the intracellular calcium sensor, Stim1. *J Biol Chem* 281(34):24979-24990.

41. DeHaven WI, Smyth JT, Boyles RR, & Putney JW (2007) Calcium Inhibition and Calcium Potentiation of Orai1, Orai2, and Orai3 Calcium Release-activated Calcium Channels. *Journal of Biological Chemistry* 282(24):17548-17556.

42. Vaeth M*, et al.* (2017) ORAI2 modulates store-operated calcium entry and T cell-mediated immunity. *Nat Commun* 8:14714.

43. Luik RM, Wu MM, Buchanan J, & Lewis RS (2006) The elementary unit of store-operated Ca2+ entry: local activation of CRAC channels by STIM1 at ER-plasma membrane junctions. *J Cell Biol* 174(6):815-825.

44. Wu MM, Buchanan J, Luik RM, & Lewis RS (2006) Ca2+ store depletion causes STIM1 to accumulate in ER regions closely associated with the plasma membrane. *J Cell Biol* 174(6):803-813.

45. Baba Y*, et al.* (2006) Coupling of STIM1 to store-operated Ca2+ entry through its consitutive and inducible movement in the endoplasmic reticulum. *Proc Natl Acad Sci U S A* 103(45):16704-16709.

46. Navarro-Borelly L*, et al.* (2008) STIM1-Orai1 interactions and Orai1 conformational changes revealed by live-cell FRET microscopy. *J Physiol* 586(22):5383-5401.

47. Xu P*, et al.* (2006) Aggregation of STIM1 underneath the plasma membrane induces clustering of Orai1. *Biochem Biophys Res Commun* 350(4):969-976.

48. Smyth JT, DeHaven WI, Bird GS, & Putney JW (2008) Ca2+-store-dependent and -independent reversal of Stim1 localization and function. *Journal of Cell Science* 121(6):762-772.

49. Partiseti M*, et al.* (1994) The calcium current activated by T cell receptor and store depletion in human lymphocytes is absent in a primary immunodeficiency. *J Biol Chem* 269(51):32327-32335.

50. Deist FL*, et al.* (1995) A primary T-cell immunodeficiency associated with defective transmembrane calcium influx. *Blood* 85(4):1053-1062.

51. Fanger CM, Hoth M, Crabtree GR, & Lewis RS (1995) Characterization of T cell mutants with defects in capacitative calcium entry: genetic evidence for the physiological roles of CRAC channels. *The Journal of Cell Biology* 131(3):655-667.

52. Feske S*, et al.* (1996) Severe combined immunodeficiency due to defective binding of the nuclear factor of activated T cells in T lymphocytes of two male siblings. *Eur J Immunol* 26(2119-2126).

53. Feske S, Prakriya M, Rao A, & Lewis RS (2005) A severe defect in CRAC Ca2+ channel activation and altered K+ channel gating in T cells from immunodeficient patients. *J Exp Med* 202(5):651-662.

54. Trebak M (2012) STIM/Orai signalling complexes in vascular smooth muscle. *J Physiol* 590(17):4201-4208.

55. Shin DM & Muallem S (2008) Skeletal muscle dressed in SOCs. *Nat Cell Biol* 10(6):639-641.

56. Abdullaev IF*, et al.* (2008) Stim1 and Orai1 mediate CRAC currents and store-operated calcium entry important for endothelial cell proliferation. *Circ Res* 103(11):1289-1299.

57. Tolhurst G*, et al.* (2009) Expression profiling and electrophysiological studies suggest a major role for Orai1 in the store-operated Ca2+influx pathway of platelets and megakaryocytes. *Platelets* 19(4):308-313.

58. Braun A*, et al.* (2009) Orai1 (CRACM1) is the platelet SOC channel and essential for pathological thrombus formation. *Blood* 113(9):2056-2063.

59. Michaelis M, Nieswandt B, Stegner D, Eilers J, & Kraft R (2015) STIM1, STIM2, and Orai1 regulate store-operated calcium entry and purinergic activation of microglia. *Glia* 63(4):652-663.

60. Gao X*, et al.* (2016) STIMs and Orai1 regulate cytokine production in spinal astrocytes. *J Neuroinflammation* 13(1):126.

61. Dou Y*, et al.* (2018) Orai1 Plays a Crucial Role in Central Sensitization by Modulating Neuronal Excitability. *J Neurosci* 38(4):887-900.

62. Tshuva RY, Korkotian E, & Segal M (2017) ORAI1-dependent synaptic plasticity in rat hippocampal neurons. *Neurobiol Learn Mem* 140:1-10.

63. Kraft R (2015) STIM and ORAI proteins in the nervous system. *Channels (Austin)* 9(5):245-252.

64. Lewis RS (2001) Calcium signaling mechanisms in T lymphocytes. *Annu Rev Immunol* 19:497-521.

65. Feske S (2009) ORAI1 and STIM1 deficiency in human and mice: roles of store-operated Ca2+ entry in the immune system and beyond. *Immunol Rev* 231(1):189-209.

66. Picard C*, et al.* (2008) STIM1 mutation associated with a syndrome of immunodeficiency and autoimmunity. *N Engl J Med* 360(19):1971-1980.

67. Lacruz RS & Feske S (2015) Diseases caused by mutations in ORAI1 and STIM1. *Ann N Y Acad Sci* 1356:45-79.

68. Parekh AB (2010) Store-operated CRAC channels: function in health and disease. *Nat Rev Drug Discov* 9(5):399-410.

69. Guzman R*, et al.* (2014) Expression of ORAII, a plasma membrane resident subunit of the CRAC channel, in rodent and non-rodent species. *J Histochem Cytochem* 62(12):864-878.

70. Xia J, Pan R, Gao X, Meucci O, & Hu H (2014) Native store-operated calcium channels are functionally expressed in mouse spinal cord dorsal horn neurons and regulate resting calcium homeostasis. *J Physiol* 592(16):3443-3461.

71. Skibinska-Kijek A, Wisniewska MB, Gruszczynska-Biegala J, Methner A, & Kuznicki J (2009) Immunolocalization of STIM1 in the mouse brain. *Acta Neurobiol Exp (Wars)* 69(4):413-428.

72. Gruszczynska-Biegala J, Pomorski P, Wisniewska MB, & Kuznicki J (2011) Differential roles for STIM1 and STIM2 in store-operated calcium entry in rat neurons. *PLoS One* 6(4):e19285.

73. Steinbeck JA*, et al.* (2011) Store-operated calcium entry modulates neuronal network activity in a model of chronic epilepsy. *Exp Neurol* 232(2):185-194.

74. Klejman ME*, et al.* (2009) Expression of STIM1 in brain and puncta-like co-localization of STIM1 and ORAI1 upon depletion of Ca(2+) store in neurons. *Neurochem Int* 54(1):49-55.

75. Berna-Erro A*, et al.* (2009) STIM2 regulates capacitive Ca2+ entry in neurons and plays a key role in hypoxic neuronal cell death. *Sci Signal* 2(93):ra67.

76. Emptage NJ, Reid CA, & Fine A (2001) Calcium stores in hippocampal synaptic boutons mediate short-term plasticity, store-operated Ca2+ entry, and spontaneous transmitter release. *Neuron* 29:197-208.

77. Baba A*, et al.* (2003) Activity-evoked capacitative Ca2+ entry: implications in synaptic plasticity. *J Neurosci* 23(21):7737-7741.

78. Korkotian E, Oni-Biton E, & Segal M (2017) The role of the store-operated calcium entry channel Orai1 in cultured rat hippocampal synapse formation and plasticity. *J Physiol* 595(1):125-140.

79. Lalonde J, Saia G, & Gill G (2014) Store-operated calcium entry promotes the degradation of the transciption factor Sp4 in resting neurons. *Sci Signal* 7(328):ra51.

80. Somasundaram A*, et al.* (2014) Store-operated CRAC channels regulate gene expression and proliferation in neural progenitor cells. *J Neurosci* 34(27):9107-9123.

81. Gemes G*, et al.* (2011) Store-operated Ca2+ entry in sensory neurons: functional role and the effect of painful nerve injury. *J Neurosci* 31(10):3536-3549.

82. Hartmann J*, et al.* (2014) STIM1 controls neuronal Ca(2)(+) signaling, mGluR1-dependent synaptic transmission, and cerebellar motor behavior. *Neuron* 82(3):635-644.

83. Venkiteswaran G & Hasan G (2009) Intracellular Ca2+ signaling and store-operated Ca2+ entry are required in Drosophila neurons for flight. *Proc Natl Acad Sci U S A* 106(25):10326-10331.

84. Kawamata H*, et al.* (2014) Abnormal intracellular calcium signaling and SNARE-dependent exocytosis contributes to SOD1G93A astrocyte-mediated toxicity in amyotrophic lateral sclerosis. *J Neurosci* 34(6):2331-2348.

85. Zhang H*, et al.* (2016) Store-Operated Calcium Channel Complex in Postsynaptic Spines: A New Therapeutic Target for Alzheimer's Disease Treatment. *The Journal of Neuroscience* 36(47):11837-11850.

86. Sun S*, et al.* (2014) Reduced synaptic STIM2 expression and impaired store-operated calcium entry cause destabilization of mature spines in mutant presenilin mice. *Neuron* 82(1):79-93.

87. Bouron A (2000) Activation of a capacitative Ca2+ entry pathway by store depletion in cultured hippocampal neurones. *FEBS Lett* 470(3):269-272.

88. Bouron A, Altafaj X, Boisseau S, & De Waard M (2005) A store-operated Ca2+ influx activated in response to the depletion of thapsigargin-sensitive Ca2+ stores is developmentally regulated in embryonic cortical neurons from mice. *Brain Res Dev Brain Res* 159(1):64-71.

89. Herring BE & Nicoll RA (2016) Long-Term Potentiation: From CaMKII to AMPA Receptor Trafficking. *Annu Rev Physiol* 78:351-365.

90. Segal M & Korkotian E (2016) Roles of Calcium Stores and Store-Operated Channels in Plasticity of Dendritic Spines. *Neuroscientist* 22(5):477-485.

91. Moccia F*, et al.* (2015) Stim and Orai proteins in neuronal Ca(2+) signaling and excitability. *Front Cell Neurosci* 9:153.

92. Bezprozvanny I & Mattson MP (2008) Neuronal calcium mishandling and the pathogenesis of Alzheimer's disease. *Trends Neurosci* 31(9):454-463.

93. Berridge MJ (2010) Calcium hypothesis of Alzheimer's disease. *Pflugers Arch* 459(3):441-449.

94. Leissring MA, *et al.* (2000) Capacitative Calcium Entry Deficits and Elevated Luminal Calcium Content in Mutant Presenilin-1 Knockin Mice. *The Journal of Cell Biology* 149(4):793-798.

95. Yoo A, *et al.* (2000) Presenilin-mediated modulation of capacitative calcium entry. *Neuron* 27(3):561-572.

96. Popugaeva E, *et al.* (2015) STIM2 protects hippocampal mushroom spines from amyloid synaptotoxicity. *Mol Neurodegener* 10:37.

97. Tong BC-K, *et al.* (2016) Familial Alzheimer's disease-associated presenilin 1 mutants promote y-secretase cleavage of STIM1 to impair store-operated Ca2+ entry. *Sci Signal* 9(444):ra89.

98. Kimelberg HK & Nedergaard M (2010) Functions of astrocytes and their potential as therapeutic targets. *Neurotherapeutics* 7:338-353.

99. Zuchero JB & Barres BA (2015) Glia in mammalian development and disease. *Development* 142(22):3805-3809.

100. Verkhratsky A, Nedergaard M, & Hertz L (2015) Why are astrocytes important? *Neurochem Res* 40(2):389-401.

101. Verkhratsky A & Nedergaard M (2018) Physiology of Astroglia. *Physiological Reviews* 98(1):239-389.

102. Anderson MA, *et al.* (2016) Astrocyte scar formation aids central nervous system axon regeneration. *Nature* 532(7598):195-200.

103. Mulligan SJ & MacVicar BA (2004) Calcium transients in astrocyte endfeet cause cerebrovascular constrictions. *Nature* 431(7005):195-199.

104. Araque A, Carmignoto G, & Haydon PG (2001) Dynamic signaling between astrocytes and neurons. *Annu Rev Physiol* 63:795-813.

105. Perea G & Araque A (2010) GLIA modulates synaptic transmission. *Brain Res Rev* 63(1-2):93-102.

106. Navarrete M*, et al.* (2013) Astrocyte calcium signal and gliotransmission in human brain tissue. *Cereb Cortex* 23(5):1240-1246.

107. Porter JT & McCarthy KD (1997) Astrocytic neurotransmitter receptors in situ and in vivo. *Prog Neurobiol* 51(4):439-455.

108. Verkhratsky A, Rodríguez JJ, & Parpura V (2012) Calcium signalling in astroglia. *Molecular and Cellular Endocrinology* 353(1-2):45-56.

109. Verkhratsky A & Parpura V (2014) Store-operated calcium entry in neuroglia. *Neurosci Bull* 30(1):125-133.

110. Volterra A, Liaudet N, & Savtchouk I (2014) Astrocyte Ca(2)(+) signalling: an unexpected complexity. *Nat Rev Neurosci* 15(5):327-335.

111. Araque A*, et al.* (2014) Gliotransmitters travel in time and space. *Neuron* 81(4):728-739.

112. Agulhon C*, et al.* (2008) What is the role of astrocyte calcium in neurophysiology? *Neuron* 59(6):932-946.

113. Hamilton NB & Attwell D (2010) Do astrocytes really exocytose neurotransmitters? *Nat Rev Neurosci* 11(4):227-238.

114. Parpura V, Grubisic V, & Verkhratsky A (2011) Ca(2+) sources for the exocytotic release of glutamate from astrocytes. *Biochim Biophys Acta* 1813(5):984-991.

115. Kanemaru K*, et al.* (2014) In vivo visualization of subtle, transient, and local activity of astrocytes using an ultrasensitive Ca(2+) indicator. *Cell Rep* 8(1):311-318.

116. Srinivasan R*, et al.* (2015) Ca(2+) signaling in astrocytes from Ip3r2(-/-) mice in brain slices and during startle responses in vivo. *Nat Neurosci* 18(5):708-717.

117. Motiani RK*, et al.* (2013) STIM1 and Orai1 mediate CRAC channel activity and are essential for human glioblastoma invasion. *Pflugers Arch* 465(9):1249-1260.

118. Kwon J*, et al.* (2017) Orai1 and Orai3 in Combination with Stim1 Mediate the Majority of Store-operated Calcium Entry in Astrocytes. *Exp Neurobiol* 26(1):42-54.

119. Moreno C, Sampieri A, Vivas O, Pena-Segura C, & Vaca L (2012) STIM1 and Orai1 mediate thrombin-induced Ca(2+) influx in rat cortical astrocytes. *Cell Calcium* 52(6):457-467.

120. Papanikolaou M, Lewis A, & Butt AM (2017) Store-operated calcium entry is essential for glial calcium signalling in CNS white matter. *Brain Struct Funct* 222(7):2993-3005.

121. Malarkey EB, Ni Y, & Parpura V (2008) Ca2+ entry through TRPC1 channels contributes to intracellular Ca2+ dynamics and consequent glutamate release from rat astrocytes. *Glia* 56(8):821-835.

122. Shirakawa H*, et al.* (2010) Transient receptor potential canonical 3 (TRPC3) mediates thrombin-induced astrocyte activation and upregulates its own expression in cortical astrocytes. *J Neurosci* 30(39):13116-13129.

123. Cornell-Bell AH, Finkbeiner SM, Cooper MS, & Smith SJ (1990) Glutamate induces calcium waves in cultured astrocytes: long-range glial signaling. *Science* 247(4941):470-473.

124. Dani JW, Chernjavsky A, & Smith SJ (1992) Neuronal activity triggers calcium waves in hippocampal astrocyte networks. *Neuron* 8:429-440.

125. Parpura V*, et al.* (1994) Glutamate-mediated astrocyte-neuron signalling. *Nature* 369:744-747.

126. Halassa MM & Haydon PG (2010) Integrated brain circuits: astrocytic networks modulate neuronal activity and behavior. *Annu Rev Physiol* 72:335-355.

127. Ventura R & Harris KM (1999) Three-dimensional relationships between hippocampal synapses and astrocytes. *J Neurosci* 19(16):6897-6906.

128. Haber M, Zhou L, & Murai KK (2006) Cooperative astrocyte and dendritic spine dynamics at hippocampal excitatory synapses. *J Neurosci* 26(35):8881-8891.

129. Perea G, Navarrete M, & Araque A (2009) Tripartite synapses: astrocytes process and control synaptic information. *Trends Neurosci* 32(8):421-431.

130. Halassa MM, Fellin T, & Haydon PG (2007) The tripartite synapse: roles for gliotransmission in health and disease. *Trends Mol Med* 13(2):54-63.

131. Martin ED*, et al.* (2007) Adenosine released by astrocytes contributes to hypoxia-induced modulation of synaptic transmission. *Glia* 55(1):36-45.

132. Harada K, Kamiya T, & Tsuboi T (2015) Gliotransmitter Release from Astrocytes: Functional, Developmental, and Pathological Implications in the Brain. *Front Neurosci* 9:499.

133. Bezzi P*, et al.* (2004) Astrocytes contain a vesicular compartment that is competent for regulated exocytosis of glutamate. *Nat Neurosci* 7(6):613-620.

134. Liu T*, et al.* (2011) Calcium triggers exocytosis from two types of organelles in a single astrocyte. *J Neurosci* 31(29):10593-10601.

135. Hertz L, Dringen R, Schousboe A, & Robinson SR (1999) Astrocytes: glutamate producers for neurons. *J Neurosci Res* 57:417-428.

136. Fields RD & Burnstock G (2006) Purinergic signalling in neuron-glia interactions. *Nat Rev Neurosci* 7(6):423-436.

137. Parpura V & Zorec R (2010) Gliotransmission: Exocytotic release from astrocytes. *Brain Res Rev* 63(1-2):83-92.

138. Montana V, Malarkey EB, Verderio C, Matteoli M, & Parpura V (2006) Vesicular transmitter release from astrocytes. *Glia* 54(7):700-715.

139. Zhang Q*, et al.* (2004) Fusion-related release of glutamate from astrocytes. *J Biol Chem* 279(13):12724-12733.

140. Zhang Q, Fukuda M, Bockstaele EV, Pascual O, & Haydon PG (2004) Synaptotagmin IV regulates glial glutamate release. *Proc Natl Acad Sci U S A* 101:9441-9446.

141. Bohmbach K, Schwarz MK, Schoch S, & Henneberger C (2018) The structural and functional evidence for vesicular release from astrocytes in situ. *Brain Res Bull* 136:65-75.

142. Mothet J-P*, et al.* (2005) Glutamate receptor activation triggers a calcium-dependent and SNARE protein-dependent release of the gliotransmitter D-serine. *Proc Natl Acad Sci U S A* 102(15):5606-5611.

143. Pascual O*, et al.* (2005) Astrocytic purinergic signaling coordinates synaptic networks. *Science* 310(5745):113-116.

144. Serrano A, Haddjeri N, Lacaille JC, & Robitaille R (2006) GABAergic network activation of glial cells underlies hippocampal heterosynaptic depression. *J Neurosci* 26(20):5370-5382.

145. Bowser DN & Khakh BS (2004) ATP excites interneurons and astrocytes to increase synaptic inhibition in neuronal networks. *J Neurosci* 24(39):8606-8620.

146. Halassa MM, Fellin T, & Haydon PG (2009) Tripartite synapses: roles for astrocytic purines in the control of synaptic physiology and behavior. *Neuropharmacology* 57(4):343-346.

147. Angulo MC, Kozlov AS, Charpak S, & Audinat E (2004) Glutamate released from glial cells synchronizes neuronal activity in the hippocampus. *J Neurosci* 24(31):6920-6927.

148. Perea G & Araque A (2007) Astrocytes potentiate transmitter release at single hippocampal synapses. *Science* 317(5841):1083-1086.

149. Fellin T*, et al.* (2004) Neuronal synchrony mediated by astrocytic glutamate through activation of extrasynaptic NMDA receptors. *Neuron* 43(5):729-743.

150. Nedergaard M & Verkhratsky A (2012) Artifact versus reality--how astrocytes contribute to synaptic events. *Glia* 60(7):1013-1023.

151. Savtchouk I & Volterra A (2018) Gliotransmission: Beyond Black-and-White. *J Neurosci* 38(1):14-25.

152. Fiacco TA & McCarthy KD (2018) Multiple Lines of Evidence Indicate That Gliotransmission Does Not Occur under Physiological Conditions. *J Neurosci* 38(1):3-13.

153. Fiacco TA*, et al.* (2007) Selective stimulation of astrocyte calcium in situ does not affect neuronal excitatory synaptic activity. *Neuron* 54(4):611-626.

154. Agulhon C, Fiacco TA, & McCarthy KD (2010) Hippocampal short- and long-term plasticity are not modulated by astrocyte Ca2+ signaling. *Science* 327(5970).

155. Rungta RL*, et al.* (2016) Ca(2+) transients in astrocyte fine processes occur via Ca(2+) influx in the adult mouse hippocampus. *Glia* 64(12):2093-2103.

156. Sherwood MW*, et al.* (2017) Astrocytic IP3 Rs: Contribution to Ca(2+) signalling and hippocampal LTP. *Glia* 65(3):502-513.

157. Okubo Y*, et al.* (2019) Inositol 1,4,5-trisphosphate receptor type 2-independent Ca(2+) release from the endoplasmic reticulum in astrocytes. *Glia* 67(1):113-124.

158. Toth AB*, et al.* (2019) CRAC channels regulate astrocyte Ca2+ signaling and gliotransmitter release to modulate hippocampal GABAergic transmission. *Sci Signal* 12(582):eaaw5450.

159. Bowser DN & Khakh BS (2007) Two forms of single-vesicle astrocyte exocytosis imaged with total internal reflection fluorescence microscopy. *Proc Natl Acad Sci U S A* 104(10):4212-4217.

160. Malarkey EB & Parpura V (2011) Temporal characteristics of vesicular fusion in astrocytes: examination of synaptobrevin 2-laden vesicles at single vesicle resolution. *J Physiol* 589(17):4271-4300.

161. Jairaman A & Prakriya M (2013) Molecular pharmacology of store-operated CRAC channels. *Channels (Austin)* 7:402-414.

162. Prakriya M & Lewis RS (2001) Potentiation and inhibition of Ca2+ release-activated Ca2+ channels by 2-aminoethyldiphenyl borate (2-APB) occurs independently of IP3 receptors. *J Physiol* 536:3-19.

163. Bates B*, et al.* (1999) Neurotrophin-3 is required for proper cerebellar development. *Nat Neurosci* 2(2):115-117.

164. Groszer M*, et al.* (2001) Negative regulation of neural stem/progenitor cell proliferation by the Pten tumor suppressor gene in vivo. *Science* 294(5549):2186-2189.

165. Wolfes AC*, et al.* (2017) A novel method for culturing stellate astrocytes reveals spatially distinct Ca2+ signaling and vesicle recycling in astrocytic processes. *J Gen Physiol* 149(1):149-170.

166. Wolfes AC & Dean C (2018) Culturing In Vivo-like Murine Astrocytes Using the Fast, Simple, and Inexpensive AWESAM Protocol. *J Vis Exp* (131).

167. Tsvilovskyy V*, et al.* (2018) Deletion of Orai2 augments endogenous CRAC currents and degranulation in mast cells leading to enhanced anaphylaxis. *Cell Calcium* 71:24-33.

168. Eckstein M*, et al.* (2019) Differential regulation of Ca2+ influx by ORAI channels mediates enamel mineralization. *Sci Signal* 12(578):eaav4663.

169. Inayama M*, et al.* (2015) Orai1-Orai2 complex is involved in store-operated calcium entry in chondrocyte cell lines. *Cell Calcium* 57(5-6):337-347.

170. Foo LC*, et al.* (2011) Development of a method for the purification and culture of rodent astrocytes. *Neuron* 71(5):799-811.

171. Abbracchio MP, Burnstock G, Verkhratsky A, & Zimmermann H (2009) Purinergic signalling in the nervous system: an overview. *Trends Neurosci* 32(1):19-29.

172. Verkhratsky A, Krishtal OA, & Burnstock G (2009) Purinoceptors on neuroglia. *Mol Neurobiol* 39(3):190-208.

173. Wang H, Ubl JJ, & Reiser G (2002) Four subtypes of protease-activated receptors, co-expressed in rat astrocytes, evoke different physiological signaling. *Glia* 37(1):53-63.

174. Junge CE*, et al.* (2004) Protease-activated receptor-1 in human brain: localization and functional expression in astrocytes. *Exp Neurol* 188(1):94-103.

175. Lee CJ*, et al.* (2007) Astrocytic control of synaptic NMDA receptors. *J Physiol* 581(Pt 3):1057-1081.

176. Shigetomi E, Bowser DN, Sofroniew MV, & Khakh BS (2008) Two forms of astrocyte calcium excitability have distinct effects on NMDA receptor-mediated slow inward currents in pyramidal neurons. *J Neurosci* 28(26):6659-6663.

177. Sofroniew MV (2014) Multiple roles for astrocytes as effectors of cytokines and inflammatory mediators. *Neuroscientist* 20(2):160-172.

178. Nicole O*, et al.* (2005) Activation of protease-activated receptor-1 triggers astrogliosis after brain injury. *J Neurosci* 25(17):4319-4329.

179. Papouin T, Dunphy J, Tolman M, Foley JC, & Haydon PG (2017) Astrocytic control of synaptic function. *Philos Trans R Soc Lond B Biol Sci* 372(1715).

180. Sahlender DA, Savtchouk I, & Volterra A (2014) What do we know about gliotransmitter release from astrocytes? *Philos Trans R Soc Lond B Biol Sci* 369(1654):20130592.

181. Henneberger C, Papouin T, Oliet SH, & Rusakov DA (2010) Long-term potentiation depends on release of D-serine from astrocytes. *Nature* 463(7278):232-236.

182. Sasaki T*, et al.* (2014) Astrocyte calcium signalling orchestrates neuronal synchronization in organotypic hippocampal slices. *J Physiol* 592(13):2771-2783.

183. Cao X*, et al.* (2013) Astrocyte-derived ATP modulates depressive-like behaviors. *Nat Med* 19(6):773-777.

184. Burrone J, Li Z, & Murthy VN (2006) Studying vesicle cycling in presynaptic terminals using the genetically encoded probe synaptopHluorin. *Nat Protoc* 1(6):2970-2978.

185. Jahn R, Hanson PI, Otto H, & Ahnert-Hilger G (1995) Botulinum and tetanus neurotoxins: emerging tools for the study of membrane fusion. *Cold Spring Harb Symp Quant Biol* 60:329-335.

186. Prakriya M & Lingle CJ (2000) Activation of BK channels in rat chromaffin cells requires summation of Ca2+ influx from multiple Ca2+ channels. *J Neurophysiol* 84(3):1123-1135.

187. Adler EM, Augustine GJ, Duffy SN, & Charlton MP (1991) Alien intracellular calcium chelators attenuate neurotransmitter release at the squid giant synapse. *J Neurosci* 11(6):1496-1507.

188. Rozov A, Burnashev N, Sakmann B, & Neher E (2001) Transmitter release modulation by intracellular Ca2+ buffers in facilitating and depressing nerve terminals of pyramidal cells in layer 2/3 of the rat neocortex indicates a target-specific difference in presynaptic calcium dynamics. *J Physiol* 531(3):807-826.

189. Deisseroth K, Bito H, & Tsien RW (1996) Signaling from synapse to nucleus: postsynaptic CREB phosphorylation during multiple forms of hippocampal synaptic plasticity. *Neuron* 16:89-101.

190. Kar P, Nelson C, & Parekh AB (2011) Selective activation of the transcription factor NFAT1 by calcium microdomains near Ca2+ release-activated Ca2+ (CRAC) channels. *J Biol Chem* 286(17):14795-14803.

191. Liu G & Tsien RW (1995) Properties of synaptic transmission at single hippocampal synaptic boutons. *Nature* 375:404-408.

192. Betz WJ & Bewick GS (1992) Optical analysis of synaptic vesicle recycling at the frog neuromuscular junction. *Science* 255(200-203).

193. Gourine AV*, et al.* (2010) Astrocytes control breathing through pH-dependent release of ATP. *Science* 329(5991):571-575.

194. Guthrie PB*, et al.* (1999) ATP released from astrocytes mediates glial calcium waves. *J Neurosci* 19(2):520-528.

195. Lalo U*, et al.* (2014) Exocytosis of ATP from astrocytes modulates phasic and tonic inhibition in the neocortex. *PLoS Biol* 12(1):e1001747.

196. Pangrsic T, *et al.* (2007) Exocytotic release of ATP from cultured astrocytes. *J Biol Chem* 282(39):28749-28758.

197. Sudhof TC (2013) Neurotransmitter release: the last millisecond in the life of a synaptic vesicle. *Neuron* 80(3):675-690.

198. Pryazhnikov E & Khiroug L (2008) Sub-micromolar increase in [Ca(2+)](i) triggers delayed exocytosis of ATP in cultured astrocytes. *Glia* 56(1):38-49.

199. Bergersen LH & Gundersen V (2009) Morphological evidence for vesicular glutamate release from astrocytes. *Neuroscience* 158(1):260-265.

200. Shigetomi E, *et al.* (2013) Imaging calcium microdomains within entire astrocyte territories and endfeet with GCaMPs expressed using adeno-associated viruses. *J Gen Physiol* 141(5):633-647.

201. Bindocci E, *et al.* (2017) Three-dimensional Ca(2+) imaging advances understanding of astrocyte biology. *Science* 356(6339).

202. Wang X, *et al.* (2006) Astrocytic Ca2+ signaling evoked by sensory stimulation in vivo. *Nat Neurosci* 9(6):816-823.

203. Tan Z, *et al.* (2017) Glia-derived ATP inversely regulates excitability of pyramidal and CCK-positive neurons. *Nat Commun* 8:13772.

204. Maggio N, *et al.* (2013) Thrombin regulation of synaptic transmission: implications for seizure onset. *Neurobiol Dis* 50:171-178.

205. Haustein MD, *et al.* (2014) Conditions and constraints for astrocyte calcium signaling in the hippocampal mossy fiber pathway. *Neuron* 82(2):413-429.

206. Tao J, *et al.* (2011) Deletion of astroglial Dicer causes non-cell-autonomous neuronal dysfunction and degeneration. *J Neurosci* 31(22):8306-8319.

207. Srinivasan R, *et al.* (2016) New Transgenic Mouse Lines for Selectively Targeting Astrocytes and Studying Calcium Signals in Astrocyte Processes In Situ and In Vivo. *Neuron* 92(6):1181-1195.

208. Gruszczynska-Biegala J & Kuznicki J (2013) Native STIM2 and ORAI1 proteins form a calcium-sensitive and thapsigargin-insensitive complex in cortical neurons. *J Neurochem* 126(6):727-738.

209. Berridge MJ (2006) Calcium microdomains: organization and function. *Cell Calcium* 40(5-6):405-412.

210. Sala C & Segal M (2014) Dendritic spines: the locus of structural and functional plasticity. *Physiol Rev* 94(1):141-188.

211. Garcia-Alvarez G, *et al.* (2015) Impaired spatial memory and enhanced long-term potentiation in mice with forebrain-specific ablation of the Stim genes. *Front Behav Neurosci* 9:180.

212. Kyung T, *et al.* (2015) Optogenetic control of endogenous Ca(2+) channels in vivo. *Nat Biotechnol* 33(10):1092-1096.

213. Majewski L, *et al.* (2017) Overexpression of STIM1 in neurons in mouse brain improves contextual learning and impairs long-term depression. *Biochim Biophys Acta Mol Cell Res* 1864(6):1071-1087.

214. Lalonde R (2002) The neurobiological basis of spontaneous alternation. *Neurosci Biobehav Rev* 26(1):91-104.

215. Kraeuter AK, Guest PC, & Sarnyai Z (2019) The Y-Maze for Assessment of Spatial Working and Reference Memory in Mice. *Methods Mol Biol* 1916:105-111.

216. Morris RG (1981) Spatial localization does not require the presence of local cues. *Learn Motiv* 12(2):239-260.

217. Vorhees CV & Williams MT (2014) Assessing spatial learning and memory in rodents. *ILAR J* 55(2):310-332.

218. Curzon P, Rustay NR, & Browman KE (2009) Cued and contextual fear conditioning for rodents. *Methods of Behavioral Analysis in Neuroscience,* Frontiers in Neuroscience, ed Buccafusco JJ (CRC Press/Taylor & Francis, Boca Raton (FL)), 2nd Ed.

219. Raybuck JD & Lattal KM (2014) Bridging the interval: theory and neurobiology of trace conditioning. *Behav Processes* 101:103-111.

220. Gwack Y*, et al.* (2008) Hair loss and defective T- and B-cell function in mice lacking ORAI1. *Mol Cell Biol* 28(17):5209-5222.

221. Seibenhener ML & Wooten MC (2015) Use of the Open Field Maze to measure locomotor and anxiety-like behavior in mice. *J Vis Exp* (96):e52434.

222. Brooks SP & Dunnett SB (2009) Tests to assess motor phenotype in mice: a user's guide. *Nature Reviews Neuroscience* 10(7):519-529.

223. Molina-García L & Barrios A (2018) Sex differences in learning — shared principles across taxa. *Current Opinion in Physiology* 6:65-74.

224. Jonasson Z (2005) Meta-analysis of sex differences in rodent models of learning and memory: a review of behavioral and biological data. *Neurosci Biobehav Rev* 28(8):811-825.

225. Maciag F*, et al.* (2019) Behavioral and electrophysiological changes in female mice overexpressing ORAI1 in neurons. *Biochim Biophys Acta Mol Cell Res* 1866(7):1137-1150.

226. Chouery E*, et al.* (2013) Report on a patient with a 12q24.31 microdeletion inherited from an insulin-dependent diabetes mellitus father. *Mol Syndromol* 4(3):136-142.

227. Bulayeva K*, et al.* (2015) Genomic structural variants are linked with intellectual disability. *J Neural Transm (Vienna)* 122(9):1289-1301.

228. Verhoeven WM*, et al.* (2015) A 12q24.31 interstitial deletion in an adult male with MODY3: neuropsychiatric and neuropsychological characteristics. *Am J Med Genet A* 167A(1):169-173.

229. Labonne JD*, et al.* (2016) An atypical 12q24.31 microdeletion implicates six genes including a histone demethylase KDM2B and a histone methyltransferase SETD1B in syndromic intellectual disability. *Hum Genet* 135(7):757-771.

230. Shigetomi E, Tong X, Kwan KY, Corey DP, & Khakh BS (2011) TRPA1 channels regulate astrocyte resting calcium and inhibitory synapse efficacy through GAT-3. *Nat Neurosci* 15(1):70-80.

231. Shigetomi E, Jackson-Weaver O, Huckstepp RT, O'Dell TJ, & Khakh BS (2013) TRPA1 channels are regulators of astrocyte basal calcium levels and long-term potentiation via constitutive D-serine release. *J Neurosci* 33(24):10143-10153.

232. Malarkey EB & Parpura V (2008) Mechanisms of glutamate release from astrocytes. *Neurochem Int* 52(1-2):142-154.

233. Zhang Y & Barres BA (2010) Astrocyte heterogeneity: an underappreciated topic in neurobiology. *Curr Opin Neurobiol* 20(5):588-594.

234. McCarthy KD (1980) Preparation of separate astroglial and oligodendroglial cell cultures from rat cerebral tissue. *The Journal of Cell Biology* 85(3):890-902.

235. Beaudoin GM, 3rd, *et al.* (2012) Culturing pyramidal neurons from the early postnatal mouse hippocampus and cortex. *Nat Protoc* 7(9):1741-1754.

236. Schmoranzer J, Goulian M, Axelrod D, & Simon SM (2000) Imaging constitutive exocytosis with total internal reflection fluorescence microscopy. *J Cell Biol* 149(1):23-32.